HHS Public Access

Author manuscript

Mater Sci Eng C Mater Biol Appl. Author manuscript; available in PMC 2021 May 01.

Published in final edited form as:

Mater Sci Eng C Mater Biol Appl. 2020 May ; 110: 110698. doi:10.1016/j.msec.2020.110698.

Recent Trends in the Application of Widely Used Natural and Synthetic Polymer Nanocomposites in Bone Tissue Regeneration

Angshuman Bharadwaz[a], **Ambalangodage C. Jayasuriya**[a,b,*]

[a]Biomedical Engineering Program, College of Engineering, The University of Toledo, Toledo OH, USA

[b]Department of Orthopaedic Surgery, College of Medicine and Life Sciences, The University of Toledo, Toledo OH, USA

Abstract

The goal of a biomaterial is to support the bone tissue regeneration process at the defect site and eventually degrade *in situ* and get replaced with the newly generated bone tissue. Nanocomposite biomaterials are a relatively new class of materials that incorporate a biopolymeric and biodegradable matrix structure with bioactive and easily resorbable fillers which are nano-sized. This article is a review of a few polymeric nanocomposite biomaterials which are potential candidates for bone tissue regeneration. These nanocomposites have been broadly classified into two groups viz. natural and synthetic polymer based. Natural polymer-based nanocomposites include materials fabricated through reinforcement of nanoparticles and/or nanofibers in a natural polymer matrix. Several widely used natural biopolymers, such as chitosan (CS), collagen (Col), cellulose, silk fibroin (SF), alginate, and fucoidan, have been reviewed regarding their present investigation on the incorporation of nanomaterial, biocompatibility, tissue regeneration, and biodegradation. Synthetic polymer-based nanocomposites that have been covered in this review include polycaprolactone (PCL), poly (lactic-co-glycolic) acid (PLGA), polyethylene glycol (PEG), poly (lactic acid) (PLA), and polyurethane (PU) based nanocomposites. An array of nanofillers, such as nano hydroxyapatite (nHA), nano zirconia (nZr), nano silica (nSi), silver nano particles (AgNPs), nano titanium dioxide ($nTiO_2$), graphene oxide (GO), that is used widely across the bone tissue regeneration research platform are included in this review with respect to their incorporation into a natural and/or synthetic polymer matrix. The influence of nanofillers on cell viability, both *in vitro* and *in vivo*, along with cytocompatibility and new tissue generation has been encompassed in this review. Moreover, nanocomposite material characterization using some commonly used analytical techniques, such as electron microscopy, spectroscopy, diffraction patterns, has been highlighted in this review. Biomaterial physical properties, such as pore size,

*Corresponding Author: Department of Orthopaedic Surgery, University of Toledo Medical Center, 3000 Arlington Avenue, Toledo, OH 43614, USA, Tel: +1-429-383-6557, Fax: +1-419-383-3526, a.jayasuriya@utoledo.edu.

Conflict of interest

The authors declare no conflict of interest

porosity, particle size, and mechanical strength which strongly influences cell attachment, proliferation, and subsequent tissue growth has been covered in this review. This review has been sculptured around a case by case basis of current research that is being undertaken in the field of bone regeneration engineering. The nanofillers induced into the polymeric matrix render important properties, such as large surface area, improved mechanical strength as well as stability, improved cell adhesion, proliferation, and cell differentiation. The selection of nanocomposites is thus crucial in the analysis of viable treatment strategies for bone tissue regeneration for specific bone defects such as craniofacial defects. The effects of growth factor incorporation on the nanocomposite for controlling new bone generation are also important during the biomaterial design phase.

Keywords

biomaterial; bone tissue regeneration; nanocomposite; nanofillers; biocompatibility

Introduction

The bone is a connective tissue that is primarily composed of minerals. It has several important functions within the body that include protection, locomotion, storage depot for calcium and phosphate in the body, housing for bone marrow, and structural integrity to the body [1]. The demand for functional bone grafting techniques has been constantly increasing all across the globe [2]. Around $45 billion is spent annually on the treatment of approximately 15 million bone disorder related patients including 1.6 million trauma-related fractures and 2 million osteoporotic bone defects [3]. Around 1.6 million patients undergo bone grafting procedures in the United States annually, accruing a total cost of around $2.5 billion [2–4]. By the turn of the decade, the total expense related to bone grafting procedures would exceed by almost two times due to several factors, including “needs of the baby boomer population” and increase in life expectancy of individuals [5].

The standard practices in bone defect repair encompass autografts, which is the tissue that is harvested from the patient, most commonly from the region of the iliac crest than from the region of the proximal tibia or distal femur. Allografts serve as an alternative to autografts, wherein the bone tissue is harvested from a donor or cadaver. Autografts are well suited for bone reconstruction methods as they are non-immunogenic, histocompatible, and osteogenic; as bone forming cells or osteoblasts within the graft promote the formation of new bone by a process called osteogenesis. These autografts also facilitate osteoconduction as the cell housing possesses a three-dimensional (3D) and porous matrix that supports ingrowth of vascular networks, tissue and other osteoprogenitor cells from the host or patient into the graft. Allografts also support osteoinduction as they contain bone morphogenetic proteins (BMPs) and other growth factors that facilitate the formation of osteoprogenitor cells by differentiation of various stem cells, especially mesenchymal stem cells [2, 6]. Although, vascularized autografting is considered as a common technique for critical bone defects several limitations, shortcomings, and complications in present clinical procedures have been reported for both autologous and allogeneic transplantations, including a decrease in the supply of grafts, infection and morbidity of the donor site, scarring, and several

surgical complications such as chronic pain, infection, bleeding [5, 7–13]. The alternatives to vascularized autografting include methods such as xenogeneic and allogenic bone grafts, but they also face considerable obstacles when it comes to a proper blood supply, immunogenicity, shortage of donor, and transmission of diseases [14, 15]. There are a few other methods of bone repair that uses BMPs, fillers such as bone cement, and distraction osteogenesis [2]. All current clinical methods of care and treatment lack the ideal features such as decreased patient morbidity, negligible size restrictions for defect site, high potential for the formation of blood vessels and preosteoblasts, longer shelf life, and reasonable costs. The key principle that governs the ideas behind bone tissue engineering explains the requirement for a regenerative environment that mimics the natural extracellular matrix (ECM) of the bone [2].

The field of Bone Tissue Engineering (BTE) is a paradigm that aims to successfully incorporate regeneration of bone at defect site of the host without any additional complications, such as donor site morbidity, immunogenicity, and poor vascularization. BTE is structured around four key components – (a) osteogenic cells that generate the bone tissue matrix, (b) a biocompatible framework, or scaffold, created with bioactive materials that mimic the ECM of the bone, (c) vascularization that provides mass transport of nutrients and wastes, and (d) morphogenetic signals to direct the cells [2, 16]. The goal of a biomaterial is to support the tissue regeneration process at the defect site and eventually get “resorbed and replaced over time” with the newly generated bone tissue [17]. Such a paradigm for bone tissue regeneration requires the biomaterial to be in possession of the following properties – (a) osteoinduction which allows the biomaterial to promote the differentiation of the progenitor cells in to osteoblasts, (b) osteoconduction that facilitates the biomaterial to support the growth of the bone tissue as well as the surrounding bone in-growth, and (c) osseointegration that supports the biomaterial to aid in integration into the surrounding bone tissue [18, 19]. Additionally, the biomaterial should be chemically and mechanically stable in the host environment, non-thrombogenic, easily sterilizable, and adequate manufacturability.

The scaffold, a 3D framework that houses the bone cells in BTE, together with the appropriate mechanical as well as biological cues stimulate and support the proliferation of bone-forming cells [20]. The scaffold should also possess the following properties for adequate bone tissue regeneration – (a) biocompatibility that requires that the scaffolds should be osteoconductive, and thus, it should support cellular activity with no toxic influence on the host tissue; the scaffold biomaterial should also allow cell adhesion and proliferation inside its pores as well as on the surface; the scaffold should be able to promote vascularization, (b) in terms of mechanical properties scaffolds should have a range of Young’s moduli around 15 to 20 GPa and 0.1 to 2 GPa for cortical and cancellous bone respectively; compressive strength should be around 100 to 200 MPa and between 2 to 20 MPa for cortical and cancellous bone respectively, (c) pore interconnectivity and size is quintessential for BTE as new bone tissue growth requires an optimum pore size of 200 to 350 μm, essential for transport of nutrients and oxygen, and (d) bioresorbability which dictates that the scaffold should be able to degrade over time *in vivo* at a controlled rate of resorption, thereby making space for the growth of the new bone tissue simultaneously [21–24]. Before the tissue regeneration process may be started, the biomaterial scaffold is

required to be fabricated to include certain features that are quintessential for cell growth and adequate bone tissue regeneration. Such properties primarily include porosity, surface-to-volume ratio, and crystallinity [25]. Some of the fabrication methods generally used for bone tissue scaffolds include foam replica method [26], electrospinning [27], freeze drying [28], gas foaming [29], solvent casting/particulate leaching [30], phase separation [31], molecular self-assembly [32]. A new dimension of 3D printing technology in the field of BTE is 3D Bioprinting. A major advantage of this 3D printing technique is the feasibility to directly implant the scaffold, right after printing, onto the patient's defect site [33]. Broadly the bioactive signal molecules, that control cell adhesion, proliferation, metabolism, and differentiation through biological cues and signals, may be broadly categorized into three groups – (a) mitogens which promote division of cells, (b) growth factors which promote cell proliferation, and (c) morphogens that control tissue generation [25]. Methods for the incorporation of these bioactive molecules into the scaffold may be categorized into two groups – a) top-down approach, that is achieved by depositing bone ECM, which is secreted by bone tissue cells or stem cells, on the scaffold, thereby creating a biomaterial scaffold-ECM hybrid structure and b) bottom-down approach, that is done by functionalizing the scaffold with growth factors and/or cytokines, as well as covalent tethering of peptides; these bioactive molecules may also be incorporated into nano or microspheres/particles that are designed for timed release of the encapsulated bioactive molecule within the ECM [34, 35]. Topological and chemical features of the bone tissue scaffolds facilitate cell adhesion to the scaffold surface, and support proliferation [36]. The scaffold also experiences enhanced interaction of the growing tissue with the nutrient microenvironment and other bioactive elements around the defect site due to the presence of chemical properties. Topographical properties of the scaffold, which are integrated onto the scaffold in the form of growth factors or other biologically active agents, support osteoconduction, osseointegration, and osteoinduction. This was evident from the enhanced osteoconductive properties of prominent studies related to natural polymeric composite bone tissue scaffolds as compared to its pristine biomaterial counterparts [37].

Nanocomposite biomaterials are a relatively new class of materials that incorporate biopolymeric and biodegradable matrix structure with bioactive and easily resorbable fillers which are nano sized [38]. The nanofillers induced into the polymeric matrix render important physical as well as chemical properties, such as large surface area, improved mechanical strength and stability, improved cell adhesion, proliferation, and differentiation, to the biomaterial important for tissue regeneration compatibility [38, 39]. This paper encompasses the summary of information dealing with the application of nanocomposites in BTE. The nanocomposites have been categorized as per the polymer and the effects of the nanoparticles incorporated into the polymer on various aspects of BTE have been highlighted. The primary objective of this paper is to introduce the concept of amalgamation of various polymers/polymer blends with nanoparticles and discuss their synergistic effect on the bone regeneration process with the help of recent research trends in bone regeneration studies. As the polymer being used for nanocomposite synthesis is quintessential for facilitating a plethora of biomimetic properties such as mechanical strength, biocompatibility, cytocompatibility etc., therefore in the subsequent sections of this paper, the nanocomposites have been categorized broadly into the ones prepared with natural

biopolymers and others with synthetic biopolymers. For each of the categorized nanocomposite group viz. chitosan based, collagen based etc. A summary of the nanocomposite synthesis/preparation techniques along with mechanical and biological compatibility results have been highlighted. The influence of the nanomaterial over the pristine material and/or biomaterial without any nanofillers has been stated. Another aim of this paper is to highlight the effects, both advantages as well as drawbacks, of the nanofillers for each of the broad polymer nanocomposite sections. This further provides an insight into the various combinations of nanofiller and polymer matrix, along with the polymer incorporation methods as well, and their subsequent positive as well as undesired effects on the overall bone regeneration process. The authors hope to provide the readers with a set of preliminary information regarding the effects of nanofillers on overall composite properties and therefore help in design and planning of future bioactive nanocomposites for bone tissue regeneration.

Natural Polymers

BTE employs polymer based biocompatible and biodegradable natural materials that provide a suitable bioactive environment and necessary mechanical support to promote the growth of new bone tissue in defect sites. Due to their superior biocompatibility and minute negative immunological influence, natural polymers such as Col, CS, alginate, silk, alginate, fucoidan, elastin, gelatin, hyaluronic acid are extensively used in BTE research [40–42].

Chitosan-Based Nanocomposites

Some of the natural polymers, like CS, can be found in abundance in the shell crusts of crustacean creatures. CS is primarily composed of β−1,4-linked N-acetyl-D-glucosamine and D-glucosamine units that are vulnerable to biodegradation [43, 44]. Because of its biodegradability and non-toxic nature, CS has been one of the most promising biomaterials in BTE. There are vast similarities between the skeleton of CS and the glycosaminoglycans (GAGs), which increases the bone regeneration rate. The presence of reactive hydroxyl and amino functional groups facilitate modifications chemically. Thus, CS-based nanocomposite materials have gained increased attention in the field of BTE [45–47]. In contrast to its source, chitin, CS has good solubility with dilute acidic solutions with a pH below 6.5 [48]. The deacetylation conditions used, as well as the biological origin of the CS, influence a host of biological and physiochemical properties in the polymer. Several *in vitro* and *in vivo* studies have confirmed the minimal toxic effects as well as biological inertness of CS. The studies have also highlighted the fact that there were no complications, such as inflammation or an allergic reaction, post-implantation of CS-based scaffolds [44]. The restrictions of pure CS, especially in terms of mechanical strength, have been addressed by the formulation of CS-based nanocomposite scaffolds, mainly with hydroxyapatite, Col, tricalcium phosphate, and synthetic polymers.

nHA has been a common nanofiller for CS based composite biomaterial in BTE. Being chemically similar with natural bone apatite material, nHA offers a plethora of benefits to the nanocomposite in terms of mechanical, thermal as well as cellular activity. An intercalated CS/nHA composite structure has been reported to be prepared using a

combination of sol-gel process and self-assembly of nHA during drying of films [49], as mentioned in Table 1. Due to the penetration of nHA in between the CS layers, X-ray Diffraction (XRD) peaks of intercalated CS has been reported in the nanocomposites which has been further confirmed by Scanning electron Microscopy (SEM) micrographs and thermal degradation profiles. SEM data has also confirmed the presence of a layered morphology for nanocomposites with 10% and 20% nHA as compared to a smooth surface observed for 5% nHA/CS composite. Mechanical testing of the nanocomposites has been reported to have an increase from 3.5 GPa to 4.4 GPa for CS only and CS/nHA 20% composites. The surface of the composite has been reported to have nHA particles in the shape of discs. The uniform shape and size of the nHA particles on the surface of the composite is desirable for avoiding inflammation reactions, as natural bone apatite is known for its regular structural characteristics [50, 51].

An increase in nHA content has also revealed an increase in surface roughness as well as hardness of the nanocomposite. Increase in nHA content also exhibits an interesting behavior of initiating a faster CS degradation up to 300 °C, which may be attributed to more efficient heat transfer aided by nHA particles [49]. However, the reverse trend for degradation rate vs. nHA content has been reported after 300 °C also. Additionally, thermal degradation of the CS matrix highlights the formation of calcium pyrophosphate as well as β-tricalcium phosphate [49]. In addition to nHA, several additional bio-ceramic nanoparticles, as listed in Table 1, have been used in the synthesis of CS-based nanocomposite porous scaffolds using freeze-drying methods [52]. The increase in nanoparticle size has been reported to have a negative impact on its distribution across the polymer matrix, as evident from Transmission Electron Microscopy (TEM) and SEM data. The roughness of the pore walls of the scaffolds has also been attributed to the deposition of nanoparticles on the pore walls, which also increases the pore wall thickness. Moreover, the swelling ratio has been reported to be lower for scaffolds prepared from nanocomposites as compared to their pristine polymer counterparts; this effect may be due to the release of the bio-ceramic nanoparticles after immersion in solution. Also, it should be noted that the water absorption of the scaffolds with nHA and nano calcium zirconate (nCZ) have been reported to have been lower than those with nZr. This may be due to the presence of a metal oxide surface on the nZr particles which is hygroscopic and attracts more water for the scaffolds prepared with nZr. Further, the presence of calcium and phosphate in nHA and calcium in nCZ may have possibly interacted with the amine and hydroxyl groups present in CS, thereby reducing its water uptake [52].

In terms of mechanical property assessment, nanomechanical property comparison reported comparable Young’s modulus across all nanocomposite groups. The increase in mechanical strength has been reported as a progression in the compressive strength and modulus of the nanocomposite scaffolds, which is around 50–55 KPa and 0.75–0.95 MPa respectively, as compared to pure CS scaffolds with 28 KPa and 0.25 MPa as the compressive strength and modulus respectively. As compared from the results of peak force quantitative nanomechanical mapping (PFQNM), the pure CS scaffolds failed to yield Young’s modulus greater than that of the CS-based nanocomposite scaffolds. The cross-interaction of zirconia-hydroxyapatite composite ceramic material may be explained as the reason for the increased mechanical strength as compared to pure hydroxyapatite nanoparticles [52].

Cell proliferation studies revealed that nCZ and nHA scaffolds were more effective scaffolds [52]. The low response rate from osteoblasts primarily towards zirconia-based scaffolds has been addressed by the nCZ/CS based composite scaffold. nCZ/CS composite biomaterial facilitated the increased proliferation of pre-osteoblasts as compared to nZr/CS composite scaffolds, as shown in Fig. 1. Also, nCZ/CS composite scaffolds had similarities in cell growth and spreading with nHA/CS composite scaffolds. This may be due to the presence of extracellular calcium on these scaffold groups that lead to more efficient osteoblast proliferation, as calcium sensing receptors enhance the chemotaxis and proliferation of the cells. The presence of calcium may have also enhanced the attachment of cells on the scaffold surface, with the cellular filopodias being reported to be have been spreading towards the nano bio-ceramic particles in each of the nanocomposite scaffolds. Increased osteopontin expression due to the presence of extracellular calcium on nHA and nCZ nanoparticles may have also contributed the efficient cell attachment on the respective nanocomposite [52].

Another novel study on bioinspired nanocomposites depicts the creation of nHA/CS/ tamarind seed polysaccharide (TSP) nanocomposites with a load proportion (nHA/CS/TSP) of 70/20/10, 70/15/15 and 70/10/20, respectively using a co-precipitation method [47]. A comparative appraisal of the properties of nHA/CS/TSP and nHA/CS nanocomposites was done by Fourier Transform Infrared Spectroscopy (FTIR), Energy Dispersive X-ray Spectroscopy (EDS), TEM, Thermal Gravimetric Analysis (TGA)/Differential Thermal Analysis (DTA), XRD, and mechanical testing. FTIR data revealed a shift of the hydroxyl group bands to a lower wavenumber in the nHA/CS/TSP as compared to nHA/CS samples, thus suggesting a strong intra and intermolecular hydrogen bonding between the three components within the nanocomposite. The hydrogen bonding may be attributed to improve the thermal stability of the nHA/CS/TSP composite, as depicted from TGA data. Agglomeration of nanoparticles was reported from TEM data to have been avoided with the addition of TSP to the nHA/CS composite, thereby revealing the inhibitory effect of TSP on particle agglomeration [47].

In the same study, the SEM data revealed the increasing trend in surface roughness of the nanocomposite with an increase in the TSP content [47]. This phenomenon may be explained as the result of an interaction between the carboxyl groups on TSP with the calcium ions from nHA and the hydroxyl groups on TSP with the amide groups on CS. The outcomes proposed strong chemical bonding between the three segments, reduced particle size, and homogeneous scattering of nHA particles in nHA/CS/TSP when contrasted with nHA/CS. Moreover, nHA/CS/TSP (70/10/20) exhibited the roughest and the most porous surface, and an improved thermal stability. The most enhanced compressive modulus and strength, 81 MPa and 4.0 MPa respectively, was reported for nHA/CS/TSP (70/10/20). This effect may be explained as the result of an increased cross-linkage between the three components of the nanocomposite system due to the increased hydrogen bonding and therefore reduced molecular mobility in the polymer matrix [47].

Additionally, the swelling characteristics of TSP incorporated scaffolds reported an increase with an increasing TSP content, thus signaling the effect of the hydrophilic nature of the TSP component in the composite [47]. Also, nHA/CS/TSP (70/10/20) displayed more

prominent swelling character, biodegradation and increased biomineralization in simulated body liquid (SBF), when compared with nHA/CS/TSP (70/20/10, 70/15/15) and nHA/CS nanocomposites. Enhancement in biomineralization may be attributed to the interaction of carboxylic groups on the TSP with the calcium ions in the SBF solution. An initial slow biodegradation rate of the nanocomposite may be explained as the inhibition of the attacking enzymes from reaching the N-acetyl glucosamine groups due to the presence of strong intermolecular hydrogen bonds between TSP and CS. But, TSP being hydrophilic and therefore prone to hydrolysis by the water content of the lysozyme, ended up being an accelerator for biodegradation of the nanocomposite [47]. A non-toxic interaction with MG-63 cells (human osteoblast cell lines) and better haemocompatibility was seen with nHA/CS-TSP (70/15/15) nanocomposites [47]. In a similar study, porous composite scaffolds were made by utilizing the freeze-drying method by blending zein (ZN), CS and nHA in various organic/inorganic weight proportions [53]. The scaffolds displayed that an increase in nHA content induced a decrease in the scaffold porosity. This phenomenon may again be attributed to the intermolecular hydrogen bonds formed between the hydroxyl groups in the nHA with the amide groups present in the CS matrix, as well as interaction of hydroxyl groups present in the CS matrix with the amide groups of ZN. Similarly, the water absorption of the scaffolds decreased with an increase in nHA content. This may be also due to the additional interactions caused between the amide and hydroxyl groups and the calcium and phosphate ions, thus reducing the hydrophilicity of ZN as well as CS. However, thermal stability data revealed the positive influence of nHA on the thermal degradation of the nanocomposite.

Furthermore, the cytocompatibility of the ZN/CS/nHA platforms was overviewed by 3-(4,5-dimethylthiazol-2-yl)- 2,5-diphenyl tetrazolium bromide (MTT) assessment and cell adhesion studies utilizing human bone cancer cells [53]. Studies revealed the non-toxic nature of the biomaterial to the cells, and the cells were observed to have adhered to the pore walls inside the scaffolds. However, the cell proliferation was observed to be more for the scaffolds with higher amounts of CS and Zn over nHA. This phenomenon may be inferred as a result of the low crystallinity of the nHA particles that induce leaching of the phosphate and calcium ions into the surrounding fluid. This increases the requirement for additional intracellular calcium and phosphate, which is fulfilled by triggering additional cell death [53].

In the literature. zirconium dioxide (ZrO_2) has also been reported as a beneficial candidate for natural nanocomposites [54]. The preparation of multifunctional ZrO_2 doped nanocomposites having CS, naturally changed montmorillonite (OMMT) and nHA has been reported in the study. Arrangement of these nanocomposites was affirmed by FTIR and XRD. XRD data revealed the synthesis of the smaller sized ZrO_2 particles through a comparatively broader nHA-ZrO_2 peak. The formation of smaller nanofiller particles induced their enhanced dispersion in the polymer which was evident from the weaker XRD peaks for the nanocomposites. Increase in OMMT content also restricts interaction of water molecules with the polymer matrix, thereby reducing water uptake by the nanocomposite. Field Emission Scanning Electron Microscopy (FESEM) data also revealed the presence of spherical and uniformly sized ZrO_2 particles. Additionally, SEM pictures uncovered uniform dispersion of OMMT and nHA-ZrO_2 into the CS lattice. This may be inferred as the effect

of the hydrophilic activity of the CS matrix that facilitates the uniform dispersion of the OMMT layers. The interaction between the calcium and phosphate ions with the amide and carboxyl groups of the CS matrix may also be the reason for observing a uniform morphology across the nanocomposite samples. Also, TEM and XRD powder analysis revealed that the OMMT was incorporated mostly within the bulk polymer [54].

Additionally, the incorporation of nZr particles also highlighted the enhancement of mechanical properties. As per the rheological analysis of the CS-OMMT-nHA-ZrO_2 nanocomposites, designated as CMZH I, II and III with 5, 10, and 15 wt. % OMMT concentration respectively, exhibited superior properties related to energy storage as compared to the viscous response of the material or the loss modulus. The intermolecular and intramolecular interaction amongst the nanocomposite components provides rigidity that may be attributed as the reason for a higher storage modulus. The uniform distribution of the nanofillers within the polymer matrix may have enhanced the storage modulus. However, the decrease in storage modulus with an increase in OMMT content may be due to the agglomeration of the nanofillers within the polymer matrix which decreases cross-linking with the composite system. Reduction in cross-linkages within the polymer system reduces elasticity of the entire composite, thereby reducing the storage modulus [54].

In the same study, the increase in OMMT content also reported an increase in antibacterial activity due to the growing concentration of antimicrobial ammonium salt in the OMMT component. Swelling rate analysis of the nanocomposites inferred the enhancement of the swelling rate with a decrease in the concentration of OMMT in the composite. The cytocompatibility analysis of the nanocomposite has been exhibited by the proliferation of human osteoblast cells (MG-63). In addition, incorporation of 5 wt.% OMMT and 5 wt.% nHA-ZrO_2 into 90 wt.% CS matrix reported an increase in tensile strength, storage modulus, swelling in water and cytocompatibility alongside strong antibacterial impact, pH and compatibility of erythrocytes. The inclusion of OMMT as a positive influence on cell proliferation was revealed from *in vitro* data, along with the decreasing trend in cell proliferation with OMMT content at 15 wt. % [54]. In another study, enhanced cellular activity due to increased pore size has been reported in nSi reinforced CS nanocomposite scaffolds, with reports about pore sizes well over 300 μm [44]. However, pore size has been reported to be independent of the CS source or its deacetylation degree. nSi particles incorporated into the CS matrix have been reported to have also increased the mechanical compression resistance by around 30%. *In vitro* experiments reported spheroidal clusters of osteoblasts proliferating. Both *in vitro* and *in vivo* test results highlight the superior biocompatibility and bone tissue regeneration supportive properties of the nSi/CS composite scaffold. As shown in Fig. 2, it took at least 8 weeks for the onset of mature bone formation using this type of scaffold [44].

Freeze-dried scaffolds synthesized from CS, CMC and AgNPs-carboxylated cellulose nanowhiskers (CCNWs) have been reported to have enhanced mechanical properties along with an antibacterial environment [55]. AgNPs-CCNWs were prepared by allowing the growth of AgNPs on CCNWs. TEM data revealed that the AgNPs were stabilized with restricted mobility on the CCNWs, which can be attributed to the affinity of the AgNPs towards the hydroxyl and carboxyl groups of the CCNWs. XRD and FESEM examination of

the nanocomposite highlighted exceptionally crystalline structure with AgNPs, which were around 5.2 nm in diameter, enhanced on approximately 200 nm long CCNWs surface. FTIR examination affirmed the collaboration between CCNWs and AgNPs. Optimization of the amount of nanofillers content of nanocomposite amid scaffold fabrication helped in accomplishing 80– 90% porosity with pore diameter going somewhere in the range of 150 to 500 μm. The increase in pore diameter may be inferred as the result of addition of nanofillers (CCNWS-AgNPs); thus, it may be attributed to the hydrogen bonds formed between the CMC matrix and nanofillers, thereby restricting the mobility of the backbone polymer chain. Additionally, carboxyl groups in the nanofillers and the CMC repel each other, thus further restricting the mobility of the backbone chain. These inhibitory effects may be the reason for fewer covalent cross-linkages in the polymer matrix, hence increasing the pore size [55].

The mechanical strength was additionally enhanced in coordination with the mechanical properties of cancellous bone for the same study [55]. The increase in mechanical strength with the addition of nanofillers may be attributed to the compact packing of the CCNWs-AgNPs and CS, due to the interaction of the carboxyl groups in the nanofillers with the amino groups in the CS matrix. The addition of nanofillers also hindered the degradation rate of the scaffolds due to the increased intermolecular interactions within the polymer and thus covering up or blocking the lysozyme attack sites. Additionally, the swelling limit of scaffolds diminished after the incorporation of the nanocomposite. This inhibitory effect may be the result of the heterogeneous and intramolecular interactions occurring between the nanofillers and the polymer matrix. Also, the addition of the CCNWs-AgNPs were also helpful in enhanced biomineralization, as the carboxyl groups present on the CCNWs interact more efficiently with the calcium ions present in the SBF. Thus, scaffold degradation was tuned to help angiogenesis and vascularization. These hybrid scaffolds, in addition to displaying exceptional antimicrobial action, also supported MG63 cell attachment and proliferation [55].

Enhancement of mechanical properties for nanocomposite scaffolds have also been studied for CS based hydrogels using a formulation of CS/glycerophosphate disodium salt (GP) gel incorporated with attapulgite (ATP) nanoparticles, as shown in Fig. 3 [56]. The tensile strength, including elongation at fracture of the hydrogels, have been reported to have increased with the incorporation of the ATP nanoparticles to 5 times in comparison to CS/GP only hydrogels; it exhibits an increasing trend with increasing ATP concentration. The fibrillar structure of the ATP nanoparticles along with its overall effect on the biomaterial surface may be explained as the reason for the increasing trend in mechanical strength. FTIR data also reveals the formation of hydrogen bonds between ATP and the CS matrix, which increases the crosslinking density of the hydrogel and supports the increased mechanical behavior of the composite. SEM analysis of the ATP incorporated hydrogels explained this observation of enhanced mechanical properties as the influence of increased compactness of the porous structure with enhanced pre-wall roughness, along with the formation of uniform small holes distributed on the pore wall. As reported by FTIR results, the hydrogen bonding between ATP and CS molecules has been attributed as the reason for the increased crosslinking of the hydrogel. Additionally, gelation speed, which may be explained as the rheological analysis on the dynamic process of sol-gel transition, was also

reported to have significantly enhanced with the incorporation of the ATP nanoparticles. It may be inferred that the nucleation effect of ATP nanoparticles induces crystallization of the CS matrix, thus increasing the gelation efficiency [56]. Bioactive glass (BG) nanoparticles with gelatin and CS based hydrogel matrix has also been used in BTE [57]. The cationic nature of the hydrogel, reported from its zeta potential at 37 °C, facilitates the interaction of negatively charged components of the bone's natural ECM. Strong hydrogel crosslinking has again been reported that may be the reason for the enhancement of mechanical strength. *In vivo* analysis using human osteosarcoma cell lines (SAOS) exhibited promising results with respect to cell viability, proving the nanocomposite's cytocompatibility [57].

Collagen-Based Nanocomposites

Col, an essential part of the bone's natural ECM, is arranged as fibers in animals [58–60]. Col may be obtained easily from fish waste, such as bones, scales, and skins [61]. Marine sources, such as cuttlefish [62], jellyfish [63], skin and muscles of marine animals [64], and waste from fish [65] is considered better than bovine sources, primarily due to the latter's high risk of transmission of spongiform encephalopathy [60]. Col is a bioactive natural polymer that exhibits favorable biocompatibility, facilitates adhesion and proliferation of bone cells, and decreased antigenicity [66, 67]. The bone's ECM is primarily composed of Col that nourishes the bone cells by facilitating proper nutrient transport [68]. Although the biocompatibility of Col facilitates cell adhesion and proliferation, the faster biodegradability rate of pure Col scaffolds, poor mechanical strength, and increased swelling instead persuade the use of Col-based composite biomaterials for BTE [69–72].

The use of functionalized nanofillers have also been noted in the literature. Nanofillers such as functionalized multiwall carbon nanotube (f-MWCNT) was used for synthesis of composite scaffolds using Col and hydroxyapatite (HA) with the help of freeze-drying technique [72]. The incorporation of f-MWCNT has exhibited enhanced biocompatibility which may be attributed to the negatively charged surfaces on the nanotubes. These charged sites act as nucleation sites for bone mineralization. Additionally, the f-MWCNT incorporation also has facilitated an interconnected porous structure with an increased surface area of around 11.746 m^2/g, and an adequate volume in its pores, which was around 0.026 cm^3/g. Intramolecular hydrogen bonding between the functional groups present on the polymer matrix and the hydroxyl groups on the f-MWCNT may be attributed to certain effects such as enhanced mechanical strength. However, the chemical interactions between the amide functional groups on the Col and CS and the carboxyl and hydroxyl groups on f-MWCNT render a decreased porosity. Moreover, the additional hydrogen bonds formed between the hydroxyl groups on the biomineralized HA and the amide groups on the polymers and other calcium ion present in HA influence the reduction in overall porosity. *In vitro* results for the nanocomposite scaffolds were superior to the control samples, along with enhanced biocompatibility, as measured using MTT assay [72].

Biphasic calcium nanoparticle (BCP) has also been used in BTE with additional incorporation of dexamethasone (DEX) [73]. The dexamethasone has been included in a way for its controlled release during the regeneration process. Controlled porosity of the scaffold structure was achieved using porogen leaching method. These scaffolds have also

displayed enhanced mechanical strength, as stated in Table 1, along with an interconnected pore structure. Human mesenchymal stem cells (hMSCs) were seen to have achieved proper osteogenic differentiation with the nanocomposite scaffold, as well as increased biocompatibility. *In vivo* analysis, subcutaneous implantation at the dorsa of "athymic nude mice", displayed facilitation of ectopic bone formation, as shown in Fig. 4. It is worth to note the facilitation of angiogenesis which may be attributed to the constant release of calcium ions from the scaffold material. Also, enhanced osteogenic differentiation of the hMSCs may be attributed to the constant release of phosphate, calcium and DEX ions from the nanocomposite scaffolds [73].

Apatite (Ap) based Col scaffolds that mimic the bone like subfibrillar nanostructure, have been reported in use in apical periodontitis bone imperfections [74]. The bone regeneration capability of the Col-Ap nanocomposite was examined by contrasting it with inorganic β-tricalcium phosphate and Col (pure and organic) by utilizing a critical-sized rat mandibular defect model. Micro-computed tomographic imaging (Micro CT) and histologic recoloring were utilized to assess new bone generation *in vivo*. When contrasted with the β-tricalcium phosphate and Col scaffolds, the Col-Ap nanocomposite-based scaffolds displayed unrivaled recovery properties portrayed by adequate deposition of new bone structures and vascularization at the imperfection site. The effects of the sub-fibrillar structure of the Col-Ap nanocomposite may be attributed to the adequate organic-inorganic phase interaction of the minerals during biomineralization [74].

Additionally, immunohistochemistry demonstrated that the transcription factor osterix (OSx) and vascular endothelial growth factor (VEGF) receptor 1 were expressed abundantly in the Col-Ap groups [74]. The outcomes demonstrate that the Col-Ap nanocomposite facilitates the growth of bone-forming cells and invigorates increasingly vascular tissue ingrowth. The formation of vascular network along with enhanced VEGF receptor 1 expression facilitates adequate nutrient transport. Moreover, the Col-Ap nanocomposite facilitates the secretion of bone ECM, as revealed by the increased expression of transforming growth factor (TGF) β −1 and mineralization of rat bone marrow stem cells [74]. Bacterial cellulose (BC) has been used in Col based scaffolds with HA and growth peptide incorporation [75]. *In vitro* assessment of nanocomposite synthesized from BC, Col, HA and osteogenic growth peptide (OGP) or its C-terminal pentapeptide (OGP) [10–14] for bone regeneration purposes has also been reported. The BC/Col nanocomposites were effectively prepared through a carbodiimide-mediated coupling, as exhibited by spectroscopy data in the study. SEM, FTIR, and ^{31}Phosphorus Nuclear Magnetic Resonance examinations revealed that *in situ* creation of HA was a successful course of action to acquire natural bone-like apatite. Moreover, BC/Col composites reported spherical apatite deposition which was composed of needle-like or plate-like apatite crystallites. These particles closely resembled the osteocalcium phosphate phase and may be attributed for the supply of secondary nucleation sites for apatite on them. Moreover, the presence of peptides along with Col may also be attributed to the nucleation and growth of plate-like apatite crystallites [75].

The incorporation of Col and HA on the BC fiber network may be attributed to be the reason for enhancement in the strain at failure for the nanocomposite [75]. This has been reported to be a helpful feature in terms of flexibility of the nanocomposite for handling purposes, as

compared to pure BC membranes. The OGP containing (BC/Col) - HA composites facilitated the early advancement of the osteoblastic phenotype. Moreover, the bonding between Col, HA, and OGP peptides has enhanced the cell development as contrasted with the OGP containing BC/HA. Additionally, none of the nanocomposites demonstrated cytotoxic, genotoxic or mutagenic impacts [75].

Other alkaline rare earth elements viz. Strontium (II) has been used in conjunction with Col for osteoporotic bone defect treatments [76]. This study encompasses the effects of strontium ion for BTE as a replacement for the standard calcium ions associated with the biological and cellular processes. Mineralized Col-type I scaffolds with Strontium (II) were used in the regeneration study instead of using calcium during scaffold preparation. Strontium was used to the degree of 25, 50, 75 and 100 mol. % by substituting the $CaCl_2$-stock arrangement with an equimolar concentration of $SrCl_2$ (0.1 M). Synchronous fibrillation and mineralization of Col prompted the arrangement of Col-mineral nanocomposites with mineral phases moving from nanocrystalline hydroxyapatite over ineffectively crystalline Sr-rich stages towards a blended mineral stage, with 1 mol.% Strontium, comprising of a shapeless strontium phosphate, which is distinguished as Collin's salt ($Sr_6H_3(PO_4)_5$ * 2 H_2O; CS) and very crystalline strontium hydroxyapatite ($Sr_5(PO_4)_3OH$; SrHA). The framed mineral stages were portrayed by TEM and Raman spectroscopy. Scaffolds made from Col/mineral nanocomposites with controlled strontium content displayed an interconnected porosity reasonable for homogenous cell seeding *in vitro*. Strontium particles (Sr^{+2}) were discharged in a continued way from the modified scaffolds, with an unmistakable connection between the discharged Sr^{+2} fixation and the level of Srsubstitution. Since the focus of Sr^{+2} in this range are known to have an osteoanabolic impact, these scaffolds are promising biomaterials for the clinical treatment of deformities in a systemically debilitated bone. [76].

Silk Fibroin-Based Nanocomposites

SF is a natural material used widely in the medicine and textile industry. SF is extracted from *Bombyx mori* cocoon, a mulberry source, and is a biocompatible material found as the core of a structural protein fiber that is coated with sericin. It has been known to possess excellent cytocompatible properties and has been used in various tissue engineering applications [77–82]. It has also been reported that SF extracted from non-mulberry sources, like tasar silkworm – *Antheraea mylitta* has enhanced mechanical properties as compared to SF isolated from mulberry sources [83]. Adhesion of osteoblasts and bone regeneration has been reported to be enhanced for non-mulberry SF [84–87]. Attachment of cells, as well as proliferation, has been reported to be enhanced due to the presence of Arg-Gly-Asp (RGD), that facilitates integrin binding [88, 89].

Titanium dioxide (TiO_2) has been used as a nanofiller in SF based polymer scaffolds. The TiO_2 nanoparticles have several benefits to its incorporation into a polymer matrix, ranging from mechanical property enhancement to improved cellular interaction [80, 90]. Halogenated TiO_2 nanoparticles, $nTiO_2$ fabricated with fluoride particles, were added to the SF matrix through phase separation technique to create SF/TiO_2-F nanocomposite scaffolds. MTT test results were utilized to affirm the biocompatibility of the platforms utilizing

human-like SaOS-2 osteoblast cell line for 1, 3 and 5 days. The mechanical properties of scaffolds have been enhanced by adjusting the amount of TiO_2-F sum up to 15 wt. %. Further increase in TiO_2-F content has been reported to be detrimental. Fluoridation of TiO_2 has been reported to have enhanced the bioactive properties of the SF/TiO_2-F scaffolds. Also, osteoblast interaction has been reported to be non-toxic with the prepared scaffolds. However, the addition of 20% by wt. of halogenated nanoparticles reported decrease in mechanical properties which may be attributed to the non-uniform dispersion of the nanofillers on the SF matrix, thereby suggesting agglomeration of the nanoparticles. The increase in scaffold degradation rates in conjunction with increased TiO2-F content was reported with the increase in acidity of the surrounding PBS solution. Additionally, the presence of fluoride ions has been highlighted to have increased the biocompatibility of the scaffold in terms of cell viability and attachment [80].

Another similar study has reported the preparation of porous scaffolds using the freeze-drying technique from SF and TiO_2 nanoparticles [90]. SF/TiO_2 scaffolds were prepared with 5, 10, 15 and 20 wt. % of the TiO_2. SaOS-2 osteoblast-like cells were used to analyze the biocompatibility of the scaffolds. Scaffolds have been reported to exhibit enhanced directional and mechanical strength with an increase in TiO_2 nanoparticle content that reduces porosity. This study reported that no porogen or inorganic solvents were required for obtaining the macroporous, interconnected and directional porous structure. However, as listed in Table 1, there was a reduction of porosity that has been reported with the increasing content of nanoparticles which may be attributed to the agglomeration of these nanofillers on the pore walls, thus, making them thicker. The increase in pore wall thickness may be further attributed to be the reason behind the enhanced mechanical properties of the nanocomposite material. The bioactivity of the prepared scaffolds was affirmed by observation of surface crystallization of the apatite layer in terms of incubation time in the SBF. Mineralization has also been reported to increase with an increase in TiO_2 content. The presence of hydroxyl groups on the nanoparticle surface induces the enhanced apatite nucleation. Moreover, the degradation rate of the prepared scaffolds exhibited an increase with an increasing amount of TiO_2. SaOS-2 osteoblast-like cells have been reported to exhibit enhanced cell attachment and proliferation, including increasing cell viability with an increase in SF content [90].

Other SF based HA nanocomposites were synthesized to access the crystallinity of Col-SF/HA nanocomposites, and reveal that the low crystalline carbonate-substituted HA constituted the inorganic phase of the composite [91]. Morphological studies also revealed that HA particles, with size ranging between 30 to 100 nm, were uniformly distributed throughout the matrix of the polymer. TEM micrographs demonstrated that the inorganic particles were made from progressively fine sub-particles, whose size measurements were somewhere in the range of 2 and 5 nm in a non-crystallographic manner. The flexural modulus of nanocomposites has been reported to have been enhanced by the incorporation of SF. *In vitro* analysis revealed that the nanocomposites exhibited adequate cell biocompatibility. Hydrogen bonding leading to intramolecular cross-linking has been attributed to a beta sheet transformation of the SF molecules in the hydrogel. However, the precipitated HA has been reported to be of lower crystallinity which may be due to the size constraints faced by the growing apatite particles with the 3D microstructure of the hydrogel

[91]. A similar study used biocompatible SF from non-mulberry tropical tasar silkworm to create SF/HA nanocomposite particles with the help of the chemical precipitation technique [92]. A comparative study, in terms of biochemical and biophysical properties of SF/HA nanocomposites, between *in situ* reinforcement and external deposition of HA particles on SF scaffolds revealed better cytocompatibility and mechanical strength for scaffolds prepared using external deposition of HA. The presence of amide and carboxyl functional groups on the SF matrix may be the reason for adequate HA nucleation. However, the presence of HA on SF fibers reduces the degradation rate due to the lower exposure rate of the degradation enzymes on the SF network. Using an osteoblast macrophage co-culture model the immune response studies revealed that both types of scaffolds exhibit very less immune responses [92].

3D printed scaffolds were also analyzed for mechanical strength and cellular activity with SF polymer matrix and *in situ* HA growth [93]. 3D printed porous scaffolds made from SF/HA nanocomposites prepared using *in situ* mineral precipitation technique, reported the use of sodium alginate (SA) as the paste binder for 3D printing of the scaffolds. Microscopic analysis of the SF/HA nanocomposite revealed a very narrow particle size distribution and uniform morphology. The 3D printed scaffolds exhibited enhanced mechanical properties, with a compressive strength range of more than 6 MPa. These scaffolds also exhibited an interconnected porous network, with 70% overall scaffold porosity and approximately 400 μm in pore size. *In vitro* analysis of the porous scaffolds revealed recrystallization of the incorporated HA and subsequent apatite formation on the scaffold surface; analysis was done by soaking the scaffold in SBF. Also, it was reported that a balance in pH, between 6.9 and 7.1, was maintained for the microenvironment of the culture medium over a month. *In vitro* analysis, as shown in Fig. 5, using human bone marrow stem cells displayed that SF/HA content played a key role in cell proliferation; both cell proliferation, as well as alkaline phosphatase (ALP) activity, displayed an increasing trend with increased SF/HA content in the scaffolds. Drug release studies of the scaffolds with bovine serum albumin, revealed a sustained manner over a course of 5 days. [93].

Cellulose-Based Nanocomposites

Cellulose, abundantly found in bacteria and plants, degrades at a very slow pace due to the absence of the enzymes that attack its bonds [94]. It has been reported that due to the biocompatible nature of cellulose, along with biodegradability, non-toxic character, presence of protein binding sites, modifiable properties, and resistance to *in vivo* breakdown, cellulose forms a vital element in BTE as well as drug delivery applications [95]. But due to the absence of a definite 3D structure, cellulose has been seldom used alone in tissue engineering scaffolds. Moreover, the low mechanical properties of cellulose are also a hindrance. Thus, cellulose is mostly coupled with other natural and synthetic polymers for use in tissue engineering applications [94, 96, 97].

Biomimetic growth of HA on CNWs has been a widely used approach for cellulose based nanocomposites for BTE [98, 99]. A concentration of 1.5 M was used for SBF to allow the biomineralization of HA. Multiple functional groups viz. phosphoric acid, hydrochloric acid, and sulfuric acid were used thereby leading to varying functionalized CNWs being obtained.

Phosphonate and sulfonate surface functional groups impact the mineralization of HA directly, which has been attributed to the presence of the negative charge on the CNW surface that aid in hydroxyapatite nucleation and growth. Wet chemical precipitation method was used to prepare hybrid CNW/HA material for comparison. Fibroblast (L929) cells were employed for biocompatibility analysis of both the hybrid samples simultaneously prepared using a biomimetic approach and wet chemical precipitation method. During an incubation period of 24 hours, the hybrid materials obtained through the biomimetic approach have been reported to exhibit superior bioactivity and biocompatibility as compared to the material prepared using the wet chemical precipitation method [98]. A similar study on functionalized CNWs using hydrochloric acid for CNW preparation, followed by chemical functionalization of amino and carboxylate groups was done to analyze efficient and selective mineralization of HA through a biomimetic approach, using SBF for an incubation period of 14 and 28 days. Results have been reported to exhibit the importance of SBF contact time and surface functionalization of the CNWs, with carboxylate and amine groups, during mineralization of HA over the CNWs. MC3T3-E1 (preosteoblasts) cells were used for the bioactivity analysis of the prepared hybrid material. During an incubation period of 24 hours, amino-functionalized CNWs with HA grown through biomimetic approach exhibit significantly higher cell viability in comparison to the CNWs functionalized with carboxylate groups [99].

Studies suggesting the use of cellulose nanocrystals (CNCs) along with halloysite nanotubes (HNTs) have been used as reinforcing agents in nanocomposite scaffolds prepared from xanthan gum (XG) and sodium alginate (SA) using freeze casting/drying technique [100]. Uniform dispersion of the CNCs and HNTs across the polymer matrix with partial orientation has been reported. Moreover, the morphology of the prepared scaffolds has been reported to exhibit interconnected pore channels with very high porosity. The electrostatic attraction as well as hydrogen bonding between CNCs, HNTs, SA and XG may be attributed for the uniform dispersion of the nanofillers. These attractive forces are also responsible for the increased storage and loss modulus of the composite system [100].

The proper interfacial attractions between the components of the composite system may be attributed to the adequate thickening of the elongated pore walls which further improve the mechanical properties of the nanocomposite [100]. The incorporation of the CNCs and/or HNTs have been also reported to have a significant effect on the reduction of porosity as well as water uptake potential of the prepared scaffolds. The reduction in water uptake may be due to the lower water intake capacity of the HNTs. CNC and/or HNT inclusion have exhibited increased cytocompatibility of the scaffolds, as analyzed using MC3T3-E1 preosteoblasts, along with an increase in thermal stability as well as compressive mechanical strength. The thermal stability of the nanocomposite may be primarily due to the encapsulation of the polymer matrix into the HNT's lumen. Increased cell viability of the nanocomposite system may be attributed to the synergistic effect of the CNCs and HNTs which deliver adequate bioactivity as well as mechanical stability to the scaffold [100].

CNCs cross-linked by chemical process to form aerogels, by using the cryo-templating technique, were also included in bone regeneration scaffolding study [101]. CNCs were surface functionalized with phosphate or sulfate groups, as determined by the acid used for

their extraction: phosphoric acid or sulfuric acid. *In vitro* studies involving Saos-2 osteoblast-like cells revealed that the cells sustained their phenotype over 7 days, as depicted from ALP assay, as well as an increase in metabolism over this period. SBF, which has been pre-treated with 0.1 M calcium chloride, was utilized for mineralization analysis *in vitro* and it exhibited hydroxyapatite growth over 14 days. *In vivo* studies using the Calvarial bone of adult male Long Evans rats, as shown in Fig. 6, revealed the superior osteoconductivity as well as increased bone growth fractions at around 33% and 50% respectively for 3rd and 12th week time periods of the sulfated aerogel, as compared to the control samples without CNC aerogel implantation. This has also been attributed to be a predictor of superior porosity of the CNC aerogel. Sulfated CNC aerogels also exhibited enhanced mechanical property of compressive strength and superior stability in liquid environments, as compared to its phosphate counterparts [101].

Electrospinning is also a widely used method for polymer based scaffold synthesis. Electrospun fibers of cellulose, derived from cotton, coupled with nHA were used to prepare nanofibrous scaffolds for bone tissue regeneration [102]. SEM data revealed that the average diameter of the nanofibers increased with an increase in nHA loading. SEM images also revealed that the size distribution of the nanofibers was well aligned with the bone's natural ECM fibers. Moreover, the electrospun nanofibers exhibited superior mechanical properties, with a modulus of elasticity of around 3.12 GPa and tensile strength of around 70.6 MPa. Biocompatibility analysis of the nanofibers, as listed in Table 1, using human dental follicle cells exhibited good cell adhesion and proliferation. Additionally, the thermal stability of the electrospun nanofibers was reported to have increased with an increase in nHA content [102]. In another study, ionic cross-linked CMC microparticles were prepared through ionic crosslinking using Zirconium (Zr) aqueous ion complex and CS complex [103]. It has been reported that the presence of Zr facilitates a rough or groovy surface along with increased stability during degradation studies with PBS. FTIR data has inferred the successful crosslinking of the CMC with CS and Zr. Cell assays accomplished by using murine preosteoblasts - OB-6 cells revealed the non-toxic nature of the microparticles, including good cell attachment and proliferation on the surface of the microparticles. The presence of Zr on the surface of the microparticles has also been attributed to significantly aid in the cell attachment and proliferation, as seen with microparticles prepared using 10% w/v zirconium tetrachloride in Fig. 7. The stability and swelling characteristics of the microparticles have been attributed to its cross-linking efficiency, as Zr ions gets replaced at a faster rate with lower cross-linking density. Also, more water molecules are taken up into the polymer matrix with lower cross-linking of the microparticles, thereby increasing the swelling. The low toxicity of the Zr ions, especially since they exist in a complex hydroxide form, have facilitated for the adequate biocompatibility of the composite. Additionally, surface roughness of the microparticles due to Zr incorporation has been attributed to the adequate cell adhesion and proliferation characteristics of the scaffold [103].

Alginate-Based Nanocomposites

Brown seaweeds supply the majority of alginate, which is primarily polysaccharides, produced industrially [104]. Several types of brown algae, such as Laminaria japonica and Macrocystis pyrifera, are sources of alginate that are initially processed to form gelatinous

precipitates and are further synthesized into water-soluble SA by purification [105]. Alginate produced from bacteria primarily originates from Pseudomonas and Azotobacter [106]. Some of the advantages of alginate gels include conformance with irregularly shaped bone defects, better control on release of various cell growth factors, ease of ligand attachment as seen with RGD attachment, and size handling. Although its biocompatibility makes alginate gels a very good biomaterial for bone tissue regeneration, yet, the poor mechanical strength of alginate gels alone drives the concept behind alginate based composites [107].

Cytocompatible bio-scaffolds from gelatin cross-linked with alginate-di-aldehyde (ADA) and (nHA) were synthesized using the method of lyophilization [108]. The use of ADA, synthesized from periodate oxidation of alginate, facilitates the crosslinking of the aldehyde and amino functional groups in ADA and gelatin respectively, and thereby improves the thermal stability of the scaffold. Wet chemical treatment was utilized to prepare nHA from egg-shell waste that exhibited adequate calcium to phosphate ratio of around 1.51, nanostructure, and crystallinity. The increased scaffold stiffness owing to the nHA affected the water absorption and biodegradation of the scaffold. XRD analysis attributed the reason for enhanced crystallinity to be a combined effect of ADA and nHA. But the proliferation of nHA within the scaffold hinders its porous structure, as analyzed from SEM micrographs [108].

In another study graphene oxide (GO), alginate and gelatin has been incorporated to fabricate scaffolds using the freeze-drying method. FTIR data revealed broadening of a characteristic peak that infers the interaction of the GO with the alginate-gelatin polymer complex. FESEM data revealed the presence of GO nanosheets that ultimately induces roughness on the scaffolds that aid in cell adhesion and proliferation. However, the increased hydrophilicity of the GO along with its increased surface area, renders the addition of the nanofiller ineffective with respect to change in scaffold porosity. However, a 0.3% increase in GO content has been reported to enhance the mechanical strength of the scaffold by around 83%. This effect may be attributed to the reinforcing property induced by the GO nanosheets within the alginate-gelatin polymer matrix. The swelling characteristics of the scaffold increase with increasing GO content, up to 0.1%, which may be due to the enhanced hydrophilicity of the GO due to the presence of functional groups on the GO particles. But further increase in GO content, above 0.1%, induces enhanced physical cross-linking within the scaffold, thereby reducing the water uptake of the scaffold. Additionally, the presence of the negatively charged functional groups viz. carboxyl, hydroxyl and epoxy groups on GO induces better cell attachment and proliferation with MG-63 cell lines. Cell differentiation, as assessed from Runx 2 and Osteocalcin expressions in Fig. 8, as well as ALP activity was reported as adequate for utilizing the scaffold for bone regeneration [109].

Fucoidan-Based Nanocomposites

Fucoidan is another natural biomaterial extracted from similar sources as alginate, such as brown seaweed and algae. Fucoidans have repeating arrangements of alternate α (1→ 3) and α (1→ 4) glycosidic bonds in the primary structure of α−1,3-linked sulfated L-fucose [110]. The primary aide provided by fucoidan includes facilitation of the supply of ALP enzyme, BMP-2, osteocalcin, and Col type I expression [111]. Lubboc®, a commercial bone

substitute made from fucoidan with low molecular weight promotes bone cell proliferation, Col type I expression, thus facilitating the increased activity of ALP enzymes [112]. The enhanced activity of ALP, coupled with superior Col type I expression, Runt-related transcription factor 2 (Runx-2), osteocalcin and osteopontin facilitates the osteogenic differentiation of stem cells derived from human adipose tissue [113]. Fucoidan based composite scaffolds enhance the biomineralization by 30% in bone tissue regeneration [112]. Several bone tissue regeneration scaffolds made from alginate, CS, and fucoidan using freeze-drying technique have displayed very promising results in new bone formation [114].

3D bioactive scaffolds prepared by freeze-drying technique from the composite structure of CS, nHA, and fucoidan exhibited reduced water absorption and retention [115]. The pore size of the scaffold ranged from 10–400 μm, along with the presence of a phosphate group which was confirmed by FTIR analysis. Nutrient supply and cell growth were aided by the scaffold's microstructure, and the scaffold facilitated the *in vitro* biocompatibility of periosteum mesenchymal stem cells (PMSCs) for proper differentiation, growth, and mineral deposition. The incorporation of nHA may be attributed as the reason for the very high porosity of the scaffolds, above 90%, which thereby facilitates vascularization. However, the dense ceramic surface of the nHA on the scaffolds resulted in a lower water absorption and retention. Additionally, SEM data revealed an adequate pore structure suggesting that the nHA did not agglomerate within the composite system. Also, the presence of carbonated nHA rich phase, obtained from salmon fish bone through alkaline hydrolysis method, may be the reason for the increased cell proliferation and biocompatibility. Further, biomineralization was reported to be enhanced with the incorporation of carbonated nHA [115].

In another study, fucoidan and nHA hybrid composite scaffolds were prepared by *in situ* chemical process and tested for response to bone tissue regeneration [116]. Biomineralization of Fucoidan/nHA composite scaffold was superior, as compared to hydroxyapatite only bone tissue regeneration environment, for human adipose-derived stem cell; this effect has been primarily attributed to the presence of fucoidan in the nanocomposite. Gene expressions, such as osteopontin, osteocalcin, Runx-2, and Col type I, were observed to have enhanced results for the fucoidan/nHA scaffolds on the 7^{th} day of implantation. *In vivo* study on rabbit model displayed new bone formation, however, the bone formation was not very dense, as shown in Fig. 9. nHA may have also benefited the osteoblastic activity which has been suggested due to the increased gene expressions for Col Type I, osteopontin and osteocalcin for nHA incorporated composite [116].

Synthetic Polymers

Specific applications in bone tissue regeneration require certain modifications to the polymer structure. This reengineering is quite difficult with natural polymers, and hence synthetic polymers, such as PCL, PLGA, PLA, are widely used in BTE [117, 118]. PCL is a relatively cheap and elastic synthetic polymer that has been approved by the FDA, USA. PLGA is another FDA approved synthetic biopolymer used in BTE. The major advantages of PLGA

include biocompatibility and controlled degradation, whereas reduced osteoconductivity of PLGA poses as a major disadvantage [119].

Polycaprolactone-Based Nanocomposites

PCL is an aliphatic and semi-crystalline polymer that exhibits superior toughness and mechanical strength along with adequate biocompatibility [120–125]. The advantage of PCL in BTE is displayed by its adequate cell adhesion and proliferation, as well as good mechanical strength, whereas it's slow degradation rate sometimes poses as a factor that impacts negatively on the bone tissue regeneration process [126, 127]. Biodegradation of PCL based scaffolds is driven by hydrolysis reactions, thereby saving the need to incorporate any enzymes or catalysts [128]. The hydrophobic nature of PCL inhibits cell adhesion and therefore proliferation, yet several osteoinductive and osteogenic inorganic compounds, such as titanium dioxide, hydroxyapatite, BG improves the mechanical as well as biological characteristics of PCL based scaffolds [129–133].

Hydroxyapatite nanorods synthesized *in situ* and reinforced on PCL has been reported in the literature [125]. The synthesis of semi-crystalline hydroxyapatite nanorods (nHAR), as affirmed by FESEM and XRD, was done at a temperature scope of 60–150 °C in an autoclave [125]. The temperature of the thermal procedure chooses the proportion of the nHAR. As observed from EDS and FTIR data, the ratio of calcium to phosphorus likewise pursues an immediate association with the processing temperature. With increase in processing temperature, the crystal growth also increases which may be due to the reduction in surface tension on some specific crystal structure faces with an increasing temperature. However, the increase in temperature also induces reduction in ion diffusion rate into the HA crystal. The *in situ* synthesis for nHAR accomplishes a higher flexible modulus and mechanical quality, around 15% more, than the result of *ex situ* technique. *In vitro* analysis in SBF reported increased bone tissue regeneration [125].

The enhancement in mechanical strength due to the incorporation of the *in situ* nanorods may be attributed to the uniform distribution of the nanofillers through the PCL matrix [125]. However, porosity also has a negative impact on the mechanical strength, as has been reported. The nanocomposite material displayed biocompatibility, as gathered from MTT data as shown in Fig. 10. The low crystallinity of the nanorods may be the reason for adequate dissolution of thermodynamically lesser stable HA nanorods in the SBF solution. This in turn rendered much help in facilitating the nucleation and growth of new HA *in situ* [125]. Another study with reduced graphene oxide (RGO), prepared by a biofriendly reduction method for ascorbic acid, induced PCL nanofibrous meshes (RGO/PCL) were prepared for bone tissue regeneration study. Around 0.25 wt. % of RGO in PCL was fabricated to mimic the fibrillar structure of bone's ECM. Also, the surface roughness in nanoscale was reported for nanofibrous mesh with RGO. The PCL chains have been reported to form hydrogen bonds with GO/RGO. The mechanical properties of the RGO/PCL nanofibrous mesh exhibited superior results, which may be attributed to attractive forces between the GO/RGO nanosheets and the PCL polymer matrix. Additionally, the roughness of the RGO/PCL composite may hinder the sliding motion of the nanofibers in the mat, thereby enhancing the mechanical stiffness [134].

Also, enhanced cell adhesion, spreading, and proliferation of osteoblast-like and fibroblast cell lines have been reported [134]. The electrospun RGO based substrate material improved the *in vitro* calcium deposition from osteoblast-like cell lines, due to the enhanced osteogenic marker expression. The rough surface on the RGO/PCL biomaterial may have improved the adsorption of osteogenic growth factors onto its surface, thus improving the mineralization during bone tissue regeneration. As shown in Fig. 11, RGO based PCL nanofibrous biomaterial displayed increased cell viability as compared to GO/PCL material, which has been depicted by the green spots for live cells. Also, RGO/PCL material displayed increased cell spreading as compared to the GO/PCL biomaterial. In general, cell spreading was enhanced with nanofibrous material as compared to PCL only. The nanofibrous mat materials, RGO/PCL and GO/PCL, exhibited enhanced cell adhesion on the substrate. This observation has been attributed to the probable effect of cell anchorage links through pseudopodia, as well as the fiber diameter and porosity of the material, thus mimicking the bone's natural ECM structure. The effect of surface roughness, thus leading to a larger surface area for cell attachment, should also be noted [134].

Another innovative approach uses magnetron sputtering for incorporating bioactive TiCaPCON films onto PCL nanofibers. EDS and X-ray photoelectron spectroscopy (XPS) analysis revealed that the highest Ti concentrations on the PCL nanofibers were reported at 2 and 2.5 A currents for the magnetron. However, at 2.5 A current, substantial damage to the nanofibrous structure, as shown in Fig. 12. Using MC3T3-E1 cell lines, the biocompatibility analysis of the scaffolds revealed adequate cell spreading with actin fibers adhering to the substrate with their tips. The cell proliferation rate and ALP activity have been reported to have increased by around 4 and 2 times respectively as compared to PCL only scaffolds [135].

Poly (lactic-co-glycolic) Acid-Based Nanocomposites

PLGA is a common organic component of BTE scaffolds. The properties of PLGA include biocompatibility, biodegradability, and controlled degradation rate [136–140]. The hydrophobic surface nature of PLGA is caused by the pendent methyl group present on the structure of PLGA chains [141]. Since PLGA alone does not exhibit the adequate mechanical strength for bone tissue regeneration, several ceramic nanoparticles like flourhydroxyapatite, BG, nHA, and tricalcium phosphate, are incorporated into the PLGA structure to create PLGA nanocomposite biomaterials [142–146].

3D scaffolds were synthesized from PLGA and titanium dioxide nanotube (TNT) composite microspheres using sintering technique. 0.5 wt. % TNT incorporated into PLGA scaffold, by sintering at 100 °C for 3 h [147]. SEM data revealed the adequate dispersion of the TNTs on the PLGA microspheres. It has been reported that the sintering temperature and time are crucial factors for controlling scaffold strength and structure. The increase in sintering temperature may induce a reduction in porosity due to stronger bonds being formed and the overall filling up of the void spaces. Therefore, the mechanical properties of the scaffolds also increased with an increase in sintering temperature which may be attributed to the increased bonding within the microspheres. Also, a sintering time above 3 h has been

reported to have created holes in the microspheres by agglomeration of molten smaller particles.

However, excessive addition of the TNTs render reduction in mechanical properties [147]. This may be due to the fact that the PLGA microspheres required close contact for bonding which is increasingly inhibited with an increasing TNT content. Although the TNTs may be able to sinter at a very high temperature, the PLGA would degrade extensively at those higher temperatures. Therefore, a very low PLGA/TNT ratio is detrimental for the mechanical properties of the scaffold. The structure of the TNTs resembles that of continuous fibers that reinforce the PLGA matrix. Excess addition of TNTs may also lead to agglomeration within the PLGA matrix, thereby causing improper dispersion of the TNTs. This would also reduce the mechanical properties of the scaffold.

Biodegradability study, using SBF, on the PLGA/0.5 wt. % TNT scaffolds and its PLGA only control scaffolds displayed a reduction in weight during the first 4 weeks [147]. This observation may be due to the slower degradation of TNTs or lower interaction of the water molecules with the ester bonds of the polymer due to TNT incorporation. Additionally, the TNTs may also impart crystallinity to the composite, thereby reducing the degradation rate. Also, ALP activity analysis and MTT assay confirmed the enhanced cell viability characteristics of PLGA/0.5 wt. % TNT nanocomposite scaffolds over its control group. *In vitro* studies on the PLGA/TNT scaffolds exhibited increased bioactivity along with stability in pH during degradation in its surroundings. However, there was significant reduction in cell viability after 3 days for the nanocomposite scaffolds. This may be attributed to the superior bioactivity of the TNTs that absorb calcium ions from the ECM at a faster rate, thus reducing the overall bioactivity of the scaffold. *In vivo* analysis of the PLGA/TNT scaffolds displayed twice the amount of new bone formation as compared to pure PLGA scaffolds. These results were supported by histologic images, as shown in Fig. 13. Mathematical modeling of scaffold mechanical properties resulted in an exponential trend with time, with progress in scaffold degradation, for both the PLGA/TNT and its control group. A monotonous distribution of stress on the PLGA/TNT scaffold was observed using a 3D finite element model, which has been attributed to the presence of TNT and thereby reducing the maximum stress on the bone [147].

In another study, nanofiber (ultrafine) scaffold was synthesized from PLGA, tussah SF, and GO using the electrospinning method [148]. Nanofiber composition comprising of 1 wt. % GO and 10 wt. % SF in PLGA displayed a reduction in fiber diameter by almost 150 nm. This may be attributed to the addition of GO that changes the viscosity and conductivity of the electrospinning solution. It has been also reported that the synthesized nanofibers were also mesoporous as compared to PLGA-tussah SF nanofibers without GO that only contained micropores. FTIR data also revealed the formation of hydrogen bonds between carbonyl groups on the polymer matrix and the hydroxyl/carboxyl groups on the nanofillers. Additionally, the SF along with GO enhanced the mechanical properties, viz. modulus of elasticity and tensile strength, by more than 3 times with respect to the control group. The enhancement of mechanical properties with the incorporation of GO may be attributed again to the strong hydrogen bonds formed between the functional groups of the polymer matrix and the nanofillers. The presence of GO along with SF also enhanced cell adhesion and

proliferation for mesenchymal stem cells from mice. The PLGA/SF/GO biomaterial exhibited increased ALP activity and mineral deposition, as shown in Fig. 14. Due to the enhanced protein absorption on GO doped composite scaffolds, the overall cell proliferation for those scaffolds were slightly higher [148].

PLGA/HA composite fibrous scaffolds were synthesized using the melt-spinning technique with BMP-2 being incorporated onto the scaffold with the help of a polymeric bridge in the form of polydopamine (PDA) [149]. The PDA coating adhered to the surface of the PLGA/HA scaffold, as confirmed by FTIR and SEM analysis. The attached PDA coating onto the PLGA/HA fibrous scaffolds enhanced the scaffold surface roughness which inherently is advantageous for cell attachment. PDA modification has been also reported to have increased the hydrophilic nature of the scaffold. The flexibility of the PDA in terms of acting as a bridge between the polymer scaffold and other interacting organic and inorganic elements or compounds is noteworthy, as it improves the attachment of various physical as well as chemical cues onto the scaffold surface for enhanced cell attachment and proliferation. Additionally, BMP-2 which has been immobilized on the PLGA/HA scaffold, released in a more sustained manner due to the effective immobilization of BMP-2 on the scaffold by PDA. *In vitro* studies on the BMP-2 immobilized fibrous scaffold improved cell adhesion and proliferation of MC3T3-E1 cells. Also, a significant increase in bone mineral deposition, ALP activity, and mRNA expression in MC3T3-E1 cells which were cultured on the BMP-2 immobilized fibrous scaffold was observed, as shown in Fig. 15 for biomineralization [149].

The use of magnetic elements as a potential candidate for BTE applications have also been touched upon [150]. Magnetic nanocomposite biomaterial was synthesized from PLGA and magnetite. PLGA synthesis was achieved by copolymerization of lactic and glycolic acid in the presence of tin octanoate [$Sn(Oct)_2$] which acts as a catalyst. Magnetite, which was prepared by co-precipitation process from $FeCl_2/FeCl_3$, which was incorporated into the nanocomposite scaffold bore size and magnetization of around 864 nm and 39.44 emu/g respectively. Magnetic properties of the nanocomposite scaffold aids in targeting by manipulation of an external magnetic field. Thermogravimetric analysis revealed the composition of the nanocomposite scaffold to be around 54 wt. % magnetite and 37 wt. % PLGA. Adequate biocompatibility and biodegradability of the nanocomposite scaffold may facilitate its use in various BTE applications [150].

Although cranial defects are successfully treated with hydrogel, yet several of these composites lack the adequate strength for load bearing application [151, 152]. Thus, porous PLGA/HA nanocomposite incorporated with poly (glycolic acid) (PGA) fibers, at different concentrations 0, 30, 50, 70 wt. % and synthesized from melt spinning with average diameter from 70 to 191 nm which depict the hybrid character of the fibers possessing both micro as well as nano structure. The study revealed that the nanocomposites required less than 100 N force for injection, which is convenient for smooth injectability of the composite without causing fatigue to surgeon [151]. The incorporation of PGA fibers increased the density of the composite due to enhanced reinforcement. PGA fibers were reported to have enhanced the fiber and matrix adhesion within the composite. The incorporation of PGA fibers into the gel matrix has proven to increase the mechanical properties – nanocomposite

with 70 wt. % PGA fibers exhibited a compressive strength of around 31.1 MPa, which was around four times as compared to the composite without any fillers. This effect may be attributed to the faster solidification rate of the composite which provides superior initial mechanical strength at the defect site. Cell viability studies, within 4 h of immersion in Minimum Essential Medium and N-methyl pyrrolidone, reported that more than 70% of cells were alive for nanocomposite paste extracts with four times dilution. The provision of the hybrid micro and nano structure within the composite may have facilitated cell and nutrient transport with adequate mechanical support [152].

Polyethylene Glycol-Based Nanocomposites

PCL nanofiber scaffolds with GO, and surface treated with PEG, were synthesized using the electrospinning method [153]. The fiber diameter displayed an increasing trend with the inclusion of GO/PEG into the nanofiber composite. It has been also noted that the addition of GO into the polymer matrix has increased the viscosity of the solution, that may have increased the fiber diameter. PCL/GO/PEG nanocomposite exhibited increased hydrophilicity along with increased modulus of elasticity, particularly at low concentrations of PEG. This effect has been attributed to the improved dispersion of GO/PEG blend. The presence of oxygenated functional groups on the GO surface along with the solubility of GO in water may be attributed as the reasons for increased hydrophilicity for the composite as compared to PCL only. Also, the grafting of PEG onto GO may have enhanced the dispersion of the nanofillers within the PCL matrix, thereby increasing the elastic modulus of the composite. However, at very high concentration of the nanofillers, agglomeration issue might have been effective in reducing the elastic modulus. Analysis with MC3T3-E1 cells on PCL/GO/PEG nanofiber mats exhibited adequate cell attachment and growth, along with adequate cytocompatibility, as shown in Fig. 16 [153].

In another study, nano calcium phosphate based nanocomposite material for guided bone regeneration has been reported in literature [154]. PCL/PEG/SF based membrane, that also incorporated nanocalcium phosphate, was developed with the intent to reduce non-functional scar tissue defects with the help of guided bone regeneration. Flame Spray Pyrolysis (FSP) technique was utilized for the synthesis of nanocalcium phosphate, that was hypothesized to improve the osteoconductivity of the membrane. A porous mechanical framework of randomly oriented fibers was incorporated into the regenerative layer, with around 12.6 μm in fiber thickness, of the bilayer membrane. The addition of calcium phosphate particles may be affecting the increase in fiber diameter as the addition of the inorganic calcium phosphate may have reduced the conductivity of the electrospinning solution.

Mechanical properties of the nanofiber membrane exhibited an increase in tensile strength due to the nanoparticles incorporated into the composite structure [154]. Increased water absorption was displayed by the nanocomposite along with hydrophilicity, as confirmed by the low water contact angle data. The effect of the solvent used during the solvent casting of PCL films may be the reason behind the reduction in water contact angle for PCL, as the polymer chains might have been rearranged. Additionally, the electrospun fibers contained hydrophilic carboxyl and amino groups from SF, thus helping in enhancement of overall hydrophilicity of the composite [154].

Also, the incorporation of nanocalcium phosphate facilitated enhanced biomineralization as compared to the control sample with no nanocalcium phosphate, as shown in Fig. 17 [154]. The addition of nano calcium phosphate may be the reason for enhanced biomineralization, as the presence of nano calcium phosphate may provide an adequate surface for the nucleation and growth of apatite based particles that form the structure of the regenerated bone. An increasing trend in cell adhesion and proliferation was observed with an increasing amount of nanocalcium phosphate. The roughness imparted by the addition of the nano calcium phosphate particles may be attributed for the adequate cell attachment behavior for the composite. Additionally, ALP activity and mineral deposition increased along with the increase in nanocalcium phosphate content. Osteogenic differentiation of the cells was aided by the addition of the calcium phosphate nanoparticles as they increased the concentration of calcium ions thereby facilitating better storage of the cells. Also, the electrospun layer of the bilayer membrane possessed adequate porosity for proper cell attachment and functionality of other biological conditions necessary for osteogenic cells [154].

Poly (lactic acid)-Based Nanocomposites

PLA is a synthetic polymer often being used in preparing tissue regeneration scaffolds due to its biocompatible and biodegradable properties, especially the ones fabricated using electrospinning technique [155, 156]. However, PLA alone lacks the adequate mechanical strength essential for bone tissue regeneration systems, and hence PLA often has been observed to undergo various fabrication methods involving polymer structural modifications, creation of blended polymer fibers, and incorporation of nanoparticles to form nanocomposite fibers [157–162]. The US FDA has approved PLA and its applications pertaining to a dynamic field of biomedical engineering [128, 163, 164].

A combination of 3D printing and thermally induced phase separation technique has been reported to have been utilized for preparing BTE scaffolds from a combination of both PLA and CS-HA hydrogel, as shown in Fig. 18 [165]. The SEM data revealed adequate adhesion of the CS and PLA polymers, which may be attributed to the interaction between the carbonyl and amino acids in the polymers. The study has reported an overall porosity of around 60% with extremely large pores of around 960 ± 50 μm pore size for the PLA structures with the incorporation of *in situ* formed HA – CS hydrogel through gelation method. The higher porosity may have facilitated the growth and differentiation of the human mesenchymal stem cells and nutrients across the scaffold. The composite hydrogel system with a high overall porosity would help in osteoinduction as well as angiogenesis, thus sustaining better cell survival. The interaction of human mesenchymal stem cells with the composite hydrogel structure at 21 days has revealed enhanced osteogenesis which has been attributed mostly to the *in-situ* mineralization of HA within the HA-CS complex. The *in situ* method of HA synthesis using non-toxic precursors such as calcite and urea phosphate allows the simultaneous existence of OCP and HA as calcium phosphate that renders better bioactivity as well as bioresorbability. The scaffolds made with composite blend of 3D printed PLA and HA-CS have been reported to have reduced elastic modulus in wet state. This may be attributed to the loss in mass from the scaffold struts made from PLA as well as the low water retention potential caused due to the HA nanoparticles [165].

Another study with electrospun coaxial PLA (core)/Poly (vinyl alcohol) - PVA (shell) nanofibers have been reported to have enhanced mechanical as well as surface wetting properties, thus, inhibiting the hydrophobic nature and poor ductility of PLA [166]. The proper coaxial structure of the polymers was reported with FTIR analysis using detection of hydroxyl and carboxyl groups on the polymers. Coaxial electrospinning has been reported to have enhanced the fiber diameter. Thermal degradation studies also revealed lower degradation rates for the coaxial fibers as compared to their pristine counterparts. PLA/PVA nanofiber mats with 27 ± 1.5° water contact angle, as compared to 110 ± 2.5° to pure PLA material, proves the improvement in hydrophilicity of PLA in the composite nanofiber material. This effect may be due to the porous nature of the PLA fiber that allows the water droplet to pass through channels into its core where it gets absorbed by the hydrophilic PVA.

In terms of mechanical properties, PLA/PVA nanofibers have also been reported to have displayed around 175% increase for failure strain, including an increase of 254% in tensile strength, given as 14.5 MPa for PLA/PVA vs 4.1 MPa for pure PLA [166]. The ductility of PLA/PVA nanofibers has also noticed an increase from 40% to 110%, for pure PLA. The enhancement in mechanical properties may be attributed to the interaction of the two polymers in a coaxial fiber structure. Also, the coaxial fiber has been reported to possess a much lower glass transition as compared to its pristine polymer counterparts. This may be the reason behind the enhanced ductility of the composite fiber. Cell adhesion and proliferation analysis, using human embryonic kidney cells – HEK-293, on PLA/PVA nanofibers, have also revealed adequate biocompatibility of the nanocomposite. The poor stability of the PVA only fibers highlights the efficiency of the PLA/PVA coaxial fiber in cell attachment [166]. The application of nHAR for BTE has been reported in the literature [167]. Nanocomposite scaffolds have been prepared from poly (D, L) lactic acid (PDLLA) and nHAR using a combined solvent casting – salt leaching method. These nHAR/PDLLA nanocomposite scaffolds exhibited macroporous structure, with overall porosity of around 84%, and an average pore size range of around 117–183 μm. FESEM data revealed the uniform dispersion of the nanorods and deposition on the pore walls, thus making them thicker and the pores smaller. Thus, an increase in nHAR content may induce a reduction in pore size and overall morphology of the scaffold. FTIR data also revealed the formation of hydrogen bonds between carbonyl group on PDLLA and the hydroxyl group on nHAR [167].

Biomineralization, with apatite formation in a flower like morphology, has been reported to have been facilitated by these nanocomposite scaffolds, after 7 days of incubation in SBF [167]. The increase in nHAR increases the nucleation sites for biomineralization which may account for the flower like morphology as compared spherical particles for samples without nHAR. As shown in Fig. 19, with an increasing time period of incubation, the nanocomposite scaffolds with a higher content of nHAR, which is around 30 wt. %, revealed superior cell attachment, cell proliferation, and cell distribution when tests were conducted on MG63 osteoblast cell lines and compared to the scaffolds with a lower percentage of nHAR. However, with increasing nHAR content, the cell viability has been reported to have reduced. This may be due to the reduction in pore size with additional nHAR that affects the cell viability negatively [167].

Incorporation of BG into electrospun fibers is another composite synthesis method for BTE scaffolds [168]. Composite nanofibers were prepared from poly-L-lactic acid (PLLA) and BG using the electrospinning method. The prepared scaffolds from the nanofibers revealed an interconnected porous structure with an average fiber diameter of around 500 nm, as analyzed from SEM, FTIR, and XRD data. The electrospinning feeding rate controls the fiber diameter. The nanofibers were plasma treated for surface modification for enhanced cell attachment [168].

hMSCs were used in the analysis of viability, growth, and proliferation. Results from several analytical assays, such as ALP activity, MTT, Alizarin Red Staining, Calcium Deposition, Col Expression, and RT-PCR, have highlighted the importance of the incorporation of BG into the nanofiber composite for enhanced bioactivity and biocompatibility of the prepared scaffolds, including added advantages for cell behavior provided by the 3D porous structure of the scaffolds, as shown in Fig. 20 [168]. The presence of bioactive elements such as calcium, phosphorous, silicon, along with a high porosity and surface area facilitates adequate cell proliferation and differentiation. Additionally, the nanofibrous structure of the scaffold may have also aided in cellular activities for bone regeneration [168]. It is known that BMPs play huge role in bone regeneration, and as such have played a significant part in biomaterial/scaffold fabrication [169]. The incorporation of BMPs in bone tissue regeneration has been widely studied for obtaining the optimal set of parameters for both scaffold properties as well as BMP concentration [169, 170]. BMP-2 carrier particles (PLA/PLGA particles) incorporated into PEG-Silk gels have proven to inhibit the burst release characteristics for BMP-2. *In vitro* studies exhibited significant stabilization of encapsulated proteins with facilitation of complete *in vitro* bioactivity. *In vivo* analysis of the composite gel exhibited scaffold biocompatibility, along with a reverse relationship of degradation rate with increased hydrophobicity due to additional reinforcement with PLA/PLGA particles. New bone formation was also reported to be maximum with PLA/PLGA – BMP-2 incorporated hydrogel [171].

Polyurethane-Based Nanocomposites

PUs have been reported to exhibit favorable mechanical, physical and biocompatible properties [172]. The segments within the PU polymeric structure is attributed widely due to its block copolymeric structure made from macro-diols that form the soft segment, and diisocyanates and diamines, also known as chain extender diols, as the hard segment of its core chain [173]. Composite scaffolds prepared with PU generally exhibit enhanced mechanical properties while retaining PU's original toughness. Incorporation of nanoparticles over microspheres reveals a superior reinforcement of PU, which has been attributed to the higher surface area-to-volume ratio of the nanoparticles over microspheres [174].

$nTiO_2$ reinforced poly (ester urethane) urea (PEUU) scaffolds were prepared from poly (ester urethane) - PEU grafted onto $nTiO_2$ particles; this process enhances the interfacial bonding of $nTiO_2$ and PEUU [175]. The $nTiO_2$ particles were functionalized with hydroxyl groups on the surface for adequate PEG grafting with isocyanate groups. Electrospinning technique was employed for scaffold creation with an average fiber diameter which is less

than 1 μm. However, the electrospun fibers synthesized without the nanofillers revealed the trend of having such a low fiber diameter. These electrospun fibers demonstrated a homogenous distribution of the composite PEU-nTiO_2 particles, as analyzed from SEM and EDS data. PEU grafting on nTiO_2 proved to be advantageous in inhibiting agglomeration of the pristine nTiO_2. The fiber morphology revealed through SEM micrographs that the uniform distribution of the nanoparticles was only reported with grafted nTiO_2. This may be attributed to the lower interaction between the non-grafted nanofillers and PEUU polymer matrix. This also resulted in presence of beads along the nanofibers synthesized during electrospinning. As reported, the ratio of nanofillers to polymer (PEUU) at 1:2 generated a smooth morphology. On the contrary, a ratio of 1:1 and 2:1 revealed more rough fibers as compared to 1:2 ratio [175].

Moreover, the PEU-nTiO_2 composite structure has been reported to have enhanced PEUU scaffold mechanical properties, especially with increased tensile stress and modulus of elasticity, as compared to unmodified nTiO_2 [175]. Scaffold reinforcement has been reported to have been the maximum at 1:1 ratio of PEUU and PEU-nTiO_2 with elastic modulus at around 49 MPa; this has been reported as a 53% increase in the Young's modulus over PEUU only scaffolds. It should be noted that the strength of interaction between the nanofillers and the PEUU matrix influence the reinforcement efficiency of the scaffold, thus influencing its mechanical properties [175].

Incubation of scaffolds in SBF over 8 weeks revealed the highest biomineralization, in terms of calcium and phosphorous, for the PEUU/ PEU-nTiO_2 scaffolds as compared to the other control groups. It should be noted that the grafted nanofillers based composite nanofibrous scaffolds showed the onset of biomineralization at around 2 weeks after incubation. Additionally, higher amounts of calcium and phosphorous was found to have been deposited on the scaffolds containing nanofillers as compared to PEUU only scaffolds. These results infer the influence of the nTiO_2 on the absorption of phosphate and carbonate ions that ultimately effect biomineralization. Bone marrow-derived mesenchymal stem cells were utilized for cytocompatibility analysis of the scaffolds, and PEUU/ PEU - nTiO_2 scaffolds displayed the highest cell proliferation as compared to the control groups, which has been shown in Fig 21. This may be inferred as the effect of the change in hydrophilicity of the nanofillers due to PEU grafting. Also, the grafting of PEU also improved the stability of the nTiO_2 which otherwise have been reported to have some toxic effects on cells [175–177]. In another study, functionalized multiwall carbon nanotube (fMWCNT) and zinc oxide nanoparticle (nZnO) reinforced PU fibers were prepared by the electrospinning process to prepare scaffolds for BTE [178]. Uniformly dispersed fMWCNT and nZnO particles, as exhibited by TEM data, revealed to have facilitated enhancement in biocompatibility, biodegradability, mineralization, mechanical strength, hydrophilic nature, electrical conductivity, and thermal stability. The increase in wt. % in fMWCNT decreases the nanofiber diameter, almost around the ultrafine scale. The presence of the polar functional groups on fMWCNT form strong hydrogen bonds with the carbonyl and amino groups of the PU polymer, thereby enhancing stress bearing capacity of the fibers. Additionally, the presence of the adequately dispersed nanofillers, fMWCNT as well as nZnO, aid in the enhancement of fiber stiffness through their electrostatic attractive forces. Cytocompatibility, as shown in Fig. 22, has been reported for a composition of 0.4 wt. % fMWCNT and 0.2 wt.

% nZnO reinforced electrospun fibers, along with the antimicrobial nature of the same. MC3T3-E1 (preosteoblasts) cells were used to analyze osteogenic differentiation of the scaffolds; increased surface to volume ratio, charge density and functionalized MWCNTs aid in the differentiation process. The presence of negatively charged groups on the nanofillers help in increased absorption of calcium and phosphorous ions that inherently increased the nucleation rate of the calcium phosphate minerals. The effective biomineralization with the nanocomposite fibrous scaffolds may be a big support in facilitating adequate biocompatibility, cell proliferation as well as cytocompatibility of the scaffolds [178].

Conclusion

Polymer nanocomposites have the capability to facilitate cell attachment, proliferation, new bone tissue growth, and biodegradation of the scaffold. Moreover, the inclusion of nanofillers into the polymer matrix creates a suitable blend of physical, chemical, and biological properties in the biomaterial that closely mimics the bone's natural ECM. Therefore, the improved ALP activity, Runx-2 activity, as well as Col type I gene expression may be attributed to the incorporation of nanomaterials into the composite structure. This hybrid structure with optimal porosity, mechanical strength, and elasticity enhance nutrient and growth factor transport across the nanocomposite scaffold, thus, improving new bone tissue development. Material preparation and fabrication is a critical step that encompasses a wide range of variables and techniques for synthesis, analysis, and quantification. The overall enhancement in the properties of the biomaterial depends on the optimal tuning of the material preparation and blending methods. Hydrogel-based polymer matrix holds a significant advantage over 3D scaffolds, as the former can be utilized as an injectable scaffold with nanofillers incorporated into the gel. Various hydrogel-nanoparticle based injectable scaffolds are therefore ideal for reducing the invasiveness of scaffold implant procedures, which can be widely utilized for the treatment of craniofacial defects. Crosslinking density of the polymer matrix holds significant importance during the biodegradation phase of the scaffold, as the integration of the new bone tissue with the host bone depends on the maintenance of optimal scaffold degradation rate and facilitation of smooth resorption of the degradation products. Natural polymers have an advantage over synthetic polymers in terms of biocompatibility and degradation; whereas, synthetic polymers provide adequate opportunity for enhancement of material properties by physical, chemical, and topographical methods that enhance cell proliferation and new tissue growth. But, the by-products of degradation of synthetic polymer-based scaffolds at times may pose certain issues, such as a buildup of acid in the surrounding tissue. Hence, the optimization of polymer blends, including the nanofillers, is quintessential for obtaining scaffold material that promotes adequate bone tissue development. Further research in the field of nanocomposite biomaterials for bone tissue regeneration is highly favorable owing to the enhanced cytocompatibility and bioactivity of the nanocomposite biomaterials with enhanced bone tissue development.

Acknowledgments

The authors would like to acknowledge funding support from the National Institutes of Health (R01DE023356).

References

[1]. Florencio-Silva R, Sasso GRD, Sasso-Cerri E, Simoes MJ, Cerri PS, Biology of Bone Tissue: Structure, Function, and Factors That Influence Bone Cells, Biomed Res Int (2015).

[2]. Amini AR, Laurencin CT, Nukavarapu SP, Bone tissue engineering: recent advances and challenges, Crit Rev Biomed Eng 40(5) (2012) 363–408. [PubMed: 23339648]

[3]. O'Keefe RJ, Mao J, Bone tissue engineering and regeneration: from discovery to the clinic—an overview, Tissue engineering part B: reviews 17(6) (2011) 389–392. [PubMed: 21902614]

[4]. Bao CLM, Teo EY, Chong MS, Liu Y, Choolani M, Chan JK, Advances in bone tissue engineering, Regenerative Medicine and Tissue Engineering, InTech2013.

[5]. Baroli B, From natural bone grafts to tissue engineering therapeutics: brainstorming on pharmaceutical formulative requirements and challenges, J Journal of pharmaceutical sciences 98(4) (2009) 1317–1375.

[6]. Parvizi J, High Yield Orthopaedics E-Book, Elsevier Health Sciences2010.

[7]. Mishra R, Bishop T, Valerio IL, Fisher JP, Dean D, The potential impact of bone tissue engineering in the clinic, Regen Med 11(6) (2016) 571–87. [PubMed: 27549369]

[8]. Dimitriou R, Jones E, McGonagle D, Giannoudis PV, Bone regeneration: current concepts and future directions, BMC Med 9(1) (2011) 66. [PubMed: 21627784]

[9]. Yaszemski MJ, Payne RG, Hayes WC, Langer R, Mikos AG, Evolution of bone transplantation: molecular, cellular and tissue strategies to engineer human bone, Biomaterials 17(2) (1996) 175–85. [PubMed: 8624394]

[10]. Finkemeier CG, Bone-grafting and bone-graft substitutes, J Bone Joint Surg Am 84(3) (2002) 454–64. [PubMed: 11886919]

[11]. Banwart JC, Asher MA, Hassanein RS, Iliac crest bone graft harvest donor site morbidity. A statistical evaluation, Spine (Phila Pa 1976) 20(9) (1995) 1055–60. [PubMed: 7631235]

[12]. Ebraheim NA, Elgafy H, Xu R, Bone-graft harvesting from iliac and fibular donor sites: techniques and complications, J Am Acad Orthop Surg 9(3) (2001) 210–8. [PubMed: 11421578]

[13]. St TJ, Vaccaro AR, Sah AP, Schaefer M, Berta SC, Albert T, Hilibrand A.J.A.j.o.o, Physical and monetary costs associated with autogenous bone graft harvesting, American journal of orthopedics (Belle Mead, NJ) 32(1) (2003) 18–23.

[14]. Gupta A, Main BJ, Taylor BL, Gupta M, Whitworth CA, Cady C, Freeman JW, El-Amin SF 3rd, In vitro evaluation of three-dimensional single-walled carbon nanotube composites for bone tissue engineering, J Biomed Mater Res A 102(11) (2014) 4118–26. [PubMed: 24443220]

[15]. Holzmann P, Niculescu-Morzsa E, Zwickl H, Halbwirth F, Pichler M, Matzner M, Gottsauner-Wolf F, Nehrer S.J.A.-A.t.a.e, Investigation of bone allografts representing different steps of the bone bank procedure via the CAM-model, ALTEX-Alternatives to animal experimentation 27(2) (2010) 97–103.

[16]. Guo B, Ma PX, Synthetic biodegradable functional polymers for tissue engineering: a brief review, Science China Chemistry 57(4) (2014) 490–500. [PubMed: 25729390]

[17]. Lanza R, Langer R, Vacanti J, Tissue engineering, 1993, pp. 920–926.

[18]. Stevens MM, Biomaterials for bone tissue engineering, Mater Today 11(5) (2008) 18–25.

[19]. Hench LL, Polak JM, Third-generation biomedical materials, Science 295(5557) (2002) 1014–7. [PubMed: 11834817]

[20]. Williams DF, There is no such thing as a biocompatible material, Biomaterials 35(38) (2014) 10009–10014. [PubMed: 25263686]

[21]. Olszta MJ, Cheng XG, Jee SS, Kumar R, Kim YY, Kaufman MJ, Douglas EP, Gower LB, Bone structure and formation: A new perspective, Mat Sci Eng R 58(3–5) (2007) 77–116.

[22]. Bose S, Roy M, Bandyopadhyay A, Recent advances in bone tissue engineering scaffolds, Trends Biotechnol 30(10) (2012) 546–54. [PubMed: 22939815]

[23]. Murphy CM, Haugh MG, O'Brien FJ, The effect of mean pore size on cell attachment, proliferation and migration in collagen–glycosaminoglycan scaffolds for bone tissue engineering, J Biomaterials 31(3) (2010) 461–466.

[24]. Williams DF, On the mechanisms of biocompatibility, Biomaterials 29(20) (2008) 2941–53. [PubMed: 18440630]

[25]. Pina S, Oliveira JM, Reis RL, Natural based nanocomposites for bone tissue engineering and regenerative medicine: A review, J Advanced Materials 27(7) (2015) 1143–1169.

[26]. Oliveira JM, Silva SS, Malafaya PB, Rodrigues MT, Kotobuki N, Hirose M, Gomes ME, Mano JF, Ohgushi H, Reis RL, Macroporous hydroxyapatite scaffolds for bone tissue engineering applications: physicochemical characterization and assessment of rat bone marrow stromal cell viability, J Biomed Mater Res A 91(1) (2009) 175–86. [PubMed: 18780358]

[27]. Chae T, Yang H, Leung V, Ko F, Troczynski T, Novel biomimetic hydroxyapatite/alginate nanocomposite fibrous scaffolds for bone tissue regeneration, J Mater Sci Mater Med 24(8) (2013) 1885–94. [PubMed: 23695359]

[28]. Liapis AI, Pikal MJ, Bruttini R, Research and development needs and opportunities in freeze drying, Dry Technol 14(6) (1996) 1265–1300.

[29]. Dehghani F, Annabi N, Engineering porous scaffolds using gas-based techniques, Curr Opin Biotech 22(5) (2011) 661–666. [PubMed: 21546240]

[30]. Hou Q, Grijpma DW, Feijen J, Porous polymeric structures for tissue engineering prepared by a coagulation, compression moulding and salt leaching technique, Biomaterials 24(11) (2003) 1937–47. [PubMed: 12615484]

[31]. Van de Witte P, Dijkstra PJ, Van den Berg J, Feijen J, Phase separation processes in polymer solutions in relation to membrane formation, J Journal of membrane science 117(1–2) (1996) 1–31.

[32]. Matson JB, Zha RH, Stupp SI, Peptide Self-Assembly for Crafting Functional Biological Materials, Curr Opin Solid State Mater Sci 15(6) (2011) 225–235. [PubMed: 22125413]

[33]. Li J, Chen M, Fan X, Zhou H, Recent advances in bioprinting techniques: approaches, applications and future prospects, J Transl Med 14(1) (2016) 271. [PubMed: 27645770]

[34]. Zhu JM, Bioactive modification of poly(ethylene glycol) hydrogels for tissue engineering, Biomaterials 31(17) (2010) 4639–4656. [PubMed: 20303169]

[35]. Kesireddy V, Kasper FK, Approaches for building bioactive elements into synthetic scaffolds for bone tissue engineering, J Mater Chem B 4(42) (2016) 6773–6786. [PubMed: 28133536]

[36]. Reilly GC, Engler AJ, Intrinsic extracellular matrix properties regulate stem cell differentiation, J Biomech 43(1) (2010) 55–62. [PubMed: 19800626]

[37]. Tripathi G, Basu B, A porous hydroxyapatite scaffold for bone tissue engineering: Physico-mechanical and biological evaluations, Ceram Int 38(1) (2012) 341–349.

[38]. Pina S, Oliveira JM, Reis RLJAM, Natural based nanocomposites for bone tissue engineering and regenerative medicine: A review, 27(7) (2015) 1143–1169.

[39]. Bonfield W, Grynpas M, Tully A, Bowman J, Abram JJB, Hydroxyapatite reinforced polyethylene--a mechanically compatible implant material for bone replacement, 2(3) (1981) 185–186.

[40]. Hasnain MS, Ahmad SA, Chaudhary N, Hoda MN, Nayak AK, 1 - Biodegradable polymer matrix nanocomposites for bone tissue engineering, in: Inamuddin, Asiri AM, Mohammad A (Eds.), Applications of Nanocomposite Materials in Orthopedics, Woodhead Publishing2019, pp. 1–37.

[41]. Saravanan S, Leena RS, Selvamurugan N, Chitosan based biocomposite scaffolds for bone tissue engineering, Int J Biol Macromol 93 (2016) 1354–1365. [PubMed: 26845481]

[42]. Sell SA, Wolfe PS, Garg K, McCool JM, Rodriguez IA, Bowlin GL, The Use of Natural Polymers in Tissue Engineering: A Focus on Electrospun Extracellular Matrix Analogues, Polymers-Basel 2(4) (2010) 522–553.

[43]. Kavya KC, Jayakumar R, Nair S, Chennazhi KP, Fabrication and characterization of chitosan/gelatin/nSiO2 composite scaffold for bone tissue engineering, Int J Biol Macromol 59 (2013) 255–63. [PubMed: 23591473]

[44]. Keller L, Regiel-Futyra A, Gimeno M, Eap S, Mendoza G, Andreu V, Wagner Q, Kyzioł A, Sebastian V, Stochel G, Arruebo M, Benkirane-Jessel N, Chitosan-based nanocomposites for the repair of bone defects, Nanomedicine: Nanotechnology, Biology and Medicine 13(7) (2017) 2231–2240.

[45]. Atak BH, Buyuk B, Huysal M, Isik S, Senel M, Metzger W, Cetin G, Preparation and characterization of amine functional nano-hydroxyapatite/chitosan bionanocomposite for bone tissue engineering applications, Carbohydr Polym 164 (2017) 200–213. [PubMed: 28325318]

[46]. Ran J, Hu J, Sun G, Chen S, Jiang P, Shen X, Tong H, A novel chitosan-tussah silk fibroin/nano-hydroxyapatite composite bone scaffold platform with tunable mechanical strength in a wide range, Int J Biol Macromol 93(Pt A) (2016) 87–97. [PubMed: 27568361]

[47]. Shakir M, Zia I, Rehman A, Ullah R, Fabrication and characterization of nanoengineered biocompatible n-HA/chitosan-tamarind seed polysaccharide: Bio-inspired nanocomposites for bone tissue engineering, Int J Biol Macromol 111 (2018) 903–916. [PubMed: 29337096]

[48]. Yi H, Wu LQ, Bentley WE, Ghodssi R, Rubloff GW, Culver JN, Payne GF, Biofabrication with chitosan, Biomacromolecules 6(6) (2005) 2881–94. [PubMed: 16283704]

[49]. Nazeer MA, Yilgör E, Yilgör I, Intercalated chitosan/hydroxyapatite nanocomposites: Promising materials for bone tissue engineering applications, Carbohydrate Polymers 175 (2017) 38–46. [PubMed: 28917880]

[50]. Pighinelli L, Kucharska M, Chitosan–hydroxyapatite composites, Carbohydrate Polymers 93(1) (2013) 256–262. [PubMed: 23465927]

[51]. Danilchenko S, Kalinkevich OV, Pogorelov MV, Kalinkevich A, Sklyar A, Kalinichenko T, Ilyashenko V, Starikov V, Bumeyster V, Sikora V, Chitosan–hydroxyapatite composite biomaterials made by a one step co-precipitation method: preparation, characterization and in vivo tests, www.amsi.ge/jbpc (2009).

[52]. Gaihre B, Jayasuriya AC, Comparative investigation of porous nano-hydroxyapaptite/chitosan, nano-zirconia/chitosan and novel nano-calcium zirconate/chitosan composite scaffolds for their potential applications in bone regeneration, Materials Science and Engineering: C 91 (2018) 330–339. [PubMed: 30033262]

[53]. Shahbazarab Z, Teimouri A, Chermahini AN, Azadi M, Fabrication and characterization of nanobiocomposite scaffold of zein/chitosan/nanohydroxyapatite prepared by freeze-drying method for bone tissue engineering, Int J Biol Macromol 108 (2018) 1017–1027. [PubMed: 29122713]

[54]. Bhowmick A, Jana P, Pramanik N, Mitra T, Banerjee SL, Gnanamani A, Das M, Kundu PP, Multifunctional zirconium oxide doped chitosan based hybrid nanocomposites as bone tissue engineering materials, Carbohydrate Polymers 151 (2016) 879–888. [PubMed: 27474636]

[55]. Hasan A, Waibhaw G, Saxena V, Pandey LM, Nano-biocomposite scaffolds of chitosan, carboxymethyl cellulose and silver nanoparticle modified cellulose nanowhiskers for bone tissue engineering applications, Int J Biol Macromol 111 (2018) 923–934. [PubMed: 29415416]

[56]. Wang Q, Chen D, Synthesis and characterization of a chitosan based nanocomposite injectable hydrogel, Carbohydrate polymers 136 (2016) 1228–1237. [PubMed: 26572466]

[57]. Moreira CDF, Carvalho SM, Sousa RG, Mansur HS, Pereira MM, Nanostructured chitosan/gelatin/bioactive glass in situ forming hydrogel composites as a potential injectable matrix for bone tissue engineering, Mater Chem Phys 218 (2018) 304–316.

[58]. Gelse K, Pöschl E, Aigner T, Collagens—structure, function, and biosynthesis, Advanced drug delivery reviews 55(12) (2003) 1531–1546. [PubMed: 14623400]

[59]. van der Rest M, Garrone R, Collagen family of proteins, FASEB J 5(13) (1991) 2814–23. [PubMed: 1916105]

[60]. Lalzawmliana V, Anand A, Mukherjee P, Chaudhuri S, Kundu B, Nandi SK, Thakur NL, Marine organisms as a source of natural matrix for bone tissue engineering, Ceram Int (2018).

[61]. Senaratne LS, Park PJ, Kim SK, Isolation and characterization of collagen from brown backed toadfish (Lagocephalus gloveri) skin, Bioresour Technol 97(2) (2006) 191–7. [PubMed: 15964191]

[62]. Nagai T, Yamashita E, Taniguchi K, Kanamori N, Suzuki N, Isolation and characterisation of collagen from the outer skin waste material of cuttlefish (Sepia lycidas), Food Chem 72(4) (2001) 425–429.

[63]. Song E, Kim SY, Chun T, Byun HJ, Lee YM, Collagen scaffolds derived from a marine source and their biocompatibility, Biomaterials 27(15) (2006) 2951–2961. [PubMed: 16457878]

[64]. Sikorski ZE, Borderias JA, Collagen in the muscles and skin of marine animals, Seafood proteins, Springer1994, pp. 58–70.

[65]. Nagai T, Suzuki N, Isolation of collagen from fish waste material—skin, bone and fins, Food Chem 68(3) (2000) 277–281.

[66]. Campbell JJ, Husmann A, Hume RD, Watson CJ, Cameron RE, Development of three-dimensional collagen scaffolds with controlled architecture for cell migration studies using breast cancer cell lines, Biomaterials 114 (2017) 34–43. [PubMed: 27838472]

[67]. Mele L, Vitiello PP, Tirino V, Paino F, De Rosa A, Liccardo D, Papaccio G, Desiderio V, Changing Paradigms in Cranio-Facial Regeneration: Current and New Strategies for the Activation of Endogenous Stem Cells, Front Physiol 7 (2016) 62. [PubMed: 26941656]

[68]. Mao H, Kawazoe N, Chen G, Cell response to single-walled carbon nanotubes in hybrid porous collagen sponges, Colloids Surf B Biointerfaces 126 (2015) 63–9. [PubMed: 25543985]

[69]. Park JE, Park IS, Neupane MP, Bae TS, Lee MH, Effects of a carbon nanotube-collagen coating on a titanium surface on osteoblast growth, Appl Surf Sci 292 (2014) 828–836.

[70]. Panda NN, Jonnalagadda S, Pramanik K, Development and evaluation of cross-linked collagen-hydroxyapatite scaffolds for tissue engineering, J Biomater Sci Polym Ed 24(18) (2013) 2031–44. [PubMed: 23905722]

[71]. Balani K, Anderson R, Laha T, Andara M, Tercero J, Crumpler E, Agarwal A, Plasma-sprayed carbon nanotube reinforced hydroxyapatite coatings and their interaction with human osteoblasts in vitro, Biomaterials 28(4) (2007) 618–624. [PubMed: 17007921]

[72]. Türk S, Altınsoy I, Çelebi Efe G, Ipek M, Özacar M, Bindal C, 3D porous collagen/functionalized multiwalled carbon nanotube/chitosan/hydroxyapatite composite scaffolds for bone tissue engineering, Materials Science and Engineering: C 92 (2018) 757–768. [PubMed: 30184804]

[73]. Chen Y, Kawazoe N, Chen G, Preparation of dexamethasone-loaded biphasic calcium phosphate nanoparticles/collagen porous composite scaffolds for bone tissue engineering, Acta Biomater 67 (2018) 341–353. [PubMed: 29242161]

[74]. Liu S, Sun Y, Fu Y, Chang D, Fu C, Wang G, Liu Y, Tay FR, Zhou Y, Bioinspired Collagen-Apatite Nanocomposites for Bone Regeneration, Journal of Endodontics 42(8) (2016) 1226–1232. [PubMed: 27377439]

[75]. Saska S, Teixeira LN, de Castro Raucci LMS, Scarel-Caminaga RM, Franchi LP, dos Santos RA, Santagneli SH, Capela MV, de Oliveira PT, Takahashi CS, Gaspar AMM, Messaddeq Y, Ribeiro SJL, Marchetto R, Nanocellulose-collagen-apatite composite associated with osteogenic growth peptide for bone regeneration, Int J Biol Macromol 103 (2017) 467–476. [PubMed: 28527999]

[76]. Quade M, Schumacher M, Bernhardt A, Lode A, Kampschulte M, Voß A, Simon P, Uckermann O, Kirsch M, Gelinsky M, Strontium-modification of porous scaffolds from mineralized collagen for potential use in bone defect therapy, Materials Science and Engineering: C 84 (2018) 159–167. [PubMed: 29519425]

[77]. Mobini S, Solati-Hashjin M, Peirovi H, Abu Osman NA, Gholipourmalekabadi M, Barati M, Samadikuchaksaraei A, Bioactivity and Biocompatibility Studies on Silk-Based Scaffold for Bone Tissue Engineering, J Med Biol Eng 33(2) (2013) 207–213.

[78]. Yan LP, Oliveira JM, Oliveira AL, Caridade SG, Mano JF, Reis RL, Macro/microporous silk fibroin scaffolds with potential for articular cartilage and meniscus tissue engineering applications, Acta Biomater 8(1) (2012) 289–301. [PubMed: 22019518]

[79]. Yan S, Zhang Q, Wang J, Liu Y, Lu S, Li M, Kaplan DL, Silk fibroin/chondroitin sulfate/hyaluronic acid ternary scaffolds for dermal tissue reconstruction, Acta Biomater 9(6) (2013) 6771–82. [PubMed: 23419553]

[80]. Johari N, Hosseini HRM, Samadikuchaksaraei A, Novel fluoridated silk fibroin/ TiO2 nanocomposite scaffolds for bone tissue engineering, Mat Sci Eng C-Mater 82 (2018) 265–276.

[81]. Correia C, Bhumiratana S, Yan LP, Oliveira AL, Gimble JM, Rockwood D, Kaplan DL, Sousa RA, Reis RL, Vunjak-Novakovic G, Development of silk-based scaffolds for tissue engineering of bone from human adipose-derived stem cells, Acta Biomater 8(7) (2012) 2483–92. [PubMed: 22421311]

[82]. Kapoor S, Kundu SC, Silk protein-based hydrogels: Promising advanced materials for biomedical applications, Acta Biomater 31 (2016) 17–32. [PubMed: 26602821]

[83]. Kundu SC, Kundu B, Talukdar S, Bano S, Nayak S, Kundu J, Mandal BB, Bhardwaj N, Botlagunta M, Dash BC, Acharya C, Ghosh AK, Invited review nonmulberry silk biopolymers, Biopolymers 97(6) (2012) 455–67. [PubMed: 22241173]

[84]. Naskar D, Nayak S, Dey T, Kundu SC, Non-mulberry silk fibroin influence osteogenesis and osteoblast-macrophage cross talk on titanium based surface, Sci Rep 4 (2014) 4745. [PubMed: 24752225]

[85]. Sharma S, Bano S, Ghosh AS, Mandal M, Kim HW, Dey T, Kundu SC, Silk fibroin nanoparticles support in vitro sustained antibiotic release and osteogenesis on titanium surface, Nanomedicine 12(5) (2016) 1193–204. [PubMed: 26772428]

[86]. Bhattacharjee P, Naskar D, Maiti TK, Bhattacharya D, Das P, Nandi SK, Kundu SC, Potential of non-mulberry silk protein fibroin blended and grafted poly(capital JE, Ukrainian-caprolactone) nanofibrous matrices for in vivo bone regeneration, Colloids Surf B Biointerfaces 143 (2016) 431–439. [PubMed: 27037780]

[87]. Sahu N, Baligar P, Midha S, Kundu B, Bhattacharjee M, Mukherjee S, Mukherjee S, Maushart F, Das S, Loparic M, Kundu SC, Ghosh S, Mukhopadhyay A, Nonmulberry Silk Fibroin Scaffold Shows Superior Osteoconductivity Than Mulberry Silk Fibroin in Calvarial Bone Regeneration, Adv Healthc Mater 4(11) (2015) 1709–1721. [PubMed: 26084249]

[88]. Datta A, Ghosh AK, Kundu SC, Purification and characterization of fibroin from the tropical Saturniid silkworm, Antheraea mylitta, Insect Biochem Molec 31(10) (2001) 1013–1018.

[89]. Patra C, Talukdar S, Novoyatleva T, Velagala SR, Muhlfeld C, Kundu B, Kundu SC, Engel FB, Silk protein fibroin from Antheraea mylitta for cardiac tissue engineering, Biomaterials 33(9) (2012) 2673–2680. [PubMed: 22240510]

[90]. Johari N, Madaah Hosseini HR, Samadikuchaksaraei A, Optimized composition of nanocomposite scaffolds formed from silk fibroin and nano-TiO2 for bone tissue engineering, Materials Science and Engineering: C 79 (2017) 783–792. [PubMed: 28629081]

[91]. Chen L, Hu J, Ran J, Shen X, Tong H, Preparation and evaluation of collagen-silk fibroin/hydroxyapatite nanocomposites for bone tissue engineering, Int J Biol Macromol 65 (2014) 1–7. [PubMed: 24412151]

[92]. Behera S, Naskar D, Sapru S, Bhattacharjee P, Dey T, Ghosh AK, Mandal M, Kundu SC, Hydroxyapatite reinforced inherent RGD containing silk fibroin composite scaffolds: Promising platform for bone tissue engineering, Nanomedicine: Nanotechnology, Biology and Medicine 13(5) (2017) 1745–1759.

[93]. Huang T, Fan C, Zhu M, Zhu Y, Zhang W, Li L, 3D-printed scaffolds of biomineralized hydroxyapatite nanocomposite on silk fibroin for improving bone regeneration, Appl Surf Sci 467–468 (2019) 345–353.

[94]. Beladi F, Saber-Samandari S, Saber-Samandari S, Cellular compatibility of nanocomposite scaffolds based on hydroxyapatite entrapped in cellulose network for bone repair, Materials Science and Engineering: C 75 (2017) 385–392. [PubMed: 28415476]

[95]. Saber-Samandari S, Saber-Samandari S, Gazi M, Cebeci FÇ, Talasaz E, Synthesis, characterization and application of cellulose based nano-biocomposite hydrogels, Journal of Macromolecular Science, Part A 50(11) (2013) 1133–1141.

[96]. Tsioptsias C, Tsivintzelis I, Papadopoulou L, Panayiotou C, A novel method for producing tissue engineering scaffolds from chitin, chitin–hydroxyapatite, and cellulose, Materials Science and Engineering: C 29(1) (2009) 159–164.

[97]. Yamaguchi K, Prabakaran M, Ke M, Gang X, Chung IM, Um IC, Gopiraman M, Kim IS, Highly dispersed nanoscale hydroxyapatite on cellulose nanofibers for bone regeneration, Materials Letters 168 (2016) 56–61.

[98]. Fragal EH, Cellet TSP, Fragal VH, Companhoni MVP, Ueda-Nakamura T, Muniz EC, Silva R, Rubira AF, Hybrid materials for bone tissue engineering from biomimetic growth of hydroxiapatite on cellulose nanowhiskers, Carbohydrate Polymers 152 (2016) 734–746. [PubMed: 27516325]

[99]. Fragal EH, Cellet TSP, Fragal VH, Witt MA, Companhoni MVP, Ueda-Nakamura T, Silva R, Rubira AF, Biomimetic nanocomposite based on hydroxyapatite mineralization over chemically modified cellulose nanowhiskers: An active platform for osteoblast proliferation, Int J Biol Macromol 125 (2019) 133–142. [PubMed: 30529209]

[100]. Kumar A, Rao KM, Han SS, Development of sodium alginate-xanthan gum based nanocomposite scaffolds reinforced with cellulose nanocrystals and halloysite nanotubes, Polymer Testing 63 (2017) 214–225.

[101]. Osorio DA, Lee BEJ, Kwiecien JM, Wang X, Shahid I, Hurley AL, Cranston ED, Grandfield K, Cross-linked Cellulose Nanocrystal Aerogels as Viable Bone Tissue Scaffolds, Acta Biomaterialia (2019).

[102]. Ao C, Niu Y, Zhang X, He X, Zhang W, Lu C, Fabrication and characterization of electrospun cellulose/nano-hydroxyapatite nanofibers for bone tissue engineering, Int J Biol Macromol 97 (2017) 568–573. [PubMed: 28087448]

[103]. Gaihre B, Jayasuriya AC, Fabrication and characterization of carboxymethyl cellulose novel microparticles for bone tissue engineering, Materials Science and Engineering: C 69 (2016) 733–743. [PubMed: 27612767]

[104]. Helgerud T, Gaserod O, Fjæreide T, Andersen P, Larsen C, 4. Alginates, Food stabilisers, thickeners gelling agents. Wiley-Blackwell, Oxford (2010) 50–72.

[105]. Lee KY, Mooney DJ, Alginate: properties and biomedical applications, Prog Polym Sci 37(1) (2012) 106–126. [PubMed: 22125349]

[106]. Remminghorst U, Rehm BH, Bacterial alginates: from biosynthesis to applications, Biotechnol Lett 28(21) (2006) 1701–12. [PubMed: 16912921]

[107]. Turco G, Marsich E, Bellomo F, Semeraro S, Donati I, Brun F, Grandolfo M, Accardo A, Paoletti S, Alginate/Hydroxyapatite biocomposite for bone ingrowth: a trabecular structure with high and isotropic connectivity, Biomacromolecules 10(6) (2009) 1575–83. [PubMed: 19348419]

[108]. Hasan MM, Khan MN, Haque P, Rahman MM, Novel alginate-di-aldehyde cross-linked gelatin/nano-hydroxyapatite bioscaffolds for soft tissue regeneration, Int J Biol Macromol 117 (2018) 1110–1117. [PubMed: 29885393]

[109]. Purohit SD, Bhaskar R, Singh H, Yadav I, Gupta MK, Mishra NC, Development of a nanocomposite scaffold of gelatin–alginate–graphene oxide for bone tissue engineering, Int J Biol Macromol 133 (2019) 592–602. [PubMed: 31004650]

[110]. Fitton JH, Therapies from fucoidan; multifunctional marine polymers, Mar Drugs 9(10) (2011) 1731–60. [PubMed: 22072995]

[111]. Cho YS, Jung WK, Kim JA, Choi IW, Kim SK, Beneficial effects of fucoidan on osteoblastic MG-63 cell differentiation, Food Chem 116(4) (2009) 990–994.

[112]. Changotade SI, Korb G, Bassil J, Barroukh B, Willig C, Colliec-Jouault S, Durand P, Godeau G, Senni K, Potential effects of a low-molecular-weight fucoidan extracted from brown algae on bone biomaterial osteoconductive properties, J Biomed Mater Res A 87(3) (2008) 666–75. [PubMed: 18189302]

[113]. Park S.-j., Lee KW, Lim D-S, Lee S.J.S.c., development, The sulfated polysaccharide fucoidan stimulates osteogenic differentiation of human adipose-derived stem cells, 21(12) (2011) 2204–2211.

[114]. Venkatesan J, Bhatnagar I, Kim SK, Chitosan-alginate biocomposite containing fucoidan for bone tissue engineering, Mar Drugs 12(1) (2014) 300–16. [PubMed: 24441614]

[115]. Lowe B, Venkatesan J, Anil S, Shim MS, Kim SK, Preparation and characterization of chitosan-natural nano hydroxyapatite-fucoidan nanocomposites for bone tissue engineering, Int J Biol Macromol 93(Pt B) (2016) 1479–1487. [PubMed: 26921504]

[116]. Young AT, Kang JH, Kang DJ, Venkatesan J, Chang HK, Bhatnagar I, Chang K-Y, Hwang J-H, Salameh Z, Kim S-K, Interaction of stem cells with nano hydroxyapatite-fucoidan bionanocomposites for bone tissue regeneration, International journal of biological macromolecules 93 (2016) 1488–1491. [PubMed: 27402459]

[117]. Tian HY, Tang ZH, Zhuang XL, Chen XS, Jing XB, Biodegradable synthetic polymers: Preparation, functionalization and biomedical application, Progress in Polymer Science 37(2) (2012) 237–280.

[118]. Rao SH, Harini B, Shadamarshan RPK, Balagangadharan K, Selvamurugan N, Natural and synthetic polymers/bioceramics/bioactive compounds-mediated cell signalling in bone tissue engineering, Int J Biol Macromol 110 (2018) 88–96. [PubMed: 28917940]

[119]. Mehrasa M, Asadollahi MA, Ghaedi K, Salehi H, Arpanaei A, Electrospun aligned PLGA and PLGA/gelatin nanofibers embedded with silica nanoparticles for tissue engineering, Int J Biol Macromol 79 (2015) 687–95. [PubMed: 26045092]

[120]. Xin X, Hussain M, Mao JJ, Continuing differentiation of human mesenchymal stem cells and induced chondrogenic and osteogenic lineages in electrospun PLGA nanofiber scaffold, Biomaterials 28(2) (2007) 316–25. [PubMed: 17010425]

[121]. Elfick A, Poly (ε-caprolactone) as a potential material for a temporary joint spacer, Biomaterials 23(23) (2002) 4463–4467. [PubMed: 12322965]

[122]. Shor L, Guceri S, Wen X, Gandhi M, Sun W, Fabrication of three-dimensional polycaprolactone/hydroxyapatite tissue scaffolds and osteoblast-scaffold interactions in vitro, Biomaterials 28(35) (2007) 5291–7. [PubMed: 17884162]

[123]. Baker SC, Rohman G, Southgate J, Cameron NR, The relationship between the mechanical properties and cell behaviour on PLGA and PCL scaffolds for bladder tissue engineering, Biomaterials 30(7) (2009) 1321–1328. [PubMed: 19091399]

[124]. Agrawal CM, Ray RB, Biodegradable polymeric scaffolds for musculoskeletal tissue engineering, J Biomed Mater Res 55(2) (2001) 141–50. [PubMed: 11255165]

[125]. Moeini S, Mohammadi MR, Simchi A, In-situ solvothermal processing of polycaprolactone/hydroxyapatite nanocomposites with enhanced mechanical and biological performance for bone tissue engineering, Bioact Mater 2(3) (2017) 146–155. [PubMed: 29744424]

[126]. Karuppuswamy P, Venugopal JR, Navaneethan B, Laiva AL, Ramakrishna S, Polycaprolactone nanofibers for the controlled release of tetracycline hydrochloride, Materials Letters 141 (2015) 180–186.

[127]. Park JS, Kim J-M, Lee SJ, Lee SG, Jeong Y-K, Kim SE, Lee SC, Surface hydrolysis of fibrous poly (ε-caprolactone) scaffolds for enhanced osteoblast adhesion and proliferation, Macromolecular research 15(5) (2007) 424–429.

[128]. Lopes MS, Jardini AL, Maciel R, Poly (lactic acid) production for tissue engineering applications, Procedia Engineer 42 (2012) 1402–1413.

[129]. Fabbri P, Bondioli F, Messori M, Bartoli C, Dinucci D, Chiellini F, Porous scaffolds of polycaprolactone reinforced with in situ generated hydroxyapatite for bone tissue engineering, J Mater Sci Mater Med 21(1) (2010) 343–51. [PubMed: 19653069]

[130]. Guarino V, Causa F, Netti PA, Ciapetti G, Pagani S, Martini D, Baldini N, Ambrosio L, The role of hydroxyapatite as solid signal on performance of PCL porous scaffolds for bone tissue regeneration, J Biomed Mater Res B 86b(2) (2008) 548–557.

[131]. Heo S, Kim S, Hyun YT, Kim D, Lee HM, Hwang YM, Park S, Shin JW, In vitro evaluation of poly ε-caprolactone/hydroxyapatite composite as scaffolds for bone tissue engineering with human bone marrow stromal cells, Key Engineering Materials, Trans Tech Publ, 2007, pp. 369–372.

[132]. Tamjid E, Bagheri R, Vossoughi M, Simchi A, Effect of particle size on the in vitro bioactivity, hydrophilicity and mechanical properties of bioactive glass-reinforced polycaprolactone composites, Mat Sci Eng C-Mater 31(7) (2011) 1526–1533.

[133]. Tamjid E, Bagheri R, Vossoughi M, Simchi A, Effect of TiO2 morphology on in vitro bioactivity of polycaprolactone/TiO2 nanocomposites, Materials Letters 65(15–16) (2011) 2530–2533.

[134]. Marrella A, Tedeschi G, Giannoni P, Lagazzo A, Sbrana F, Barberis F, Quarto R, Puglisi F, Scaglione S, “Green-reduced” graphene oxide induces in vitro an enhanced biomimetic mineralization of polycaprolactone electrospun meshes, Materials Science Engineering: C 93 (2018) 1044–1053. [PubMed: 30274035]

[135]. Manakhov A, Permyakova ES, Ershov S, Sheveyko A, Kovalskii A, Polčák J, Zhitnyak IY, Gloushankova NA, Zajíčková L, Shtansky DV, Bioactive TiCaPCON-coated PCL nanofibers as a promising material for bone tissue engineering, Appl Surf Sci 479 (2019) 796–802.

[136]. Tahriri M, Moztarzadeh F, Preparation, characterization, and in vitro biological evaluation of PLGA/nano-fluorohydroxyapatite (FHA) microsphere-sintered scaffolds for biomedical applications, Appl Biochem Biotechnol 172(5) (2014) 2465–79. [PubMed: 24395697]

[137]. Nojehdehian H, Moztarzadeh F, Baharvand H, Nazarian H, Tahriri M, Preparation and surface characterization of poly-L-lysine-coated PLGA microsphere scaffolds containing retinoic acid for nerve tissue engineering: in vitro study, Colloids Surf B Biointerfaces 73(1) (2009) 23–9. [PubMed: 19520554]

[138]. Nojehdehian H, Moztarzadeh F, Baharvand H, Mehrjerdi NZ, Nazarian H, Tahriri M, Effect of poly-L-lysine coating on retinoic acid-loaded PLGA microspheres in the differentiation of carcinoma stem cells into neural cells, Int J Artif Organs 33(10) (2010) 721–730. [PubMed: 21058269]

[139]. Tahriri M, Moztarzadeh F, Hresko K, Khoshroo K, Tayebi L, Biodegradation properties of PLGA/nano-fluorhydroxyapatite composite microsphere-sintered scaffolds, Dental Materials 32 (2016) e49–e50.

[140]. Masaeli R, Kashi TSJ, Dinarvand R, Rakhshan V, Shahoon H, Hooshmand B, Abbas FM, Raz M, Rajabnejad A, Eslami H, Khoshroo K, Tahriri M, Tayebi L, Efficacy of the Biomaterials 3 wt %-nanostrontium-hydroxyapatite-enhanced calcium phosphate cement (nanoSr-CPC) and nanoSr-CPC-incorporated simvastatin-loaded poly(lactic-co-glycolic-acid) microspheres in osteogenesis improvement: An explorative multi-phase experimental in vitro/vivo study, Mat Sci Eng C-Mater 69 (2016) 171–183.

[141]. Wang Y, Shi X, Ren L, Yao Y, Zhang F, Wang DA, Poly (lactide co glycolide)/titania composite microsphere sintered scaffolds for bone tissue engineering applications, Journal of Biomedical Materials Research Part B: Applied Biomaterials 93(1) (2010) 84–92.

[142]. Lu L, Garcia CA, Mikos AG, In vitro degradation of thin poly(DL-lactic-co-glycolic acid) films, J Biomed Mater Res 46(2) (1999) 236–44. [PubMed: 10380002]

[143]. Eslami H, Solati-Hashjin M, Tahriri M, The comparison of powder characteristics and physicochemical, mechanical and biological properties between nanostructure ceramics of hydroxyapatite and fluoridated hydroxyapatite, Mat Sci Eng C-Bio S 29(4) (2009) 1387–1398.

[144]. Boccaccini AR, Blaker JJ, Maquet V, Chung W, Jérôme R, Nazhat SN, Poly (D, L-lactide) (PDLLA) foams with TiO2 nanoparticles and PDLLA/TiO2-Bioglass® foam composites for tissue engineering scaffolds, Journal of materials science 41(13) (2006) 3999–4008.

[145]. Lv Q, Nair L, Laurencin CT, Fabrication, characterization, and in vitro evaluation of poly (lactic acid glycolic acid)/nano hydroxyapatite composite microsphere based scaffolds for bone tissue engineering in rotating bioreactors, Biomedical Materials Research Part A: An Official Journal of The Society for Biomaterials 91(3) (2009) 679–691.

[146]. Ehrenfried LM, Patel MH, Cameron RE, The effect of tri-calcium phosphate (TCP) addition on the degradation of polylactide-co-glycolide (PLGA), J Mater Sci Mater Med 19(1) (2008) 459–66. [PubMed: 17607516]

[147]. Eslami H, Lisar HA, Kashi TSJ, Tahriri M, Ansari M, Rafiei T, Bastami F, Shahin-Shamsabadi A, Abbas FM, Tayebi L, Poly(lactic-co-glycolic acid)(PLGA)/TiO2 nanotube bioactive composite as a novel scaffold for bone tissue engineering: In vitro and in vivo studies, Biologicals 53 (2018) 51–62. [PubMed: 29503205]

[148]. Shao W, He J, Sang F, Wang Q, Chen L, Cui S, Ding B, Enhanced bone formation in electrospun poly (l-lactic-co-glycolic acid)–tussah silk fibroin ultrafine nanofiber scaffolds incorporated with graphene oxide, Materials Science Engineering: C 62 (2016) 823–834. [PubMed: 26952489]

[149]. Zhao X, Han Y, Li J, Cai B, Gao H, Feng W, Li S, Liu J, Li D, BMP-2 immobilized PLGA/hydroxyapatite fibrous scaffold via polydopamine stimulates osteoblast growth, Mater Sci Eng C Mater Biol Appl 78 (2017) 658–666. [PubMed: 28576035]

[150]. Tudorachi N, Chiriac AP, Mustata F, New nanocomposite based on poly(lactic-co-glycolic acid) copolymer and magnetite. Synthesis and characterization, Compos Part B-Eng 72 (2015) 150–159.

[151]. Montufar EB, Traykova T, Gil C, Harr I, Almirall A, Aguirre A, Engel E, Planell JA, Ginebra MP, Foamed surfactant solution as a template for self-setting injectable hydroxyapatite scaffolds for bone regeneration, Acta Biomaterialia 6(3) (2010) 876–885. [PubMed: 19835998]

[152]. Zhu Y, Wang Z, Zhou H, Li L, Zhu Q, Zhang P, An injectable hydroxyapatite/poly(lactide-co-glycolide) composite reinforced by micro/nano-hybrid poly(glycolide) fibers for bone repair, Mater Sci Eng C Mater Biol Appl 80 (2017) 326–334. [PubMed: 28866171]

[153]. Scaffaro R, Lopresti F, Maio A, Botta L, Rigogliuso S, Ghersi G, Electrospun PCL/GO-g-PEG structures: Processing-morphology-properties relationships, Compos Part a-Appl S 92 (2017) 97–107.

[154]. Turkkan S, Pazarceviren AE, Keskin D, Machin NE, Duygulu O, Tezcaner A, Nanosized CaP-silk fibroin-PCL-PEG-PCL/PCL based bilayer membranes for guided bone regeneration, Mat Sci Eng C-Mater 80 (2017) 484–493.

[155]. Yang F, Murugan R, Wang S, Ramakrishna S, Electrospinning of nano/micro scale poly(L-lactic acid) aligned fibers and their potential in neural tissue engineering, Biomaterials 26(15) (2005) 2603–2610. [PubMed: 15585263]

[156]. Cacciotti I, Fortunati E, Puglia D, Kenny JM, Nanni F, Effect of silver nanoparticles and cellulose nanocrystals on electrospun poly(lactic) acid mats: morphology, thermal properties and mechanical behavior, Carbohydr Polym 103 (2014) 22–31. [PubMed: 24528696]

[157]. Lee JH, Park TG, Park HS, Lee DS, Lee YK, Yoon SC, Nam JD, Thermal and mechanical characteristics of poly(L-lactic acid) nanocomposite scaffold, Biomaterials 24(16) (2003) 2773–8. [PubMed: 12711524]

[158]. Shi Q, Zhou C, Yue Y, Guo W, Wu Y, Wu Q, Mechanical properties and in vitro degradation of electrospun bio-nanocomposite mats from PLA and cellulose nanocrystals, Carbohydr Polym 90(1) (2012) 301–8. [PubMed: 24751045]

[159]. Li H, Qiao T, Song P, Guo H, Song X, Zhang B, Chen X, Star-shaped PCL/PLLA blended fiber membrane via electrospinning, J Biomater Sci Polym Ed 26(7) (2015) 420–32. [PubMed: 25671790]

[160]. Qiao TK, Song P, Guo HL, Song XF, Zhang BC, Chen XS, Reinforced electrospun PLLA fiber membrane via chemical crosslinking, Eur Polym J 74 (2016) 101–108.

[161]. Lou T, Wang X, Song G, Gu Z, Yang Z, Fabrication of PLLA/β-TCP nanocomposite scaffolds with hierarchical porosity for bone tissue engineering, Int J Biol Macromol 69 (2014) 464–470. [PubMed: 24933519]

[162]. Kim HW, Lee HH, Knowles JC, Electrospinning biomedical nanocomposite fibers of hydroxyapatite/poly(lactic acid) for bone regeneration, J Biomed Mater Res A 79(3) (2006) 643–9. [PubMed: 16826596]

[163]. Scaffaro R, Lopresti F, Botta L, Rigogliuso S, Ghersi G, Preparation of three-layered porous PLA/PEG scaffold: relationship between morphology, mechanical behavior and cell permeability, J Mech Behav Biomed 54 (2016) 8–20.

[164]. Salerno A, Fernández-Gutiérrez M, del Barrio JSR, Domingo C, Bio-safe fabrication of PLA scaffolds for bone tissue engineering by combining phase separation, porogen leaching and scCO2 drying, The Journal of Supercritical Fluids 97 (2015) 238–246.

[165]. Rogina A, Pribolšan L, Hanžek A, Gómez-Estrada L, Gallego Ferrer G, Marijanović I, Ivanković M, Ivanković H, Macroporous poly(lactic acid) construct supporting the osteoinductive porous chitosan-based hydrogel for bone tissue engineering, Polymer 98 (2016) 172–181.

[166]. Alharbi HF, Luqman M, Khalil KA, Elnakady YA, Abd-Elkader OH, Rady AM, Alharthi NH, Karim MR, Fabrication of core-shell structured nanofibers of poly (lactic acid) and poly (vinyl alcohol) by coaxial electrospinning for tissue engineering, Eur Polym J 98 (2018) 483–491.

[167]. Nga NK, Hoai TT, Viet PH, Biomimetic scaffolds based on hydroxyapatite nanorod/poly(d,l) lactic acid with their corresponding apatite-forming capability and biocompatibility for bone-tissue engineering, Colloids and Surfaces B: Biointerfaces 128 (2015) 506–514. [PubMed: 25791418]

[168]. Shamsi M, Karimi M, Ghollasi M, Nezafati N, Shahrousvand M, Kamali M, Salimi A, In vitro proliferation and differentiation of human bone marrow mesenchymal stem cells into osteoblasts on nanocomposite scaffolds based on bioactive glass (64SiO2–31CaO-5P2O5)-poly-l-lactic acid nanofibers fabricated by electrospinning method, Materials Science and Engineering: C 78 (2017) 114–123. [PubMed: 28575950]

[169]. Mohammadi M, Alibolandi M, Abnous K, Salmasi Z, Jaafari MR, Ramezani M, Fabrication of hybrid scaffold based on hydroxyapatite-biodegradable nanofibers incorporated with liposomal formulation of BMP-2 peptide for bone tissue engineering, Nanomedicine 14(7) (2018) 1987–1997. [PubMed: 29933024]

[170]. Segredo-Morales E, García-García P, Évora C, Delgado A, BMP delivery systems for bone regeneration: Healthy vs osteoporotic population. Review, Journal of Drug Delivery Science and Technology 42 (2017) 107–118.

[171]. Ma D, An G, Liang M, Liu Y, Zhang B, Wang Y, A composited PEG-silk hydrogel combining with polymeric particles delivering rhBMP-2 for bone regeneration, Materials Science and Engineering: C 65 (2016) 221–231. [PubMed: 27157747]

[172]. Zdrahala RJ, Zdrahala IJ, Biomedical applications of polyurethanes: a review of past promises, present realities, and a vibrant future, J Biomater Appl 14(1) (1999) 67–90. [PubMed: 10405885]

[173]. Shahrousvand M, Mir Mohamad Sadeghi G, Salimi A, Artificial extracellular matrix for biomedical applications: biocompatible and biodegradable poly (tetramethylene ether) glycol/poly (epsilon-caprolactone diol)-based polyurethanes, J Biomater Sci Polym Ed 27(17) (2016) 1712–1728. [PubMed: 27589493]

[174]. Paul DR, Robeson LM, Polymer nanotechnology: Nanocomposites, Polymer 49(15) (2008) 3187–3204.

[175]. Zhu Q, Li X, Fan Z, Xu Y, Niu H, Li C, Dang Y, Huang Z, Wang Y, Guan J, Biomimetic polyurethane/TiO2 nanocomposite scaffolds capable of promoting biomineralization and mesenchymal stem cell proliferation, Materials Science and Engineering: C 85 (2018) 79–87. [PubMed: 29407160]

[176]. Chen Z, Wang Y, Ba T, Li Y, Pu J, Chen T, Song Y, Gu Y, Qian Q, Yang J, Jia G, Genotoxic evaluation of titanium dioxide nanoparticles in vivo and in vitro, Toxicology Letters 226(3) (2014) 314–319. [PubMed: 24594277]

[177]. Nogueiras R, Habegger KM, Chaudhary N, Finan B, Banks AS, Dietrich MO, Horvath TL, Sinclair DA, Pfluger PT, Tschöp M.H.J.P.r., Sirtuin 1 and sirtuin 3: physiological modulators of metabolism, 92(3) (2012) 1479–1514.

[178]. Shrestha BK, Shrestha S, Tiwari AP, Kim J-I, Ko SW, Kim H-J, Park CH, Kim CS, Bio-inspired hybrid scaffold of zinc oxide-functionalized multi-wall carbon nanotubes reinforced polyurethane nanofibers for bone tissue engineering, Materials & Design 133 (2017) 69–81.

Highlights

- Improved osteoconductive properties for nanocomposites over the pure biomaterial.
- Nanocomposites offer adjustment of the matrix to obtain desired scaffold properties.
- Natural polymer based nanocomposites display superior biocompatibility.
- Synthetic polymer based nanocomposites can be optimized for strength and bioactivity.

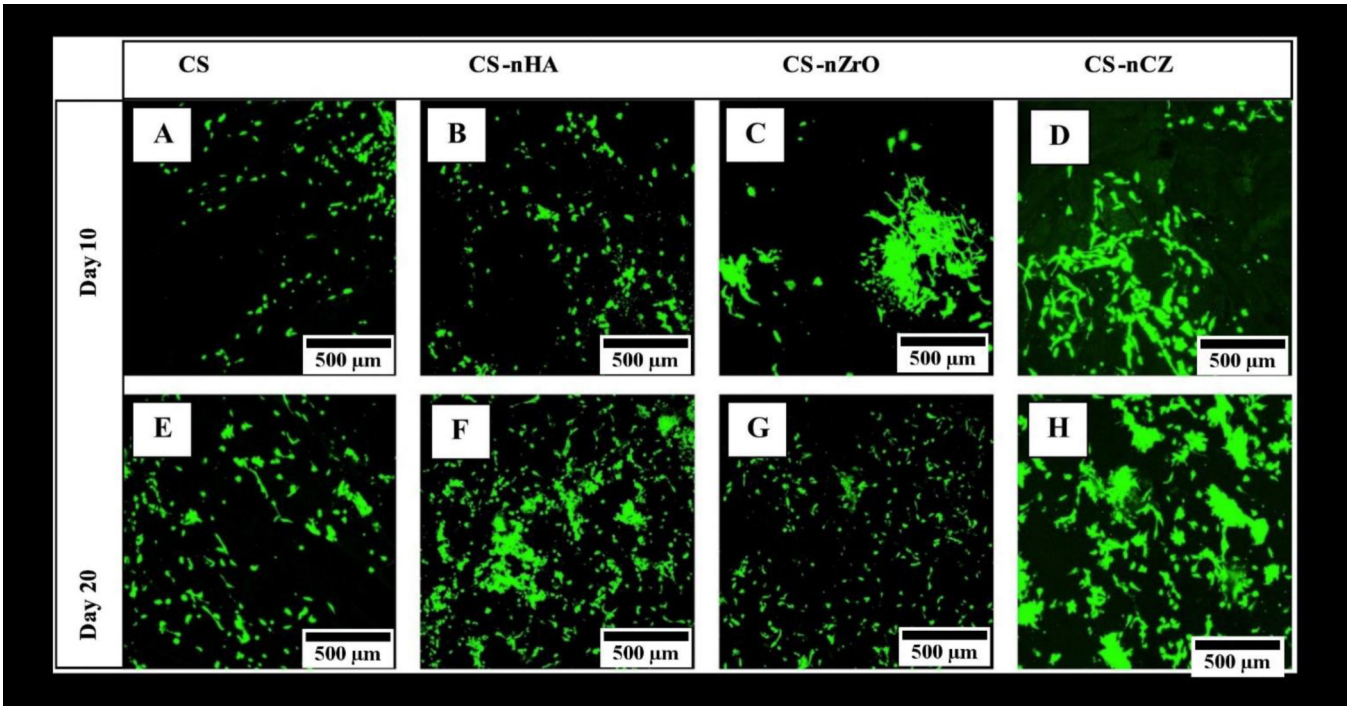

Fig. 1.

Proliferation of OB-6 pre-osteoblasts on CS and CS composite scaffolds at day 10 and 20. The proliferation was better on CS-nHA and CS-nCZ groups; scale = 250 μm [52].

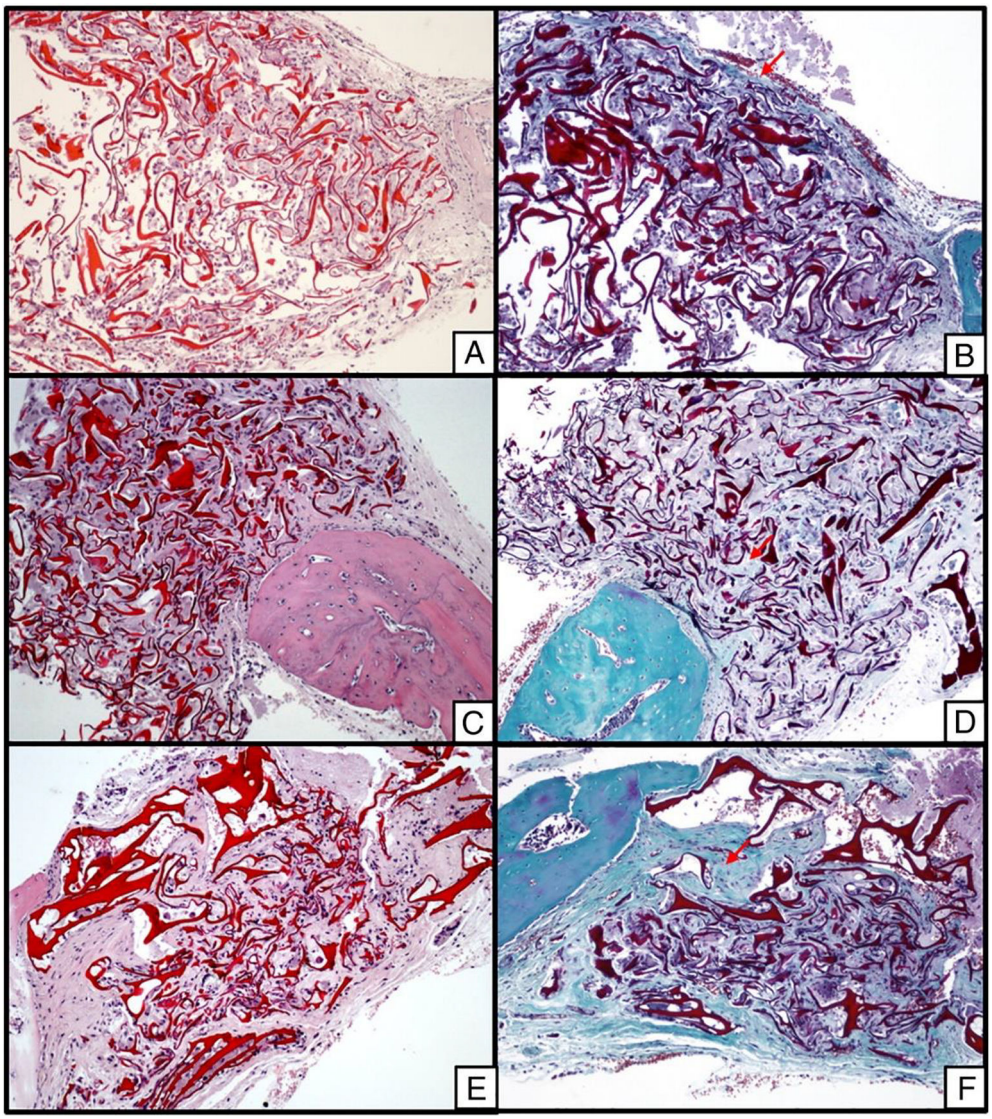

Fig. 2.

Histological Images of nSI/CS composite scaffold. A (2 weeks), C (4 weeks), and E (8 weeks) with H&E staining. B (2 weeks), D (4 weeks), and F (8 weeks) with Mallory's trichrome staining [44].

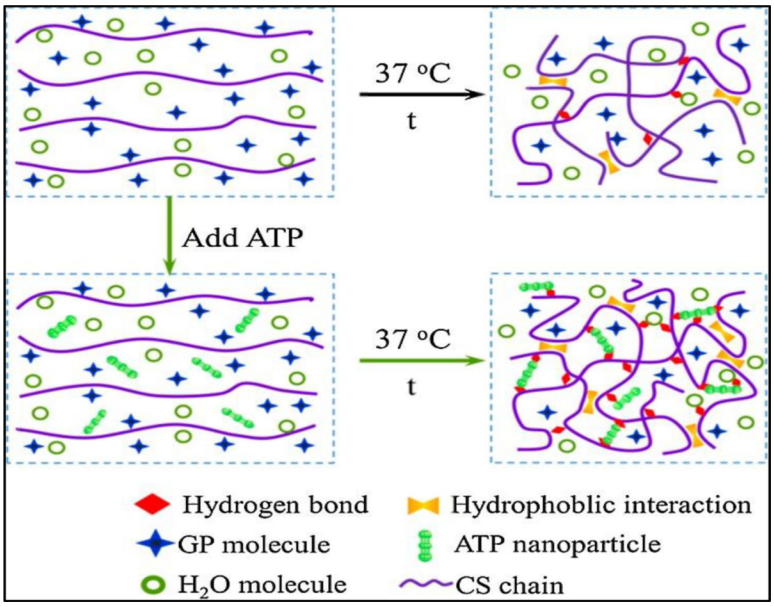

Fig. 3.
Influence of ATP nanoparticles on CS/GP hydrogel crosslinking [56].

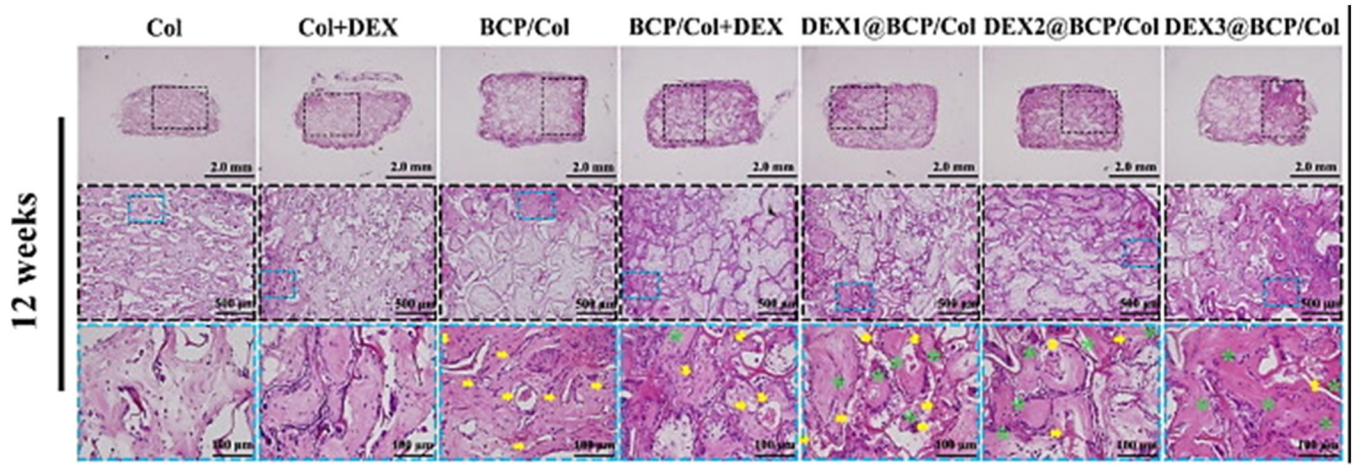

Fig. 4.

H&E Staining after 12 weeks of implantation along the decalcified regions; green stars signifies new bone formation whereas yellow arrows identify new blood vessels [73].

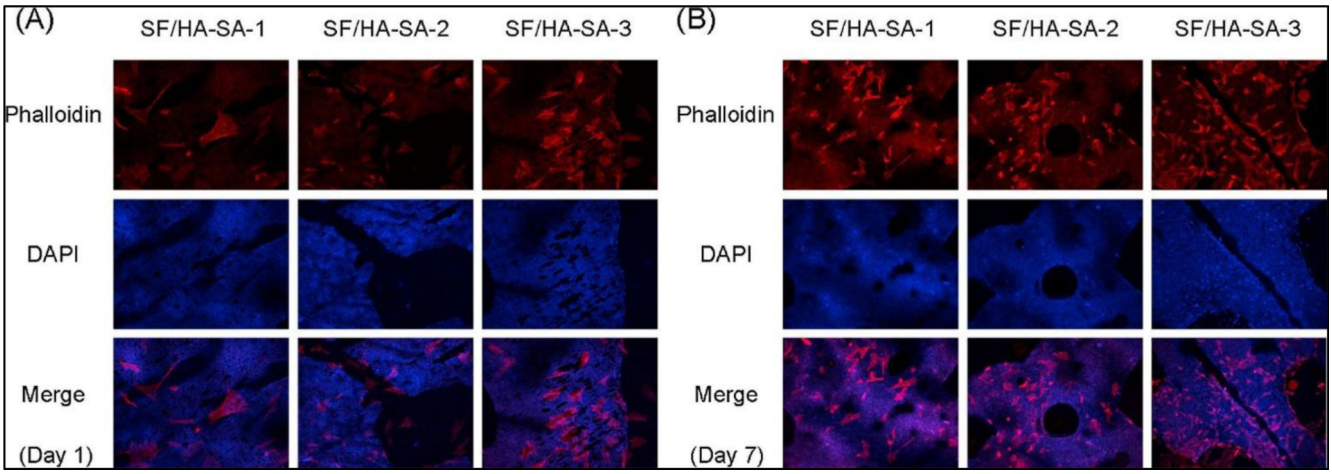

Fig. 5.

Fluorochrome-labelling analysis of the hBMSCs for cell proliferation for the three scaffold groups with varying amounts of the paste binder; culture done for (A) 1 day, (B) 7 days; cell nuclei in blue and actin in red [93].

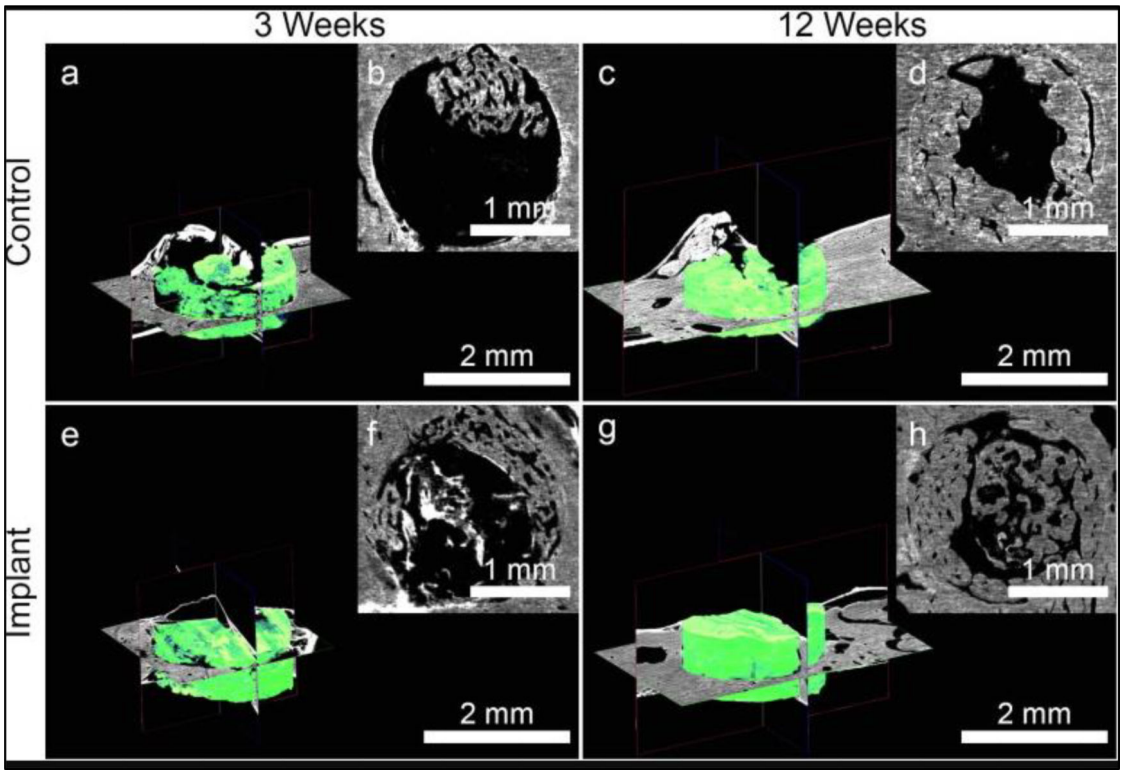

Fig. 6.

Control sample bone growth from only bone defect wall (a,b,c,d) and contact and distance osteogenesis from the center as well as wall of the bone defect in sulfated CNC aerogel implanted samples (e,f,g,h) [101].

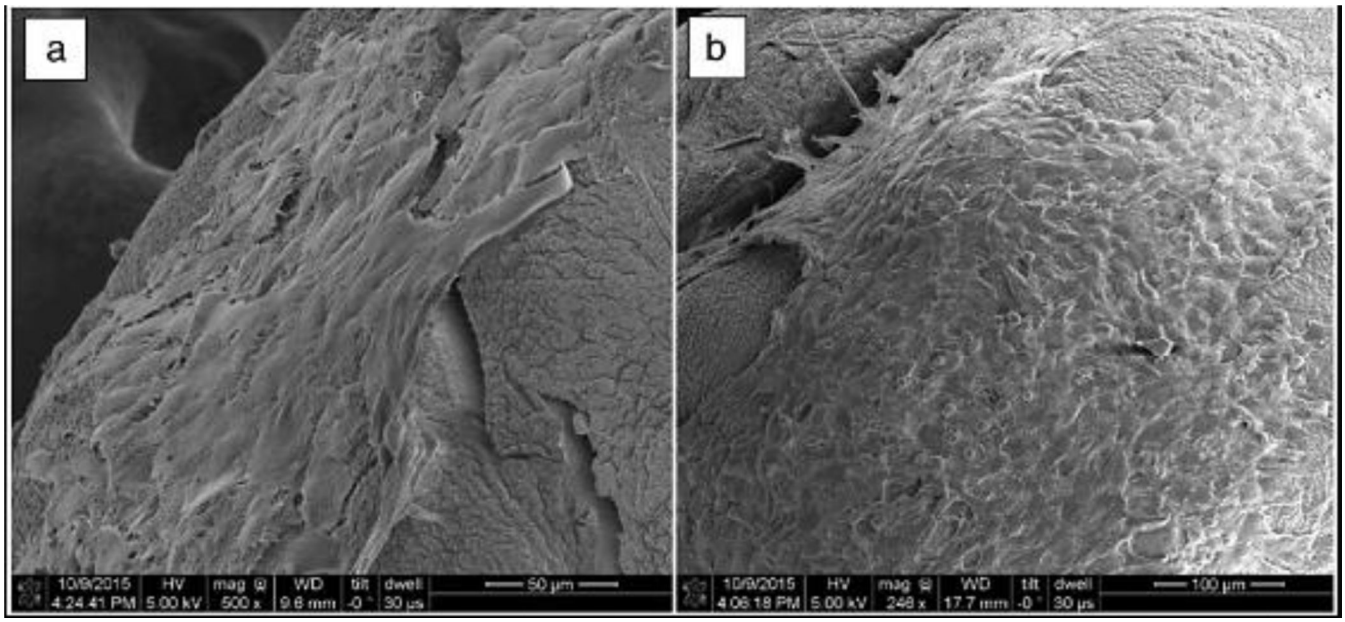

Fig. 7.

OB-6 preosteoblasts proliferating along cracks on the microparticles on day 10 prepared (a) with 5% w/v $ZrCl_4$ and (b) with 10% w/v $ZrCl_4$ [103].

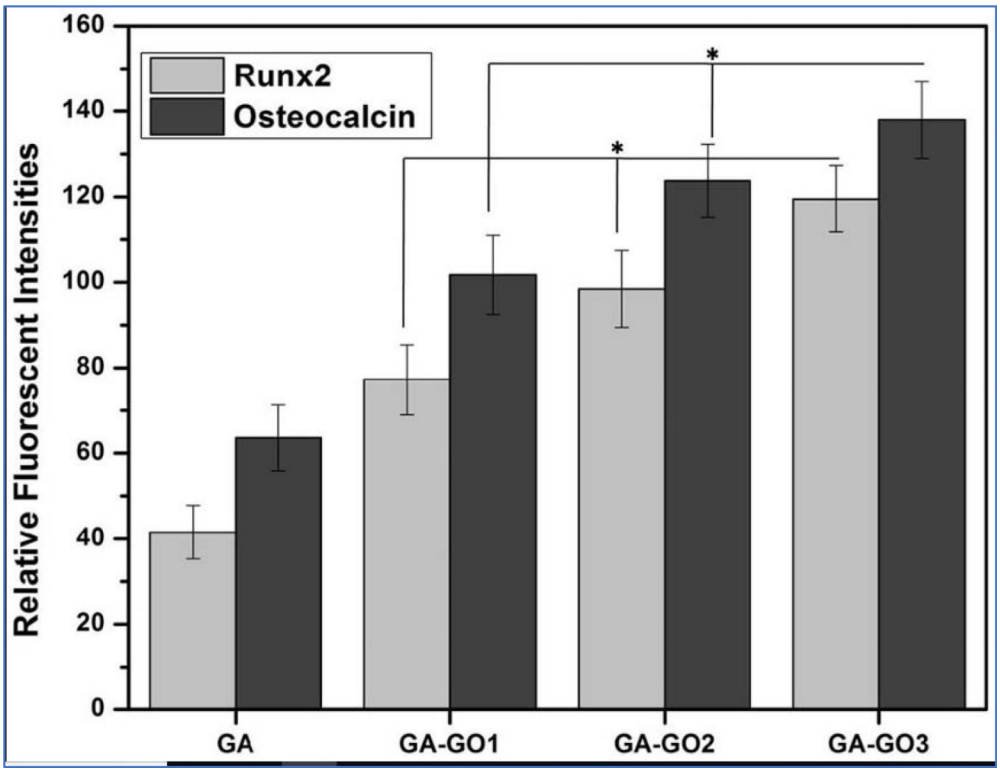

Fig. 8.
Runx2 and Osteocalcin expression data in Relative Fluorescence Intensity [109].

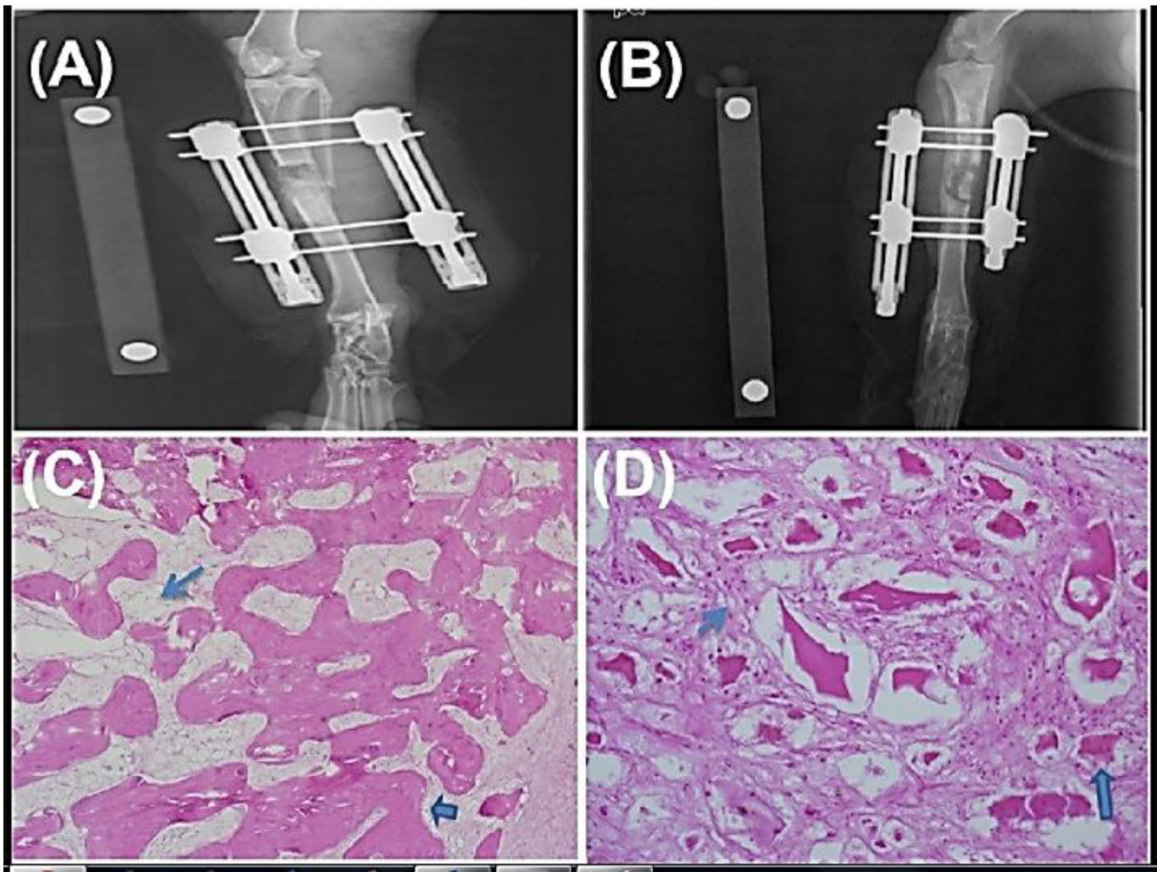

Fig. 9.

(A) Radiographs of nHA only and (B) Fucoidan/nHA nanocomposite scaffold. H&E staining (x100) displaying (C) the filling of bone defect with Fucoidan/nHA nanocomposite biomaterial, and (D) identification of osteoblasts (represented by ➡) and fat cells (represented by ➡) [116].

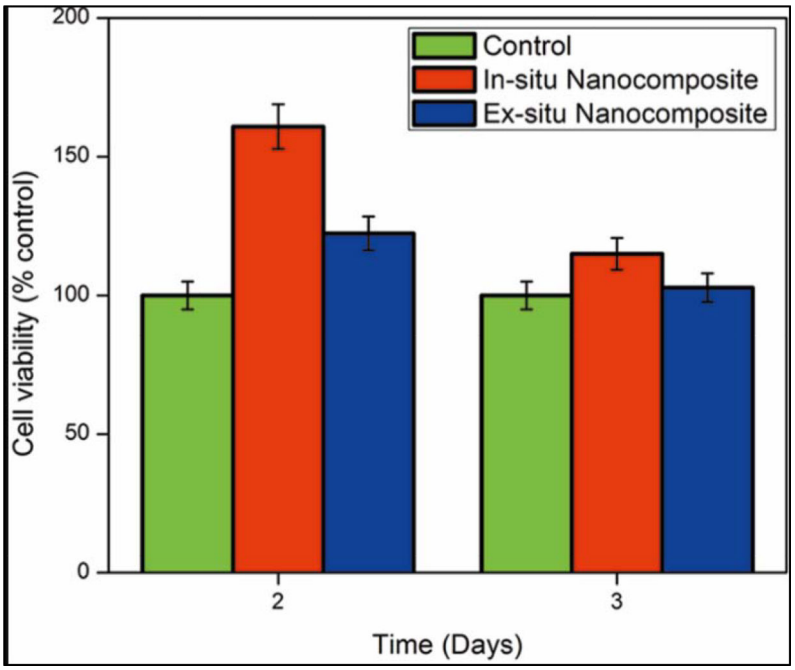

Fig. 10.

PCL/HA (20%) nanocomposite incubation data in human osteosarcoma cell lines for analysis of cell viability; p-value > 0.05; n=5 for statistical significance [125].

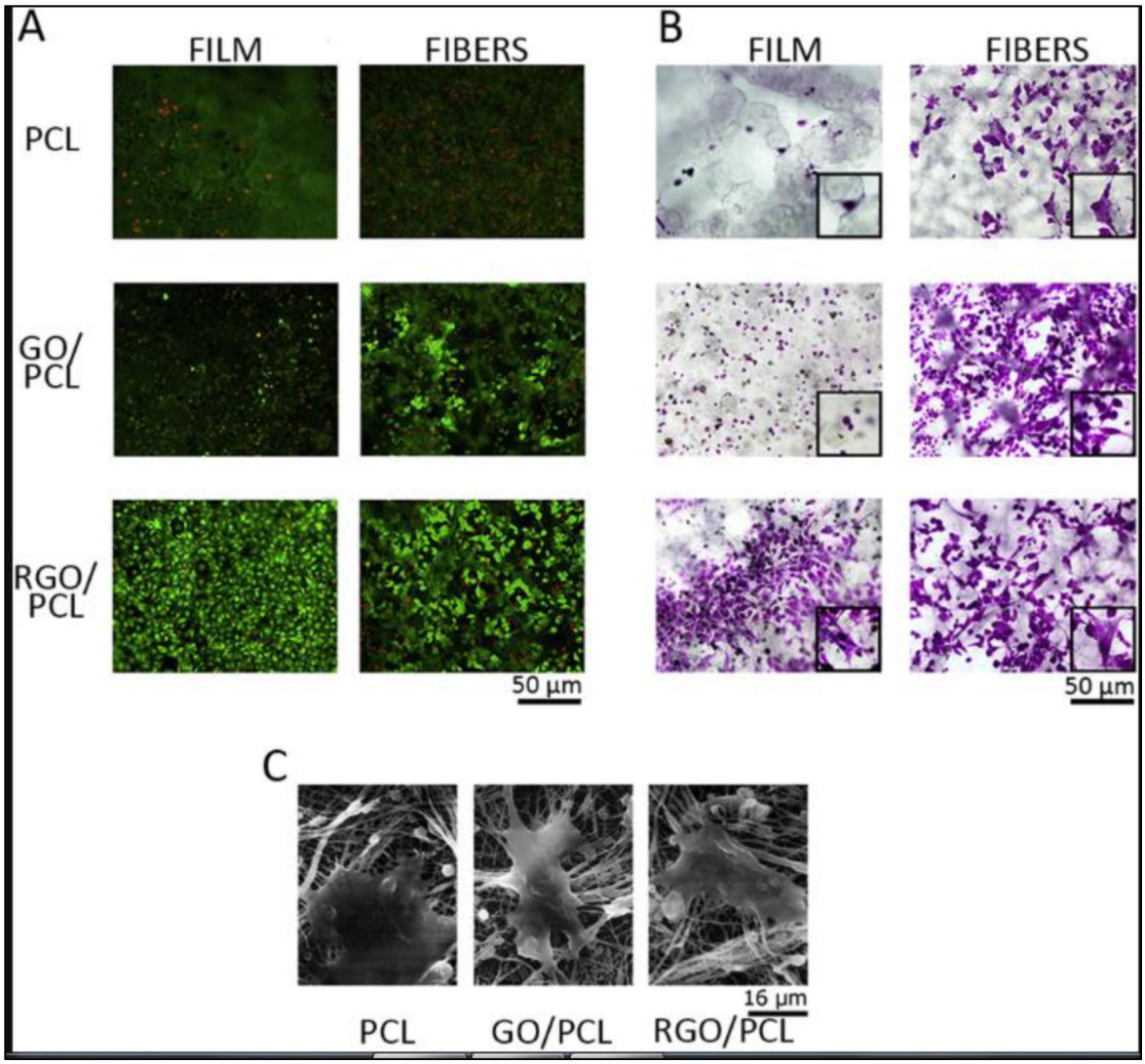

Fig. 11.

(A) Fluorescent images denoting live cells (in greens spots) and dead cells (in red spots) for cell viability analysis on RGO/PCL nanofibrous mat and other control samples. (B) Cell spreading analysis (using toluidine blue staining) of 3T3s after 24 hours of culture on RGO/PCL biomaterial as well as other control samples. (C) Cell adhesion analysis (using SEM micrographs) for 3T3s on RGO/PCL nanofibrous mat as well as other control samples after 24 hours of cell culture [134].

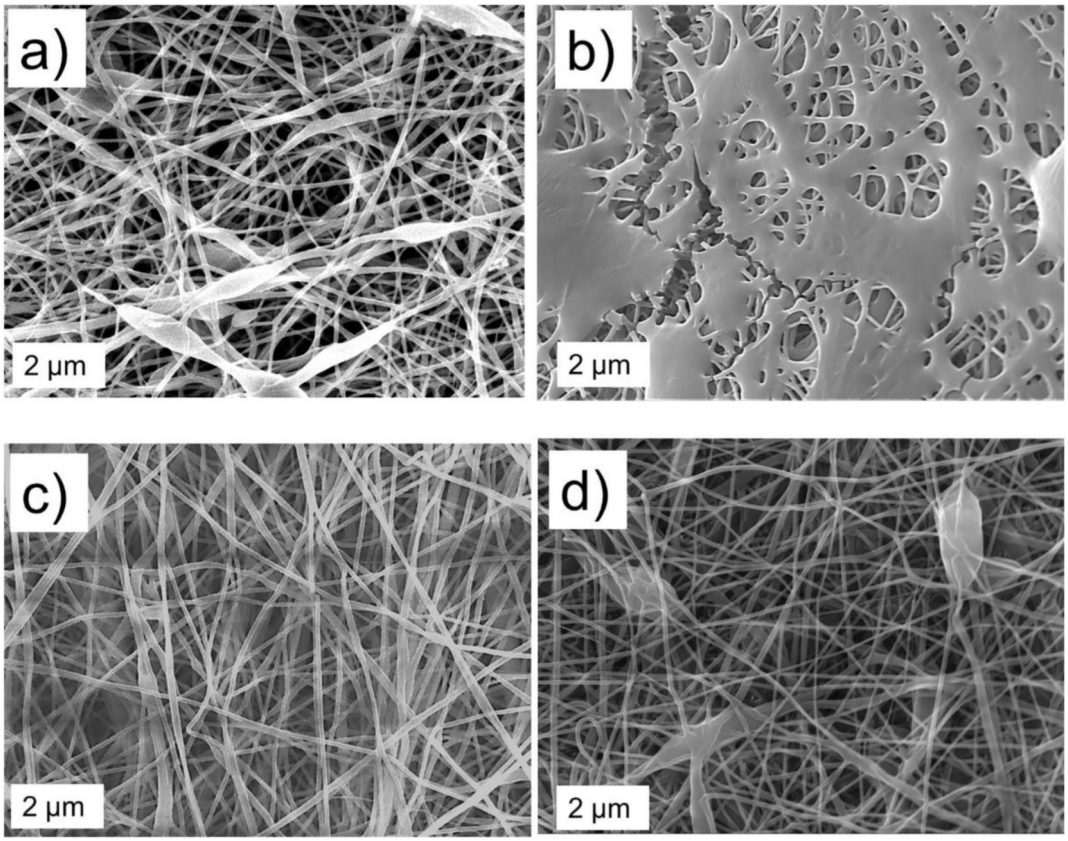

Fig. 12.

Scanning electron microscope images showing a) PCL nanofibers only, b) PCL/TNT at 2.5A, c) PCL/TNT at 2A, and d) PCL/TNT at 1.5 A magnetron current [135].

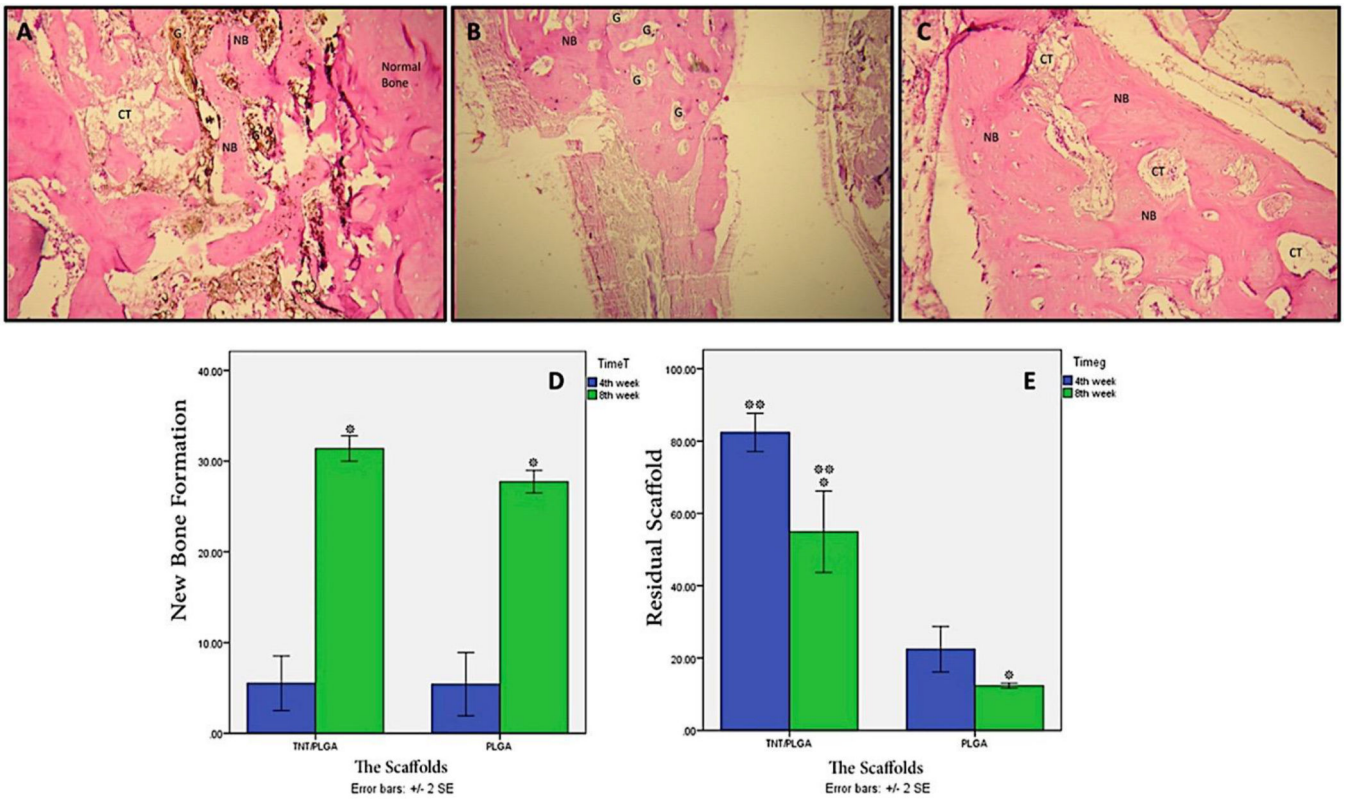

Fig. 13.

Histologic images: (A) PLGA/TNT, (B) pure PLGA, (C) empty defect. Histomorphometric analysis: (D) new bone formation (%), (E) residual scaffold (%). G – Graft, NB – New bone formation, and CT – connective tissue. Asterisk and double asterisk denote the significant difference between time points and scaffolds respectively [147].

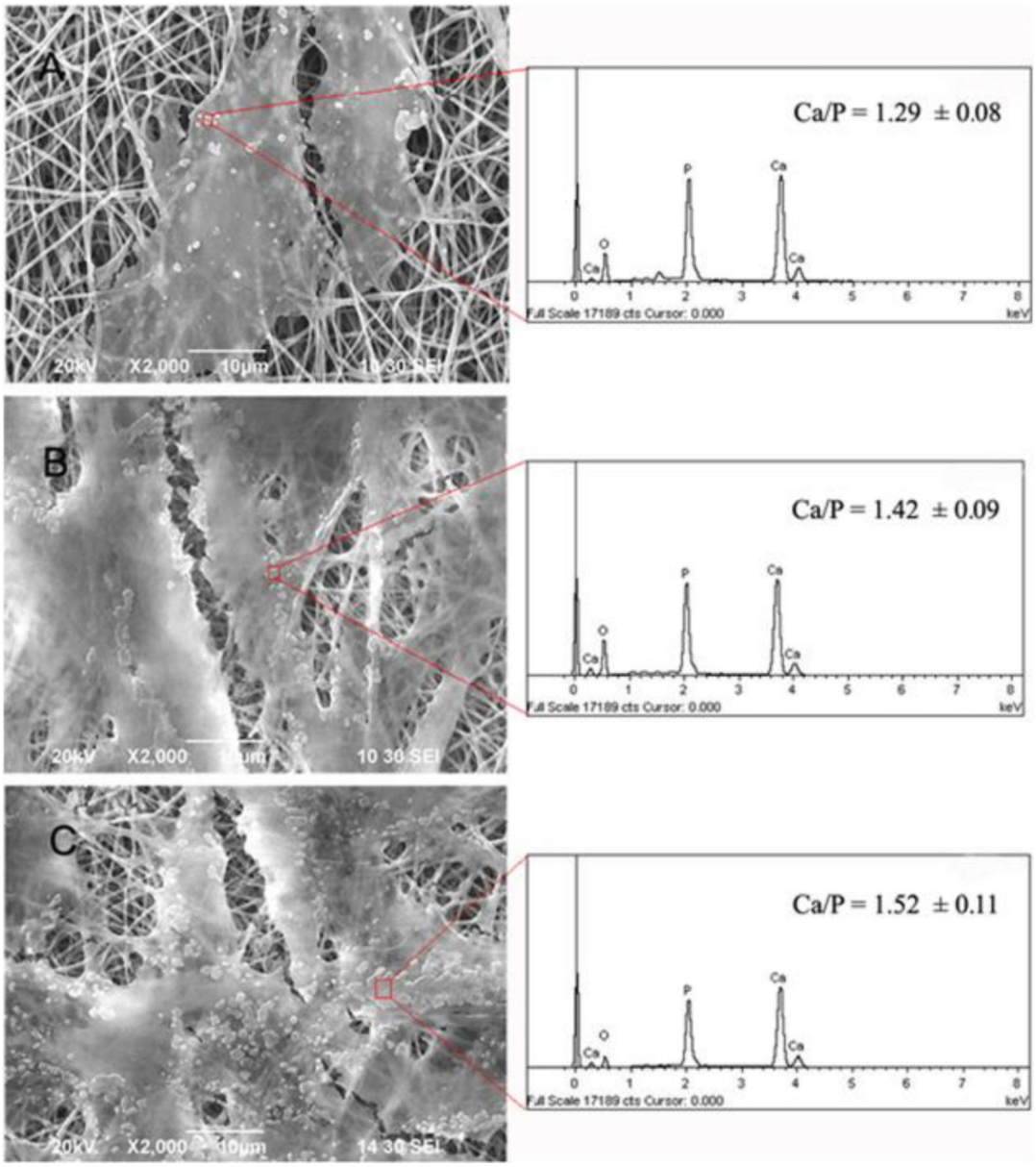

Fig. 14.

SEM images for biomineralization by mesenchymal stem cells on PLGA (A), PLGA/SF (C), and PLGA/SF/GO nanofiber scaffolds 14 days post implantation; corresponding EDS images for mineral identification are given along with on the right [148].

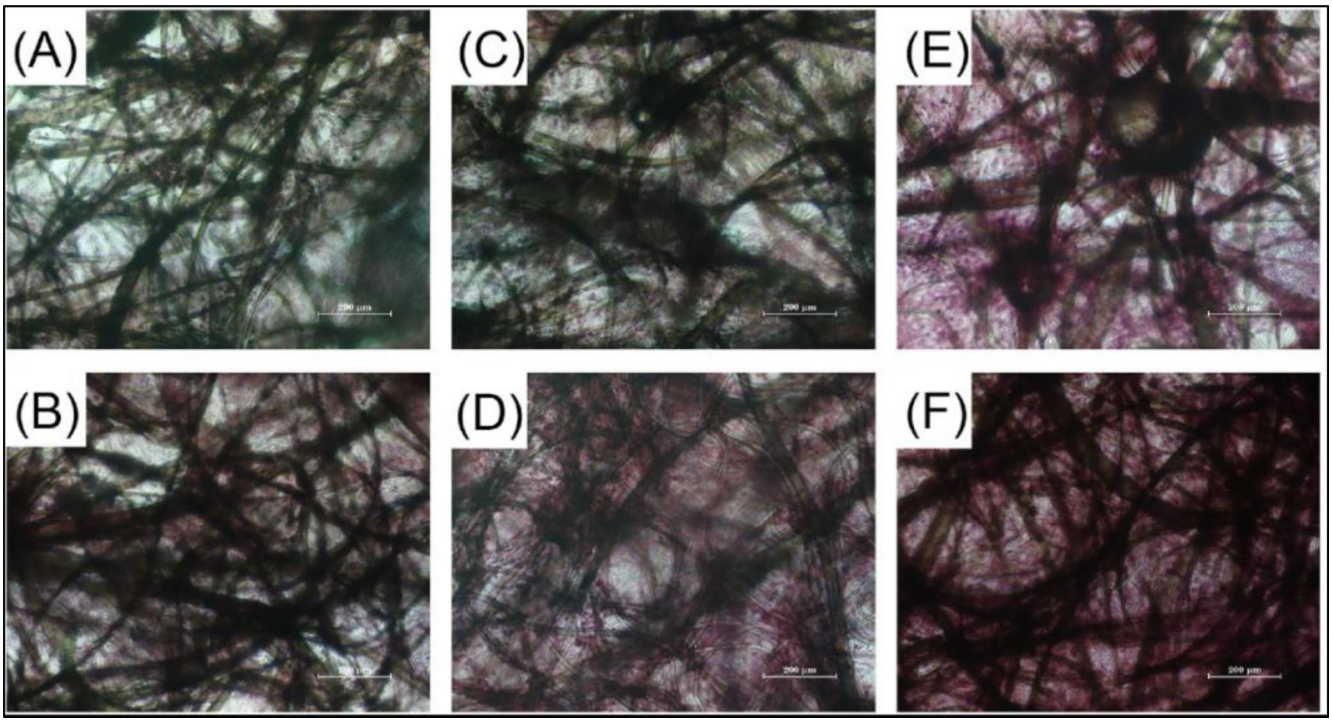

Fig. 15.

Alizarin Red staining of MC3T3-E1 cells (on 21st day of cell culture) on (A) PLGA, (B) PLGA/HA, (C) PDA-PLGA, (D) PDAPLGA/HA, (E) PDA-PLGA/BMP-2, and (F) PDA-PLGA/HA/BMP-2. [149]

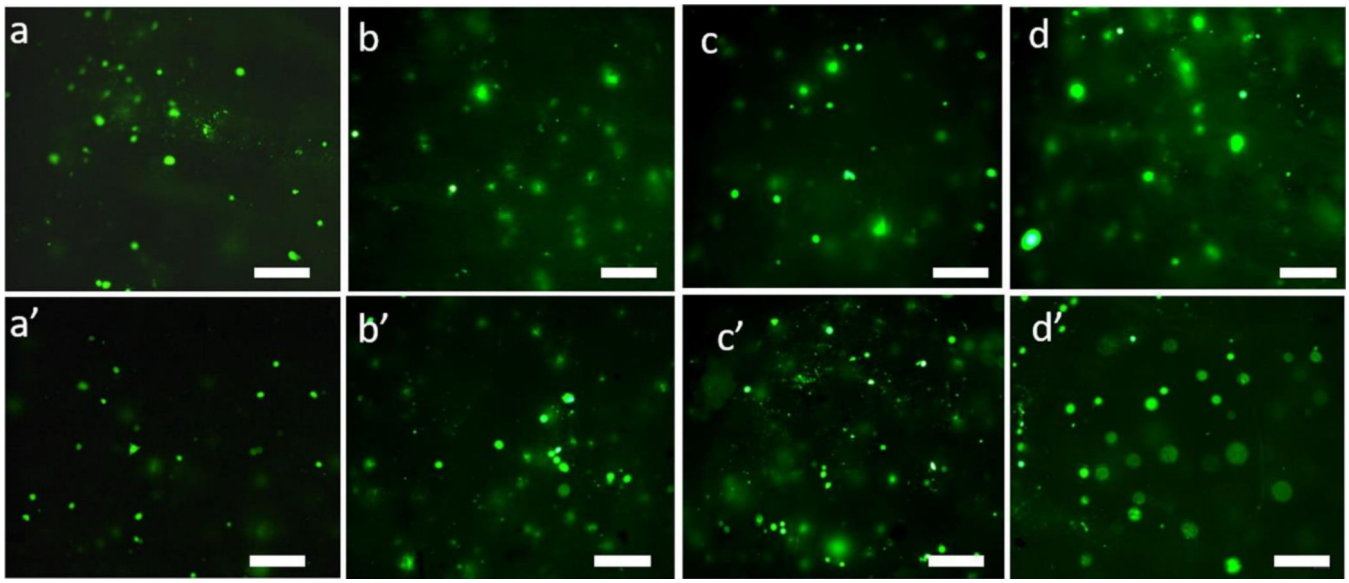

Fig. 16.

Cell viability analysis of MC3T3-E1 cells on (a, b. c. d) electrospun PCL and (a', b', c', d') electrospun PCL/GO/PEG (at 0.25 wt.%); cell culture done for 1 (a, a'), 5 (b, b'), 7 (c, c'), and 9 (d, d') days respectively; scale at 200 μm [153].

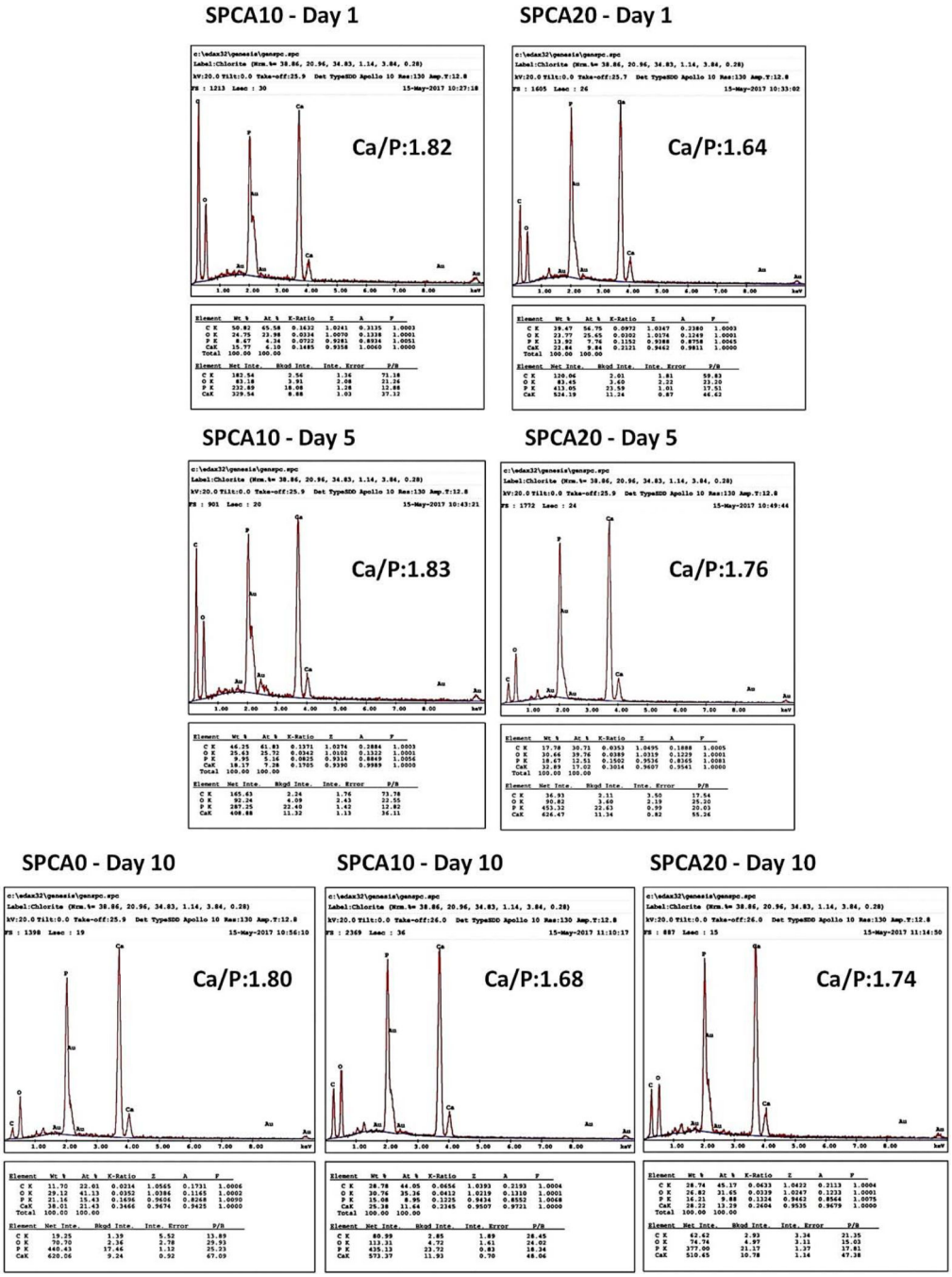

Fig. 17.

Energy dispersion spectroscopy for detecting apatite-like formation on the nano calcium membranes after 10 days of SBF incubation [154].

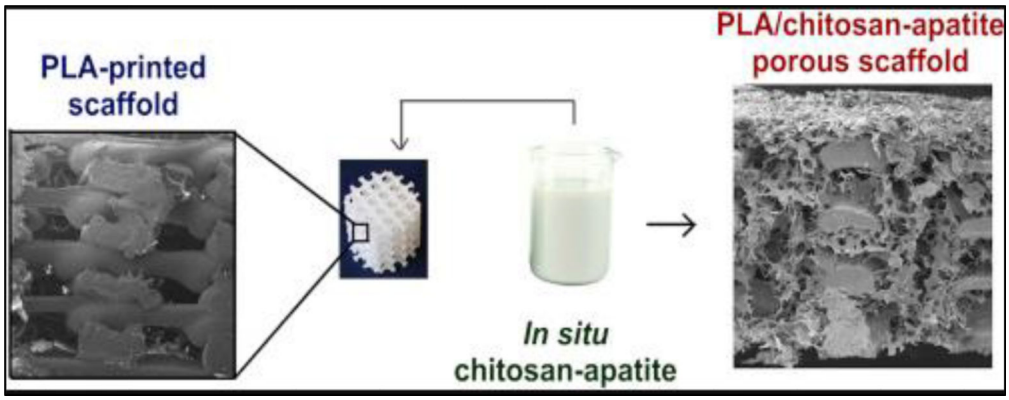

Fig. 18.

Schematic for preparation of 3D printed PLA/HA-CS composite hydrogels through freeze gelation technique [165].

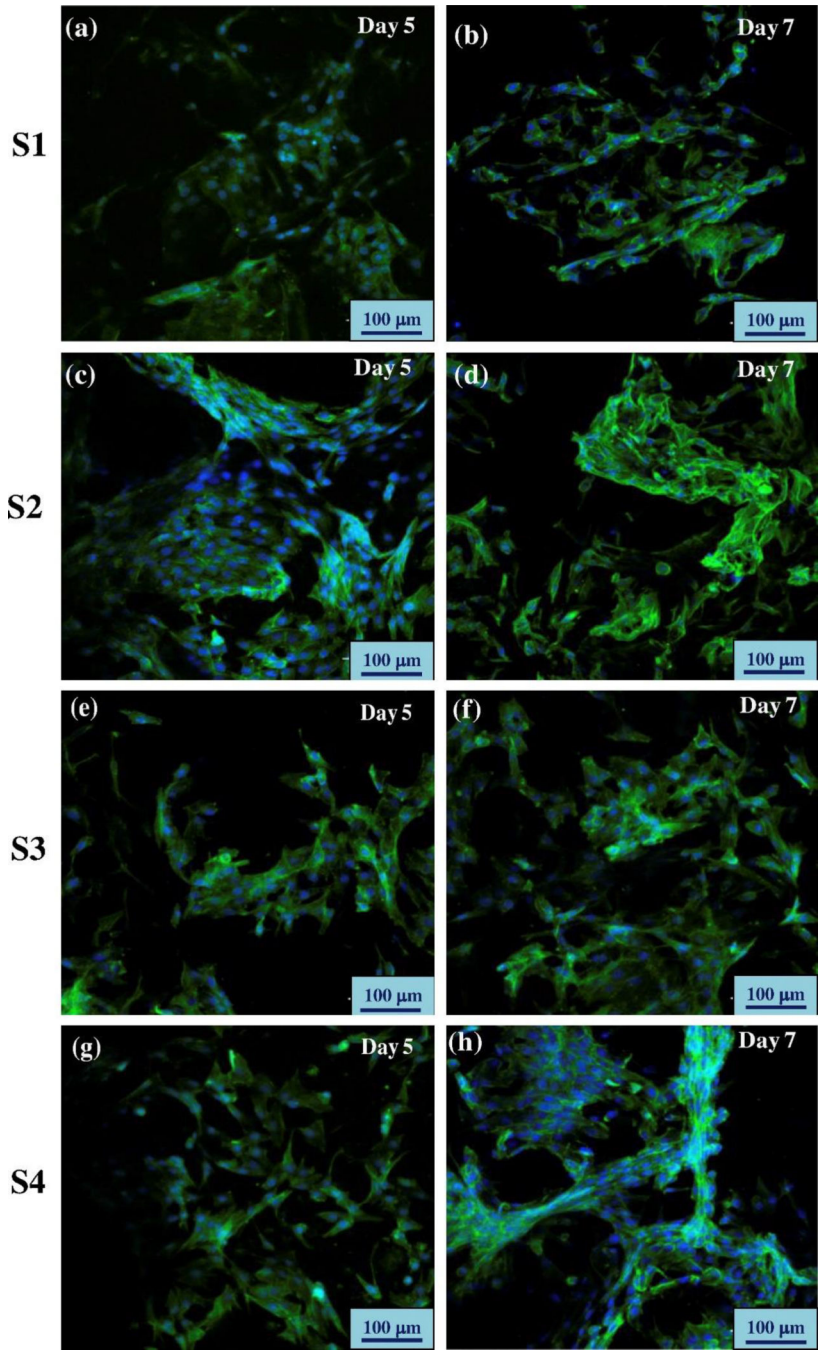

Fig. 19.

MG 63 cells stained with DAPI (blue) and actin filaments with Oregon Green 488 phalloidin (green) after 5^{th} and 7^{th} day culture (images captured using confocal laser scanning microscopy). (a) and (b) – S1 (0 wt.% nHA), (c) and (d) – S2 (10 wt.% nHA), (e) and (f) – S3 (20 wt.% nHA), and (g) and (h) – S4 (30 wt.% nHA); scale bars are representing 100 µm [167].

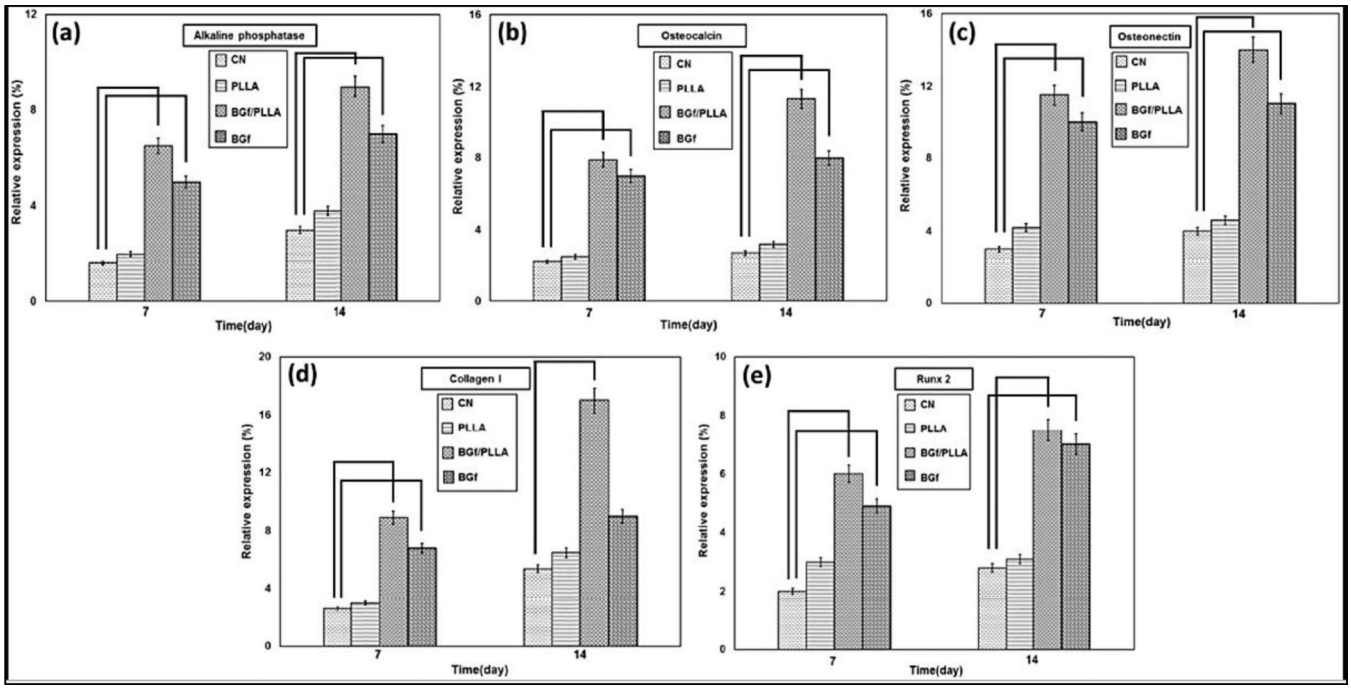

Fig. 20.

Relative gene expressions (alkaline phosphatase (a), osteocalcin (b), osteonectin (c), collagen I (d), and Runx 2 (e)) at 7th day (with osteogenic differentiation of human mesenchymal stem cell lines) for control sample, PLLA nanofiber only, BG/PLLA nanocomposite scaffold, and BG nanofiber only; between group significant difference at $P < 0.05$ [168].

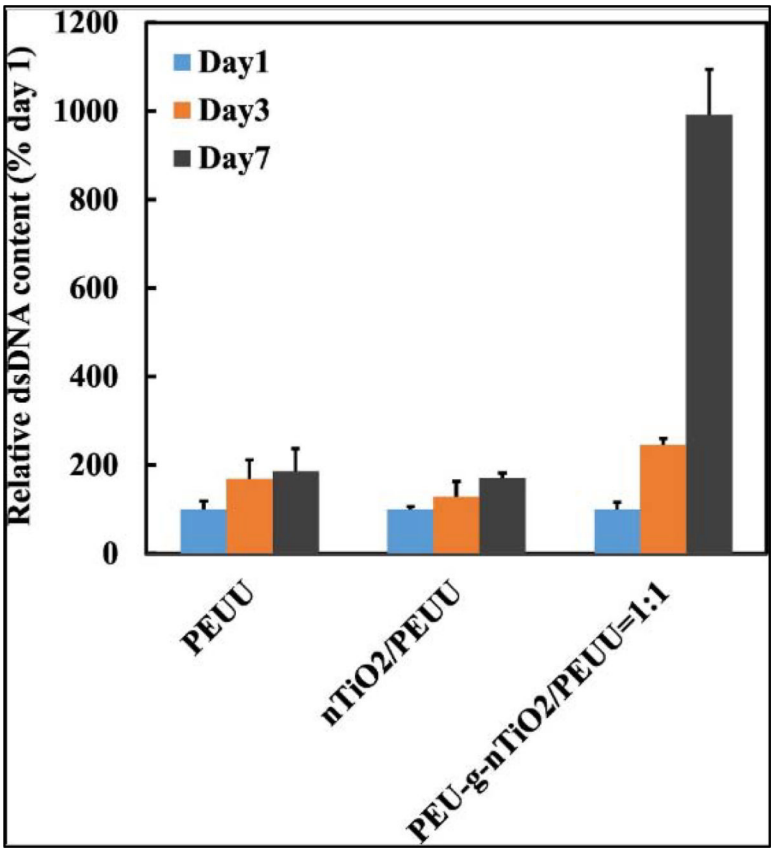

Fig. 21.
Cell growth using bone marrow-derived mesenchymal stem cells on various scaffold compositions [175].

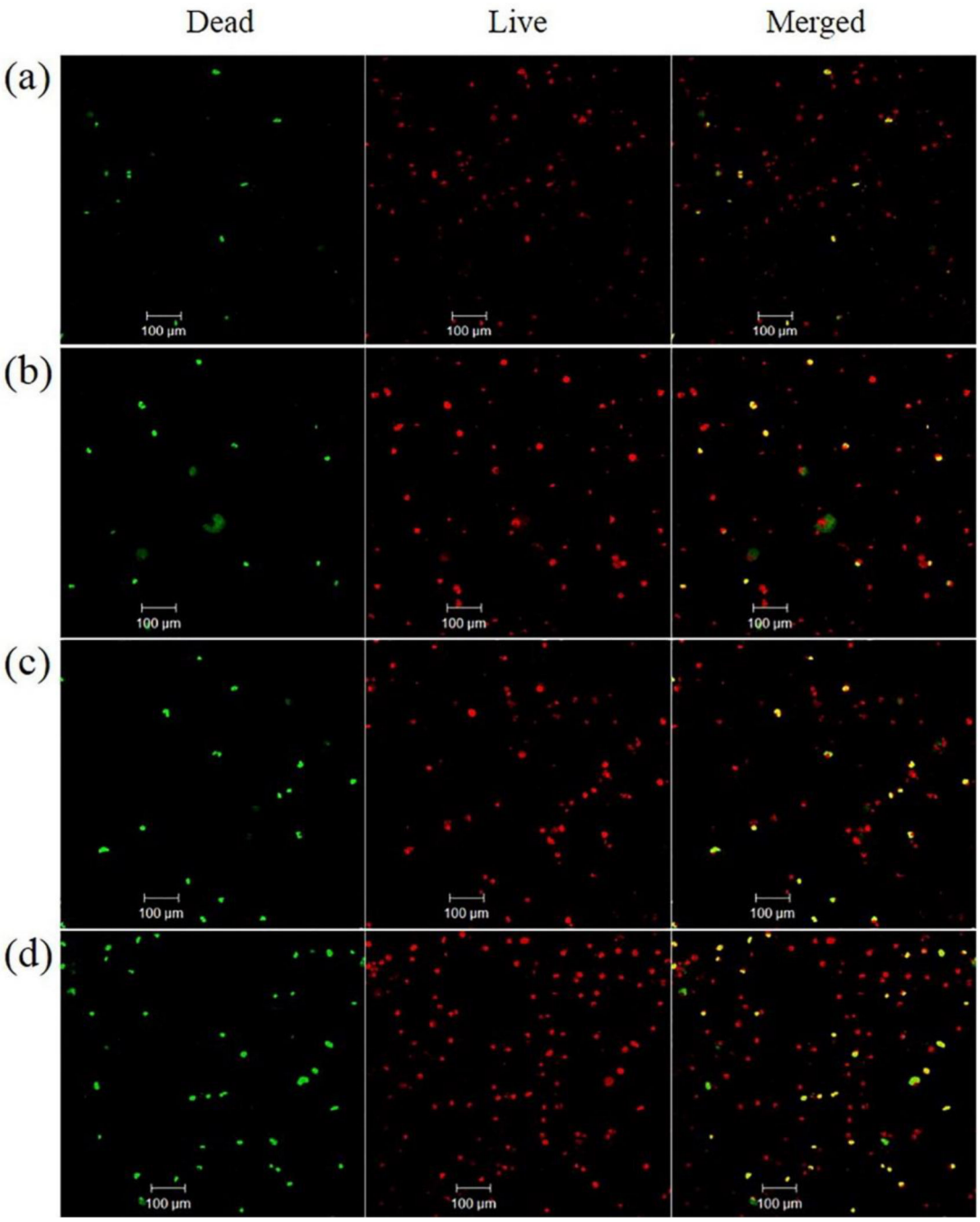

Fig. 22.

MC3T3-E1 Cell Viability and Proliferation for a 5-day period with live cells (red) and dead cells (green) for scaffolds – Electrospun scaffolds of (a) PU (pure), (b) PU/ZnO-fMWCNTs (0.1 wt.%), (c) PU/ZnO-fMWCNTs (0.2 wt.%), and (d) PU/ZnO-fMWCNTs (0.4 wt.%) [178].

Table 1

Summary of some natural polymer-based nanocomposites which have been listed with respect to nanomaterial used. Significant advantages and disadvantages due to the incorporation of the particular nanomaterial have been listed along with their effect on the mechanical properties.

Nanomaterial	Synthesis Method	Polymer Incorporation Method	Scaffold Preparation & Mechanical Properties	Biological Activity	Advantages	Drawbacks	References
nHA	• Sol-gel method; co-precipitation. • Wet chemical method (egg shells)	• 2% formic acid – CS suspension; nHA addition while 60 min magnetic stirring followed by sonication (30 min.). • 2% acetic acid – CS suspension; 40% w/w nanoparticles with magnetic stirring followed by sonication at 40 °C. • 1% acetic acid – CS/TSP solution co-precipitation. • Col/SF blend with *in situ* HA formation • 5 wt. % Gelatin and ADA mixed with nHA and $CaCl_2$ (for gelation). • 2.5 % CH solution, 0.1 g Fucoidan and 2.5 g of nHA	• Freeze-drying. • Compressive Modulus: • 0.24 MPa – Pure CS • 0.76 MPa - CS/nHA • Young's Modulus: • ~3.0 GPa – Pure CS • >3.5 GPa - CS/nHA • Tensile strength of 69 MPa for CS/nHA films. • Compressive modulus and strength are enhanced with TSP incorporation • Col/SF/HA scaffolds report increased elastic modulus.	• MG-63 cell lines showed increased cell viability for nHA/CS/TSP biomaterial. • Higher biomineralization and degradation with increase in TSP content. • Cell proliferation on CS-nHA and CS-nCZ better than that on CS-nZrO. Filopodia extensions towards non bioceramic materials. • Col/SF/HA reports more cell growth with MG-63. • ADA/ Gelatin/nHA showed cytocompatibility with Vero cell line. • Adequate cell proliferation and growth with CS/ Fucoidan/nHA scaffolds for periosteum derived-mesenchymal stem cells (PMSC).	• Surface roughness of nHA/Cs/TSP higher than CS/ nHA, which is also more than pure CS material. • Increased mechanical strength of scaffold. • Improved thermal stability for nHA/CS/TSP and CS/nHA. • Uniform particle distribution. • Higher swelling ratio with TSP incorporation into nHA/CS. • Presence of calcium in nanoparticles (especially nHA) has been reported to have increased the binding efficiency of the engineered biomaterial with osteocalcin; and enhanced osteopontin expression and synthesis leading to more Arg-Gly-Asp oligopeptide binding sites. This helps in cell spreading across the scaffold. • Thermal stability increases with increase in nHA in ADA and Gelatin scaffolds. • Higher mineralization for CS/ Fucoidan/nHA scaffolds.	• Without TSP incorporation, water absorption and porosity capacity decrease as compared to pure CS. • Irregular crystal structure with wet chemical method. • Pore size decreased with increase in nHA above 2% in ADA and Gelatin matrix. • Slower degradation rate with increase in stiffness due to increase in nHA content in ADA and Gelatin matrix. • CS/ Fucoidan/nHA scaffolds show slight decrease in porosity and lower efficiency in water absorption/ retention with nHA incorporation.	[49], [47], [91], [108], [115]
nZrO/nCZ	Co-precipitation	• 2% acetic acid – CS suspension • 40% w/w nanoparticles with magnetic stirring followed by	• Freeze-drying. • Compressive Modulus: 0.774 MPa - CS/nZrO 0.97 MPa - CS/nCZ • Young's Modulus: >3.5	• OB-6 preosteoblast cell proliferation on CS/nZrO better than CS only scaffolds. • Cell proliferation on	• Increased mechanical strength of scaffold. • Uniform particle distribution.	-	[52]

Nanomaterial	Synthesis Method	Polymer Incorporation Method	Scaffold Preparation & Mechanical Properties	Biological Activity	Advantages	Drawbacks	References
		sonication at 40 °C.	GPa - CS/nZrO, CS/nCZ.	CS-nCZ better than that on CS-nZrO. Filopodia extensions towards non bioceramic materials.			
nSi	Stöber method	• CS solutions (in acetic acid) and nSi put together in Eppendorf tubes and frozen.	• Freeze-drying. • Young's modulus of around 173.3 MPa.	Human primary osteoblast cells were reported to have formed three-dimensional conformation.	• 3D conformation of cells enhances cellular metabolic activity.	• No significant changes in pore size between samples with varying nanofillers amount.	[43]
CCNWs/ AgNPs	• Acid hydrolysis – Carboxylation (CCNWS). • Metallic Reduction Method (AGNPs/ CCNWS)	• CS/CMC polymer blend mixed with CCNWs/ AGNPS.	• Freeze-drying. • Enhanced compressive strength with increase in nanofillers content to polymer matrix.	• Adequate MG-63 cell adhesion to scaffolds. • Suitable protein absorption at low CCNWS/AgNPs content.	• Antimicrobial activity. • Larger pore size with increasing nanofillers content.	• Reduction in swelling and porosity (%) and increase in half-life for degradation with increase in nanoparticles.	[55]
BG	Stöber method	• 0.1 M acetic acid CS solution and 2% gelatin (in DI water). • BG dispersion in varying amounts.	• Hydrogel based injectable scaffold. • Elastic and viscous modulus (at both 25 and 37 °C) increase with	• Adequate cell proliferation (SAOS cells).	• Reduction in gelation time with gelatin and BG incorporation.	• No effect on porosity	[57]
MWCNT	Acid oxidative process (functionalization of MWCNT)	• Col hydrogel synthesized using acetic acid for fibril homogenization	• Freeze-drying. • Compressive stress and elastic modulus increased with fMWCNT/CS/Col scaffolds. • Biomineralization of scaffolds resulted in doubling of these properties.	• Enhancement in MG-63 cell proliferation and overall scaffold biocompatibility with nanoparticle incorporation	• Enhanced regularity and interconnected pore size rate. • Increased biomineralization on nanostructured surface. • Biomineralization reduces hydrophilicity	• Reduced swelling with nanofiller incorporation and biomineralizetion	[72]
BCP	Calcium nitrate tetrahydrate added dropwise to ammonium phosphate dibasic	• 2.5% (w/v) Col solution. • 50:50 (w/v) BCP/Col solution to ice particles.	• Freeze-dried. • Increased Young's modulus for all nanoparticle incorporated scaffolds.	• Human mesenchymal stem cells (hMSC) adhesion adequate. • DEX-BCP scaffolds reported increased cell proliferation.	• Adequate interconnected pores at BCP/Col mass ratio of 1:1 • Increased pore surface roughness	• Osteogenic expressions significantly enhanced with combined effect of DEX/BCP.	[73]
$nTiO_2$	Fluoride modification of $nTiO_2$ using HF	• 2% (w/v) SF blended with homogenously dispersed TiO2-F	• Freeze-dried. • Increase in compressive strength (approx. 0.7 to 1.7 MPa) with increase in nanofiller content up to 15 wt. %	• Higher biomineralization with spherical apatite particles. • SAOS-2 cell viability and attachment increased with nanofiller content up to 15 wt. %	• Degradation rate increases with increased nanofiller content	• Decrease in pore size with increase in TiO2-F content	[80, 90]
CNWs	Acid hydrolysis followed by lyophilization	• *In situ* HA formation –	• Homogenously dispersed in medium.	• MC3T3-E1 cell lines reported cytocompatibility.	• Controlling acidic groups on CNWs can	• CNWs tend to aggregate.	[98, 99]

Nanomaterial	Synthesis Method	Polymer Incorporation Method	Scaffold Preparation & Mechanical Properties	Biological Activity	Advantages	Drawbacks	References
		biomimetic method. • Physical blending of CNWs and HA particles synthesized using wet chemical method.		• L929 cells reported viability to be higher for CNW with biomimetically produced HA.	influence HA nucleation characteristics	• Thermal degradation of cellulose irrelevant of HA growth.	
CNCs	Acid hydrolysis; TEMPO oxidation reaction	• Cryo-templating to form CNC aerogel.	• CNCs synthesized with sulfuric acid hydrolysis exhibited higher compressive strength than CNCs created through phosphoric acid hydrolysis.	• Adequate cell proliferation and metabolism exhibited using SAOS-2 cell lines; significantly increased ALP activity with S-CNC over P-CNC; adequate biomineralization of pretreated CNC aerogels.	• High porosity (above 80%) for both S-CNC and P-CNC. • Large surface area for improved cell adhesion. • Tunable degradation characteristics of the aerogel by controlling the aldehyde and hydrazide content on CNC surfaces and limiting the number of hydrazine bonds.	• Lower cell metabolism for P-CNC(from phosphoric acid) due to low stiffness as compared to S-CNC (from sulfuric acid).	[100, 101]

Table 2

Summary of some synthetic polymer-based nanocomposites. The summary has been categorized with the nanoparticle in focus. Significant advantages and disadvantages due to the incorporation of the particular nanomaterial have been listed along with their effect on the mechanical properties.

Nanomaterial	Synthesis Method	Polymer Incorporation Method	Scaffold Preparation & Mechanical Properties	Biological Activity	Advantages	Drawbacks	References
nHA	*In situ* solvo-thermal method on PCL	• PCL/nHA dissolved in DMC with stirring.	•Salt leaching and freeze-drying. • Compressive strength and elastic modulus of *in situ* PCL/nHA has been reported to be more as compared to PCL/nHA (*ex situ*).	• Human osteosarcoma cells report higher cell viability with *in situ* PCL/nHA.	• Adequate nanofillers dispersion through the polymer matrix, owing to an increase in mechanical strength for *in situ* PCL/nHA. • Reduced hydrophobicity of PCL. • Reduced particle aggregation in *in situ* PCL/nHA.	• Spherical nHA (*ex situ*) less uniformly distributed. • Minor reduction in ductility of biomaterial.	[125]
RGO	Reduce GO using L-ascorbic acid.	• 0.25 wt. % GO-RGO/PCL composite solution with 20% (w/v) PCL on total volume.	•Electrospinning: nanofibrous mats. • Young's modulus of around 2.09 MPa for nanofibrous mats with GO-RGO/PCL, which is 38% increase as compared to PCL only mats.	• Mouse fibroblast (NIH-3T3) cell lines reported increased cell viability with RGO incorporation. • 3T3, HOS, MG-63 cell lines reported increased cell proliferation with RGO (both fibrous and films). • Enhanced biomineralization with RGO/PCL nanofibrous mats.	• Increased surface roughness owing to heterogeneous topography.	• No significant effect on the ductility of the nanofibrous mat.	[134]
TNT	PLGA/TNT microspheres synthesized using modified emulsion and solvent evaporation process.	• 10% (w/v) PLGA dissolved in methylene chloride mixed with TNT was added in drops t PVA solution while being stirred.	•Sintered microsphere procedure. • PLGA/TNT (0.5 wt. %) sintered at 120 °C and for 3 hours exhibited the maximum compressive strength and modulus, >10 MPa and > 350 MPA respectively.	• G-292 (osteoblast) cell proliferation had no adverse effects due to TNT incorporation. • Increased bioactivity for PLGA/TNT scaffolds; SAOS-2 cell lines reported adequate attachment, proliferation as well as migration. • *In vivo* studies revealed adequate bone	• Increased surface roughness for microspheres. • Reduce hydrophobicity of the scaffold enforced by PLGA. • Mesoporosity and nanoscale surface topography aids in adequate cellular behavior.	• Nanofillers incorporation efficiency may reduce with increase in TNT content; reduction in PLGA/TNT ratio will decrease scaffold mechanical strength. • Decrease in degradation rate of scaffolds.	[147]

Nanomaterial	Synthesis Method	Polymer Incorporation Method	Scaffold Preparation & Mechanical Properties	Biological Activity	Advantages	Drawbacks	References
				formation in direct contact with the composite material.			
Grafted - GO	• Oxidation of natural graphite (Tour's method). • Surface grafted GO on PEG synthesized with amino-PEG and GO aqueous suspension.	• Electrospinning mixture made by blending GO-g-PEG with PCL using dichloromethane and ethanol; 10 wt. % of PCL with 1 wt. % maximum GO-g-PEG concentration.	•Electrospun fibers; increase in tensile stress; 0.25 wt. % GO-g-PEG/PCL reported enhanced elastic modulus and overall reinforcement of nanocomposite as compared to GO only incorporation.	• MC3T3-E1 cells have been reported to have more affinity towards PCL/GO-g-PEG nanocomposite. • GO-g-PEG enhances cellular adhesion as compared to pristine PCL scaffolds.	• GO-g-PEG nano sheets reported with deep lamellar structure owing to adequate 3D porous network. • Nanofiber diameter distribution increased with GO-g-PEG information;	• Reduction in ductility with GO-g-PEG addition. • Lower interaction between PCL matrix and nanofillers owing to lower heterogeneous crystallinity.	[153]
Nano calcium phosphate	Flame Spray Pyrolysis method.	• Solvent casted and electrospun bilayer membranes with 10% (w/v) PCL, 5% (w/v) SF.	•Electrospun SF/PCL-PEG-PCL with nano calcium phosphate. • Increase in ultimate tensile strength with increase in nano calcium phosphate content	• Human dental pulp stem cells (DPSC) cell lines reported significant enhancement in osteogenic differentiation of cells. • High porosity of membranes facilitated cell attachment.	• Increased hydrophilicity with increasing nano calcium phosphate content. • Increased roughness and thickness of nanofibers with increasing nano calcium phosphate content. • Enhanced nucleation of apatite with addition of nanofillers; increased elastic behavior of nanofibers with nanofillers addition.	• Very slight increase in water uptake with nanofillers addition.	[154]
BG	Sol-gel method; BG nanofibers synthesized using tetraethyl orthosilicate, tetraethyl phosphate, hydrochloric acid, calcium nitrate, polyvinylpyrrolidone.	• BG nanofibers dispersed in ethanol were applied onto the plasma treated PLLA nanofibers and dried at room temperature.	•Electrospun BG and PLLA nanofibers synthesized as nanocomposite	• Increased biocompatibility. • MSCs show the highest growth in PLLA BG nanofiber composites with lower toxicity. • Highest ALP activity for nanocomposite as compared to BG only and PLLA only nanofibers.	• Adequate interconnected porous and completely fibrous structure.	-	[162]